Mechanism of Dynamin-catalyzed Membrane Fission

A Thesis

Submitted in partial fulfillment of the requirements

of the degree of

Doctor of Philosophy

By

Srishti Dar

20113117

Indian Institute of Science Education and Research Pune

2016

Acknowledgements

I would like to express my sincere gratitude to my supervisor, Dr. Thomas Pucadyil, without whose guidance, understanding, and patience this project would not have reached completion. I appreciate and envy his expertise and vast knowledge in all areas and especially his skills in writing reports and giving presentations. It is owing to his efforts that I have become disciplined, focused, and developed a keen interest in science. He provided me with direction;support and most importantly,lessons on how to do good science; and overtime became more of a mentor and friend, than a supervisor. I doubt that I will ever be able to convey my appreciation fully, but I owe him my eternal gratitude

I would also like to thank my parents for their constant faith in my abilities and for the encouragement they have provided me through my entire life. I would not have been here if it were not for them. A special thanks to my friends, Neha Nirwan, Darshika Tomar and Mansi Mungee for not just the scientific discussions and lending reagents and consumables but also our philosophical discussions, debates and venting of frustration after a hard day in the lab. They have tremendously helped enrich my journey. I would also like to thank Shreyash Tandon, without whose support I would not have survived these 5 years. PhD is a very long arduous struggle where there are more failures and very few successes. His friendship and motivation has made this journey immensely enjoyable and one that I will always cherish. He has always brought out the best in me.

I must also acknowledge Professor L.S.Shashidhara, who despite his busy schedule, has always managed to help me in the hour of need. I must also acknowledge my lab members, without their help, encouragement and editing assistance, I would not have reached here.

In conclusion, I recognize that this research would not have been possible without the financial assistance and facilities provided by IISER and my fellowship from CSIR and express my gratitude to those agencies.

Declaration

This thesis is a presentation of my original research work. Wherever contributions of others are involved, every effort is made to indicate this clearly, with due reference to the literature, and acknowledgement of collaborative research and discussions. The work was done under the guidance of Dr. Thomas Pucadyil, at the Indian Institute of Science Education and Research, Pune.

Srishti Dar

In my capacity as supervisor of the candidate's thesis, I certify that the above statements are true to the best of my knowledge.

Dr. Thomas Pucadyil

Table of Contents

Table of Figures

Synopsis

Membrane proteins are sorted to different cellular compartments by a process termed as vesicular transport, wherein membrane proteins are sorted into a membrane bud that is severed to form a vesicle. This process allows cells to take up nutrients, ensures inheritance of organelles after cell division and manages synaptic transmission thus making it fundamental to life. The process of vesicle release requires dynamic interplay between the protein and membrane. Protein binding induces curvature stress that remodels planar membranes into narrow tube-like intermediates, leading to scission. The formation of a constricted neck-like intermediate requires the bilayer to approach distances closer than 4 nm (lesser than the thickness of a bilayer) and is hence energetically unfavorable and necessitates the requirement of specific protein machinery. Cells have therefore evolved highly sophisticated protein machineries to execute the fission reaction. Proteins implicated in the severing reaction belong to a highly conserved family of GTPases. Dynamin represents the paradigmatic member of this family and functions to generate synaptic vesicles for fast neurotransmission. It is recruited at late stages of clathrin-mediated membrane budding where it scaffolds the constricted neck of a coated pit and hydrolyzes GTP to affect membrane fission.

While genetic screens identified dynamin as a membrane fission catalyst in the late 80's, its mechanism of action remains elusive even today. The complex environment of the cell involving myriads of proteins, gives limited insights into the mechanism by which this protein catalyzes scission of membranes. This is because defects in any of the sub-processes of membrane binding, scaffolding and membrane fission produce similar phenotypes in such assays. Investigating this reaction *in vitro* has been equally challenging due to the lack of quantitative assays. Fission leading to the release of vesicles has been reproduced using purified cell membranes, and cytosol. However the biochemical complexity of these systems hinders our understanding of the underlying mechanism of dynamin-catalyzed membrane fission. The more evolved reconstitution approaches involve EM analysis of liposomes. Although, the observations from these studies have contributed significantly to our current understanding of the tube severing reaction, one cannot monitor the dynamics of the fission reaction in real-time. Collectively, all studies seem to indicate that the severing reaction is typically carried out in a

confined region of the membrane enclosed within a 10 nm wide, 2-rung scaffold comprised of ~26 molecules of dynamin.

In keeping with the membrane topology at the site of dynamin action, the current research focuses on recruiting dynamin on membrane tubes. Conventionally, membrane tubes are formed by tugging at a large vesicle using sophisticated micromanipulators or optical traps or by employing tedious reconstitution schemes using motor proteins. Quantitative analysis of fluorescence changes on the widely used assay system of membrane tethers pulled from giant unilamellar vesicles is difficult because of their out-of-focus movements in solution, not to mention the experimental challenge in recording statistically significant numbers of fission events because these systems allow recording of only a single fission event at a time. Thus, events leading to membrane severing have been difficult to probe. Current models proposed to explain membrane fission either imply a GTP hydrolysis-induced conformational change or a local sculpting of membrane lipids into non-bilayer configurations. Notably however, many of the proposed models are based on read-outs from indirect conductance- or molecular modeling-based approaches. While static EM-based analysis have offered some insights into the nature of membrane intermediates generated during this process, assays that provide a direct and reliable visualization of membrane dynamics during membrane fission has been conspicuously absent.

Chapter 1 of this thesis gives an introduction to vesicular transport, and dynamin with an emphasis on the different reconstitution approaches that have been used to understand its function and the proposed models for dynamin-catalyzed membrane fission.

Chapter 2 describes a novel facile assay system of arrayed supported membrane tubes (SMrT), resting on a passive surface and contained in a flow cell to allow accurate monitoring of dynamin-catalyzed membrane fission. The membrane tube dimensions can be controlled to mimic the topology of necks of clathrin-coated buds, the physiological substrate for dynamin. The SMrT assay is robust, easy to set-up and highly economical with respect to lipid consumption. Biochemical parameters such as size, lipid diffusion, lipid distribution and stability have been characterized. Given the simplicity of our assay and its potential widespread applicability, we anticipate our assay system of SMrT templates to be of broad interest in understanding the mechanisms by which protein scaffolds function during vesicular transport

Chapter 3describes how using the SMrT assay we have been able to dissect the molecular events leading to membrane fission catalyzed by dynamin. For the first time in the

field of membrane fission, we now can trace the evolution of membrane intermediates to nanometer precision as the dynamin scaffold wraps around a membrane tube, constricts it in response to GTP hydrolysis leading to scission of the tube. Using a correlative fluorescence microscopy-based analysis of scaffold dynamics and membrane topological intermediates generated during the scission reaction, we have identified a GTP hydrolysis-dependent membrane constriction process catalyzed by an intact scaffold that culminates in a highly constricted tubular intermediate of 7.2 nm radius prior to scission. I believe these results unambiguously establish a role for GTP hydrolysis in bringing about a membrane constriction reaction and would serve to constrain current models proposed for membrane fission.

Chapter 4 attempts to understand the functional relevance of the pleckstrin homology domain in dynamin-mediated membrane fission. Dynamin engages with the plasma membrane via a pleckstrin-homology domain (PHD) that recognizes the phosphatidylinositol-4,5-bisphosphate (PIP_2) head group in a stereo-selective manner and its importance is underscored in centronuclear myopathies that map to point mutations in the PHD. The PHD however is conspicuously absent among extantmembers of the dynamin superfamily such as the bacterial and mitochondrial dynamins,where its functions are substituted by disordered loops. Inspired by the design of theseextant dynamin family members, we engineered a dynamin mutant where specific PHD-PIP_2interactions are replaced by a generic polyHis-Ni2+-lipid association. Using the SMrT assay, we find that this mutant canremarkably catalyze membrane fission. However, the fission reaction is characterizedby highly variable rates of scaffold assembly-induced membrane constriction and long-lived(15-30s) prefission intermediates which slow down kinetics of fission by 3-fold. We conclude that thephysiological requirement for a fast-acting membrane fission apparatus appears to have been fulfilled by the adoption of the PHD by dynamin family members.

Chapter-1

Introduction

1. Introduction

1.1 Membrane Trafficking and Vesicular Transport

Cell compartmentalization is a prominent feature of all eukaryotic cells. Each compartment is enclosed by a lipid bilayer that separates the contents of the organelle from the outside environment thereby maintaining specificity and ensuring efficiency of chemical reactions. However for cellular homeostasis to occur, cells must constantly incorporate material from their environment or exchange material between compartments. This is achieved through transport of membrane-bound vesicles between the donor and the acceptor compartment.

This process of vesicular transport involves deformation of the donor membrane into a bud, encapsulation of proteins, separation of bud from the parent membrane and subsequent fusion with the donor compartment. Membrane budding and fission are crucial stages during vesicular transport generating intracellular carriers of cargo. Membrane fission involves non-leaky division of one membrane into two. Fission from the plasma membrane ensures internalization of proteins from the external environment into the cell, fission from the Golgi and ER is necessary for the secretory function of these organelles, and vesicle release from endosome and lysosome regulates receptor recycling (Schmid 1997; Mironov et al., 1997; Griffiths 2000; Lipincott-Schwartz 2001). In all, this process ensures a dynamic exchange of proteins and lipids across different compartments.

Although critical to vesicular transport, the molecular mechanisms underlying membrane fission remain poorly understood. In particular, the actual dynamics of lipid bilayer division and the corresponding role of protein machinery driving this process are poorly characterized. There are two reasons for this lack of understanding; a) fast kinetics of the fission reaction makes it impossible to trap intermediates and follow the process in real-time with any technique, and b) lack of common fission machinery across different compartments.

Protein machineries implicated in membrane fission are dynamin, COPI and COPII, epsin homology domain containing proteins and ESCRTIII complex (Schmid 1997; Rothman 1994; Schekman and Orci 1996; Naslavsky and Caplan 2012; McCullough et al., 2014). Although widely different in their sites of action, a striking common feature across these proteins and complexes is their ability to polymerize and deform membranes. The general principle governing membrane fission is the ability of the protein coat to drive constriction of the

underlying membrane bringing them in close proximity until they fuse (Chernomordik and Kozlov 2003). This is an energetically unfavorable process and involves the formation of a very narrow neck (Kozlovsky and Kozlov 2000). Dynamin was identified as the first protein to be directly involved in carrying out this unfavorablefission reaction (Koening and Ikeda 1989; van der Bliek et al., 1993; Chen et al., 1991).

1.2 Dynamin

1.2.1 Introduction

The dynamin superfamily of proteins is associated with diverse cellular processes such as release of endocytic vesicles during clathrin-mediated endocytosis (CME), fusion and fission of mitochondria, division of chloroplast, cell division and antiviral proteins (Heyman and Hinshaw 2009). Dynamin1, the paradigmatic member of this family, has been shown to drive membrane fission by forming helical collars on necks of endocytic vesicles (Sweitzer and Hinshaw 1998; Takei et al., 1998). Dynamin assembly on negatively charged membranes *in vitro* has been shown to induce curvature stress, constricting the underlying membrane to form a narrow tube. Early evidence implicating dynamin in membrane fission came from mutants defective in GTP hydrolysis (van der Bleik et al., 1993, Herkovits et al., 1993; Damke et al., 1994; Marks et al., 2001). It was therefore speculated that GTP hydrolysis triggers conformational changes in the dynamin polymer that brings the inner monolayer of the bilayers closer to the thickness of the bilayer (3-5nm) at which point the membranes fuse leading to a non-leaky membrane fission event (Bashkirov et al., 2008).

Bilayer integrity is maintained by strong hydrophobic effects (Tannford 1973). Membrane fission is speculated to proceed via a pathway involving progressive membrane deformation followed by rapid membrane remodeling (Kozlovsky and Kozlov 2003; Chermomordik and Kozlov 2003). Theoretical analysis of membrane fission proposes the formation of a narrow neck, which upon further constriction transitions into a hemi-fission intermediate and fission follows spontaneously. This progression from a constricted neck to the hemi-fission intermediate is thermodynamically unfavorable and is speculated to be driven by the energy released from hydrolysis of GTP.

1.2.2 Discovery

Dynamin was originally identified as a microtubule binding protein, which in the presence of ATP causes microtubules to slide past each other (Shpetner and Valee 1989). Because of its similarity to an ATP-dependent motor protein it was named dynamin (derived from dynamic). However cloning and sequencing studies revealed 70% homology to the *shibire* gene in Drosophila, suggesting a role for dynamin in endocytosis (Obar et al., 1990). The temperature sensitive *shibire* flies showed rapid and reversible paralysis on being shifted to non-permissive temperature (Grigliatti et al., 1973). Ultra-structural analysis of the synaptic termini of these flies revealed a block in endocytosis (Kosaka and Ikeda 1983; Koening and Ikeda 1989). This arrest in synaptic transmission was characterized by depletion of synaptic vesicles and accumulation of constricted omega shaped buds at the membrane with electron-dense collars decorating the neck. This observation was followed by studies overexpressing the GTPase-defective mutant of dynamin, which inhibited endocytosis in cells (van der Bleik et al., 1993; Herkovits et al., 1993, Damke et al., 1994). Further studies by Takei et al., in rat synaptosomes treated with the non-hydrolysable analogue of GTP, GTPγS, showed accumulation of long necks attached to the plasma membrane at one end and coated with clathrin at their base. *In vitro* reconstitution with recombinant dynamin1 on negatively charged templates revealed formation of helical scaffolds that deformed underlying membrane into tubes (Sweitzer and Hinshaw 1998). These structures were very similar to the electron-dense collars in *shibire* and striated tubules in rat synaptosomes. These and similar studies suggested a possible role for dynamin in endocytosis.

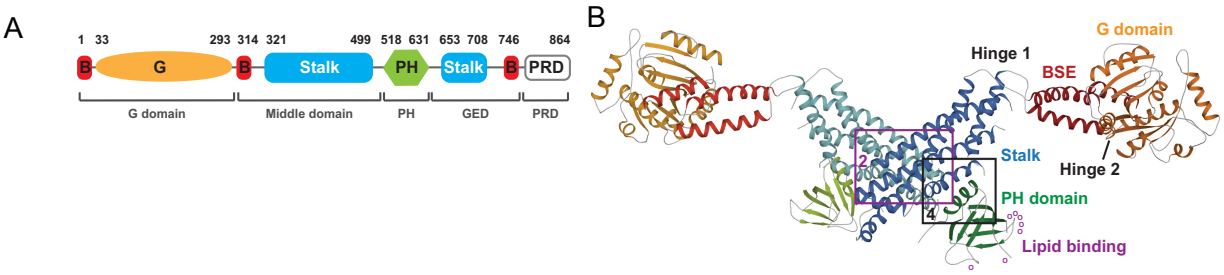

Figure 1-1. Domain organization and structure.(A) Domain organization of dynamin. (B) Structure of dynamin colour-coded according to schematic shown in (A). Images reproduced from Faelber et al., 2011.

1.2.3 Domain Organization

The crystal structure of the full-length human neuronal dynamin 1 without the PRD was reported only recently (Faelber et al., 2011; Ford et al., 2011). The superfamily of dynamins shares a highly conserved N-terminal G (GTPase) domain. The C-terminal of the G Domain is comprised of a helical Bundle Signalling Element (BSE) called the neck. The middle domain of dynamin is unique, lacking sequence homology with any known structural motif. The N terminus of the middle domain, which is 72% similar between dynamin1 and dynamin2 (Warnock and Schmid 1996), is a coiled-coil domain involved in oligomerization. The C- terminus of the middle domain is where sites for alternative splicing for all three dynamin isoforms have been mapped. The PH domain, around 100 residues in length, derives its name from the protein pleckstrin, a substrate for Protein Kinase C in platelets. The PH domain present at the foot of the dynamin dimer module binds with high affinity to acidic phospholipids, particularly PI(4,5)P2, present in the inner leaflet of the plasma membrane via highly conserved lysine residues (Ramachandran et al; 2009). Although the affinity of the isolated dynamin PH domain for the membrane is low (>1 mM), the net binding affinity is increased by both charge-dependent interactions and dynamin polymerization on membranes. PH domain mutants have been shown to exert dominant negative effects on CME (Ramachandran et al; 2009). The GTPase Effector Domain or GED is a coiled-coil that interacts with the G domain upon dimer formation thereby stimulating rates of GTP hydrolysis. The stimulation of GTPase activity has been shown to be cooperative and reflects the co-operativity in self-assembly (Warnock et al., 1996). The GED and the middle domain interact to form a stalk connecting the lipid binding PH domain to the G domain. The stalk dimerizes in a criss-cross arrangement to form a dimer, which is the basic unit where individual G domains are oriented in opposite directions. The C-terminus of dynamin, ~100 residues long, is highly unstructured and predicted to be projecting away from the membrane upon dynamin assembly. This is a highly positively charged stretch enriched in PXXRP motifs and is therefore called the Proline-Arginine Rich domain or PRD. The PRD serves as a substrate for many SH3 domain-containing proteins. Although the PRD-SH3 interactions are not very strong, the presence of multiple PRD residues in dynamin as well as its tendency to polymerize enhance this interaction which in turn regulates dynamin recruitment to clathrin-coated pits. The significance of this interaction is evident as dynamin lacking the PRD

cannot rescue endocytic defects in dynamin-knockout fibroblasts (Ferguson 2009). Human dynamin1 exists as a tetramer in solution. Purified dynamin spontaneously polymerizes into helical arrays or rings in solutions of low ionic strength and on membrane templates containing negatively-charged lipids

1.2.4 Genetic Diversity

A single dynamin gene with multiple isoforms has been reported in both *Drosophila melanogaster* and *Caenorabditis elegans* (van der Bleik et al., 1993; Clark et al., 1997). In mammals, dynamin is represented by 3 genes with multiple splice variants (Cao et al., 1998). Dynamin1 is the predominant neuronal isoform regulating synaptic vesicle recycling (Nakata et al., 1991; Ferguson et al., 2007). Dynamin2 is ubiquitous and the major fission molecule in clathrin-mediated endocytosis in all non-neuronal cell types (Cook et al., 1994; Sontag et al., 1994; Diatloff-Zito et al., 1995). Dynamin3 is present along with Dyn1 but at extremely low levels in the neurons (Raimondi et al., 2011), besides it is also reported to be present in the lungs and testis where it is involved in formation of tubulobulbar structures releasing sperm cells from the cells of Sertoli (Vaid et al., 2007). While the core domains are 80% homologous indicating a similar molecular mechanism across these isoforms, differences exist in their rates of GTP hydrolysis, membrane binding and assembly-induced constriction and fission efficiencies (Raimondi et al., 2011; Liu et al., 2011). Major differences appear in the protein binding C-terminal PRD, which engages with different partner proteins depending on the isoform and its site of expression (Raimondi et al., 2011).

1.2.5 Dynamin Superfamily Members

The dynamin superfamily includes classical dynamin and dynamin-like proteins (DLPs). Classical dynamins includes all those proteins which share sequence homology with the *shibire* gene in *Drosophila* and are characterized by the presence of 5 domains, G domain, Middle domain, PH domain, GED and the PRD. DLPs on the other hand have only the G, Middle and GED domains, and are implicated in various processes like mitochondrial fission and fusion, chloroplast and peroxisome division, cytokinesis and protection against viral infections. Dynamin superfamily members are characterized by very low binding affinities for GTP and high basal rates of GTP hydrolysis and therefore do not require additional guanine exchange

factors (GEFs) or GTPase activating proteins (GAPs) like members of the Ras family of GTPases. This lack of need for a GEF and assembly-stimulated GTP hydrolysis is a feature that is found conserved across all members of the dynamin superfamily.For all dynamin family members the cycle of nucleotide binding and hydrolysis is tightly coupled to their ability to catalyze vesicle release. The conformational changes occurring during cycles of GTP hydrolysis are propagated along the length of the polymer and are speculated to trigger forces leading to membrane fission (Chappie et. al., 2011).

1.2.6 Structural Insights

Early insights into the role of individual domains in dynamin function came from site-specific mutations. Over the past 2 decades many structural and functional studies of individual domains, chimeric constructs and EM reconstructions have yielded useful insights into the molecular determinants of polymer assembly and fission. The full-length protein has been difficult to crystallize due to its propensity to polymerize. A breakthrough in dynamin crystallization came about when two groups solved the crystal structure of full-length dynamin1 (without its PRD) by using self assembly-defective mutants (Ford et al., 2011; Faelber et al., 2011). While the wild type is present as a tetramer in solution (Muhlberg et al., 1997), these mutants were crystalized as dimers in the apo- and the nucleotide-bound state. This was followed by a more recent report from the collaborative efforts of a number of groups who managed to crystallize a more native form of the dynamin tetramer by reducing the severity of the assembly defects, which in turnhas given profound insights into key interfaces and determinants of higher order assembly (Reubold et al., 2015).

The G-domain is highly conserved across all DRPs and is extended by αβ fold made of 2 β-sheets surrounded by 2 α-helices (Niemann et al., 2006). It is characterized by the presence of 5 motifs- G1-G5, P-loop that binds GTP, and switches I and II. The G-domain is positioned on a lever-like arm formed by 3 α-helices constituting a structural domain called the bundle-signaling element (BSE) (Chappie et al., 2009; Gao et al., 2011; Faelber et al., 2011; Ford et al., 2011). The BSE is derived from non-contiguous sequences from the N and Ctermini of the G-domain and the C-terminus of the GED. The middle and the GED domain together form a rigid coiled-coil structure called the stalk (Gao et al., 2011; Faelber et al., 2011; Ford et al., 2011). The stalk domains of two monomers interact to yield a criss-cross dynamin dimer, which is the basic unit

of higher order assembly. The tetramer is a dimer of dimer and is characterized by 4 interaction interfaces. Interface 2 is where the stalks of the dimers form a criss-cross such that the G-domains of the monomers are oriented in the opposite directions. Further oligomerization between the dimers is facilitated via interface 1 and 3 that leads to tetramerization (Reubold et al., 2015). The PH domain-stalk interactions are highly conserved and this interaction is speculated to keep the PH domain in a closed conformation preventing untimely oligomerization. This autoinhibiton is only relieved upon membrane binding and is a key regulator of assembly (Mehrotra et al., 2014; Reubold et al., 2015).

The BSE functions like a toggle. Nucleotide and membrane binding introduces a bent in the dimer conformation thus facilitating formation of a helix as opposed to a ring. This also relieves the PH domain, inhibited due to interaction with the stalk interface, facilitating higher order assembly (Mehrotra et al., 2014; Reubold et al., 2015). G-domain dimerization of adjacent rungs of the helix triggers GTP hydrolysis (Chappie et al., 2011). Structural studies predict a long-range transmission of GTPase induced conformational changes from the G-domains via the BSE to the stalk finally causing membrane fission (Faelber et al., 2012).

However the most striking piece of information has come from the crystal structure of the minimal dynamin1 G-GED chimera (Chappie et al., 2011). The fusion protein crystallized in presence of GDPAlF_4^-, unravels information about the dimer in the transition state. This G-domain dimerization is only observed in the transition and not in the apo or with the non-hydrolysable analogue GMPPCP. The GED fragment docks into the hydrophobic cleft between the N- and C-terminal helices of the GTPase domain.In a dynamin spiral,the G-domain dimerization is predicted to occur between G-domains of adjacent rungs thereby optimally positioning key residues in trans for stimulated GTPase activation.

Current evidence points to the existence of a dynamic equilibrium among 3 states of dynamin- tetramer, dimer and monomer with the predominant species being the tetramer (Muhlberg et al., 1997). These tetramers undergo further assembly into higher order structures forming spirals and helical rings (Hinshaw and Schmid 1995; Carr and Hinshaw 1997). Formation of such rings can be triggered in vitro by lowering salt concentration, presence of a negatively charged lipid template (Switzer and Hinshaw 1998) or addition of BAR domain proteins like amphiphysin1 that engage with the C-terminal PRD (Takei et al., 1999).

1.2.7 Biochemical Characterization

On the basis of its GTPase activity, dynamin is extremely divergent from the canonical Ras family of small GTPases. At physiological salt concentration the basal rates GTP hydrolysis for Dynamin has been reported to be ~1 s^{-1} (Warnock et al., 1993; Song and Schmid 2003). These are 4orders of magnitude higher than the k_{cat} ($1.3x10^{-4}s^{-1}$) reported for members of the Ras family of small GTPases. Their affinity for GTP is also very different. While Ras has an extremely low K_m = 0.2-0.5 uM, necessitating the requirement of exchange factors or GEFs to facilitate transition between the GTP-bound active state and the GDP-bound inactive state, dynamin on the other hand has very low affinity for GTP (K_m= 10-150 uM)(Warnock and Schmid 1996). The GTPase activity can be stimulated 100-fold upon assembly. When dynamin is assembled either by recruitment on a negatively charged lipid template or by lowering salt concentration, it triggers dimerization of G-domains of adjacent rungs and optimal positioning of key catalytic residues leading to concomitant stimulation in hydrolysis rates (Mears et al., 2007; Chappie et al., 2011).

1.2.8 *In vitro* Reconstitution of Dynamin Function

Dynamin was the first protein to display tubulation activity on protein free liposomes (Swietzer and Hinshaw 1998). Although its membrane binding property is independent of GTP, several reports indicate the role of negative charge (Tuma et al., 1993) and curvature (Roux et al., 2010)as key determinants for regulating dynamin polymerization. Most studies that have looked at dynamin-induced membrane tubulation have been carried out on SUVs made either with 100% PS or purified brain lipids supplemented with PIP_2. Purified dynamin when added to negatively charged liposomes forms helical polymers tubulating the underlying membrane. These helical polymers were visualized via electron microscopy (EM) and reconstructed by CryoEM (Chen et al., 2004; Mears et al., 2007). In the apo state dynamin forms a right-handed helix with 14.3 dimers per helical turn. The distance between adjacent rungs is 13 nm and the outer diameter of the helix has been reported to be 50 nm (Zhang and Hinshaw 2001; Chen et al., 2004). The dimensions of the tube and the surrounding helix are the same whether the protein is assembled on a lipid template or on its own. Once assembled on the membrane, the BSE tilts each unit by an angle to facilitate packing of 14.3 subunits in a helix (Mears et al., 2007; Chappie

et al., 2009). These scaffolds of dynamin appeared to be more ordered for dynamin1 lacking the C-terminal PRD than the full-length protein. The PRD is an unstructured domain speculated to be projecting out from the helical polymer. In cells it is actively engaged with SH3 domain containing BAR proteins that are proposed to form a copolymer with dynamin important for effective constriction and fission (Grabs et al., 1997; Shpetner et al., 1997; Shupliakov et al., 1997; Farsad et al., 2001; Lundmark et al., 2004; Ferguson et al., 2009).

When GTP and dynamin are added together, liposomes fragment releasing smaller vesicles that are 20-30 nm in diameter. CryoEM data of GTP addition to dynamin decorated tubes recorded at different time points to two distinct intermediates; a) super constricted dynamin-coated tubes are seen within 60 seconds and b) disassembly of the protein and bulging-out of the underlying membrane was visualized for tubes imaged after 200 seconds (Stowell et al., 1999; Marks et al., 2001; Danino et al., 2004). Upon constriction, the dynamin helix reducesfrom 50 to 40 nm in diameter with the pitch lowering to 9.3 nm, suggesting compaction of the helix. The more significant and reproducible observation is however the reduction in the number of units in the scaffold from 14.3 in the non-constricted state to 13.3 in the constricted state.

A comprehensive understanding of conformational changes taking place in the dynamin polymer and its relation to membrane fission in response to GTP hydrolysis has remained elusive. Assays that probe conformational states or dynamics in proteins are largely EM- or spectroscopy-based and hence not amenable to probe dynamic remodeling of membranes leading to fission. Recent results of docking of crystal structures of isolated domains of dynamin locked in the GTP-bound and transition states to the CryoEM reconstructions of helical polymers suggest that a concerted state transition is necessary for tube scission. However, the proposed conformational changes are yet to be experimentally validated in a membrane fission assay.

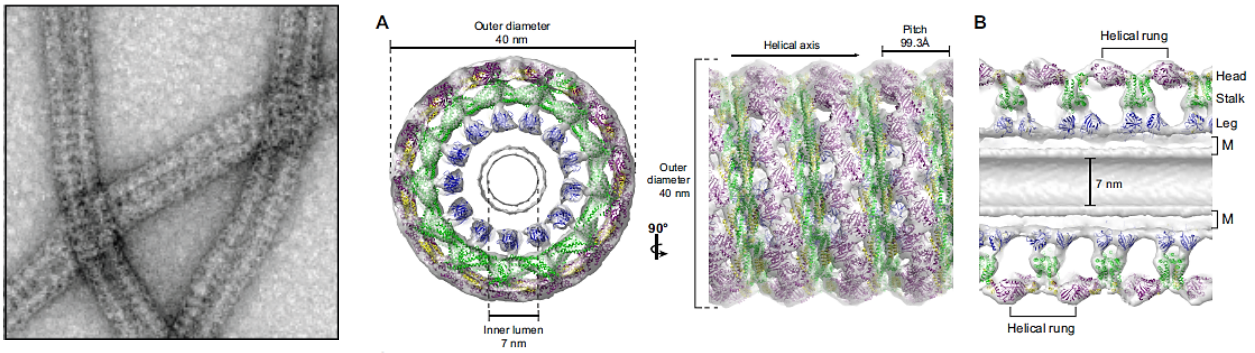

Figure 1-2. Dynamin scaffold organization on the membrane.(A) Negative-stain EM of dynamin assembled on 100% PS liposomes. (B) CryoEM reconstruction of dynamin polymer on a membrane. Purple represents apposing G-domains, green represents the stalk and blue represents the PH domain. Images are reproduced from Sweitzer and Hinshaw 1998 (A); Chappie and Dyda 2013 (B).

1.3 Current Models for Dynamin-catalyzed Membrane Fission

Although dynamin's role in fission has been investigated for more than 20 years, it was only recently shown that dynamin alone is sufficient to mediate fission. Studying dynamin behaviour on membranes in the constant presence of GTP has proved to be extremely challenging due the rapid kinetics of its association and disassembly from membranes. Models have only looked at the organization of dynamin on membranes or the conformational changes the enzyme undergoes upon assembly and nucleotide-binding, without correlating it to fission. Importantly, the exact sequence of events taking place during fission still remains obscure. *Invitro* reconstitution on protein-free liposomes have made use of either EM or light scattering approaches. While EM has offered some insights, changes in light scattering could be interpreted as membrane dissociation of dynamin and/or membrane fission. The recent advances made in our understanding of the structure of dynamin and conformational changes seen upon GTP-binding are inconclusive with regards to understanding conformational changes required for fission.

1.3.1 The "Constriction" Model

In 2006, Roux et al for the first time reconstituted the fission reaction in real-time identifying dynamin as the first independent membrane-fission catalyst (Roux et al., 2006). Dynamin in the presence of GTP was added to an array of membrane tubes pulled out of giant

unilamellar vesicles by the action of kinesin motor proteins. Fluorescence microscopy revealed fragmentation of these tubes and release of numerous vesicles under conditions of constant GTP turnover. However, in another experiment, where GTP was added to dynamin decorated tubes, tubules that were free at one end underwent spontaneous supercoiling and retraction back to the membrane reservoir, but the ones that were tethered were severed. Moreover, polystyrene beads conjugated with dynamin underwent a rotatory motion upon GTP addition suggesting a conformational twist of the helix in response to GTP. This observation was in agreement with the earlier data from Sweitzer and Hinshaw (1995), who showed that attachment of dynamin coated tubules to a substrate (EM grids), provided the tension necessary to catalyze fission. *In vivo*, this tension could be generated by the actin cytoskeleton, which is a key player in endocytosis and is co-localized with dynamin at clathrin-coated pits (Itoh et al., 2005; Kaksonen et al., 2005). More data in support of the role of tension and membrane rigidity in dynamin-mediated membrane fission came from Morlot et al., (2012). Membrane tethers pulled from GUVs of different composition indicate a positive dependence of tension on rates of fission. On the basis of the existing data, the authors proposed a corkscrew model (Mears et al., 2007), speculating that fission is triggered by GTP hydrolysis induced torque, which propagates throughout scaffold, leading to sliding and twisting of individual rungs of the spiral. This model also suggests that membrane tension is as a major player in regulating kinetics of the fission process (Roux et al., 2006; Morlot et al., 2012).

1.3.2 "Squeeze and Release" or "Assembly-Disassembly" Model

In cells, vesicle release is followed by disassembly of the dynamin polymer (Cremona et al., 1999; Chang-Ileto et al., 2011; Milosevic et al., 2011)and is triggered bythe action of the PIP_2-hydrolyzing enzyme synaptojanin (McPherson et al., 1996; Chang-Ileto et al., 2011; Milosevic et al., 2011). Taylor et al, using TIRF showed that fission at necks of coated pits coincided with the arrival of synaptojanin a PIP_2phosphatase. Interestingly, depolymerization of preassembled dynamin scaffolds in response to GTP addition has also been reported earlier on liposomes (Danino et al., 2004) and independently by fluorescence-based studies (Ramachandran and Schmid 2008). In 2008, two different groups using independent approaches with high spatial and temporal resolution, proposed a 'squeeze and release' mechanism for fission. Pucadyil and Schmid recapitulated dynamin-catalyzed membrane fission on a novel assay of tethers pulled

from SUPER templates (Pucadyil and Schmid 2008; Pucadyil and Schmid 2010). These are membranes with excess reservoir adsorbed on silica beads and organized in folds. These templates offer the unique advantage of simultaneous microscopy- and sedimentation-based bulk analysis of membrane fission. Addition of dynamin to SUPER templates led to the growth of fluorescently labeled dynamin-coated tubules. GTP addition to these tubes was accompanied by loss of dynamin signal from the tubes followed by retraction of these tubes into the membrane reservoir. In an independent study with NBD-labeled dynamin, similar results were reported suggesting that disassembly precedes fission (Ramachandran and Schmid 2007). Further support for this model came from a conductance-based assay (Bashkirov et al., 2008). Dynamin was assembled on nano-tubes of fixed dimensions pulled from supported bilayers, and the corresponding changes in lumenal radius were followed by monitoring conductance changes across the bilayer. GTP addition to preassembled dynamin lead to a monotonous increase in conductance, followed by a sudden drop to zero. The initial rise was interpreted as widening of the tube, caused by scaffold disassembly, and the drop to zero indicates tube scission. Together these results indicate cycles of assembly and disassembly of dynamin polymer as a possible mechanism for membrane fission. Another interesting observation from the SUPER template assay was that, even flow-induced tubes that were flaccid and under no external tension underwent dynamin-catalyzed scission in constant presence of GTP (Pucadyil and Schmid 2008). These results are further supported by *in vivo* data on cells kept under different osmotic condition. Cocucci et al. examined the effect of tension on the number of dynamin molecules required to catalyze a scission event (Cocucci et al., 2014). When a cell is exposed to a hypoosmotic solution, the plasma membrane becomes flaccid, thereby lowering membrane tension. Under these conditions more dynamin molecules get recruited at necks of coated pits. However, no difference was observed in the number of dynamin molecules required to catalyze fission in cells kept in a hyperosmotic or isotonic solution. Based on theseresults, there appears to be a threshold requirement of dynamin molecules for a scission event irrespective of membrane tension.

1.3.3 The “Hemi-fission” Model

Nonleaky membrane fission reactions involving a tubular neck-like intermediate, such as the one catalyzed by dynamin (Bashkirov et al., 2008), are proposed to involve a tube-

constriction step in order that the enclosing lipid bilayer is brought to close proximity, at which point spontaneous formation of a hemifission intermediate leads to tube scission (Frolov et al., 2015; Kozlovsky and Kozlov, 2003). Membrane recruitment via PH domain-lipid interactions and intermolecular interactions between adjacent stalks promote dynamin self-assembly as stable helical polymers. CryoEM reconstructions indicate the polymer to be a right-handed helix of 50 nm in diameter and comprised of 14 subunits per turn with a pitch of 9.9 nm. Polymerization distorts the membrane into a tube with an inner lumen of 7 nm in diameter and also reorients catalytic residues in apposing G-domains, which leads to stimulation in its basal rates of GTP hydrolysis (Chappie and Dyda, 2013). The mechanism that couples GTP hydrolysis induced conformational changes in the polymer to membrane fission remains unclear. Recent results of docking of crystal structures of isolated domains of dynamin locked in the GTP-bound and transition states to the CryoEM reconstructions of the helical polymers suggest that a concerted state transition is necessary for tube scission. However precise conformational changes occurring during GTP hydrolysis that drive membrane remodeling leading to scission are yet to be experimentally validated in a membrane fission assay.

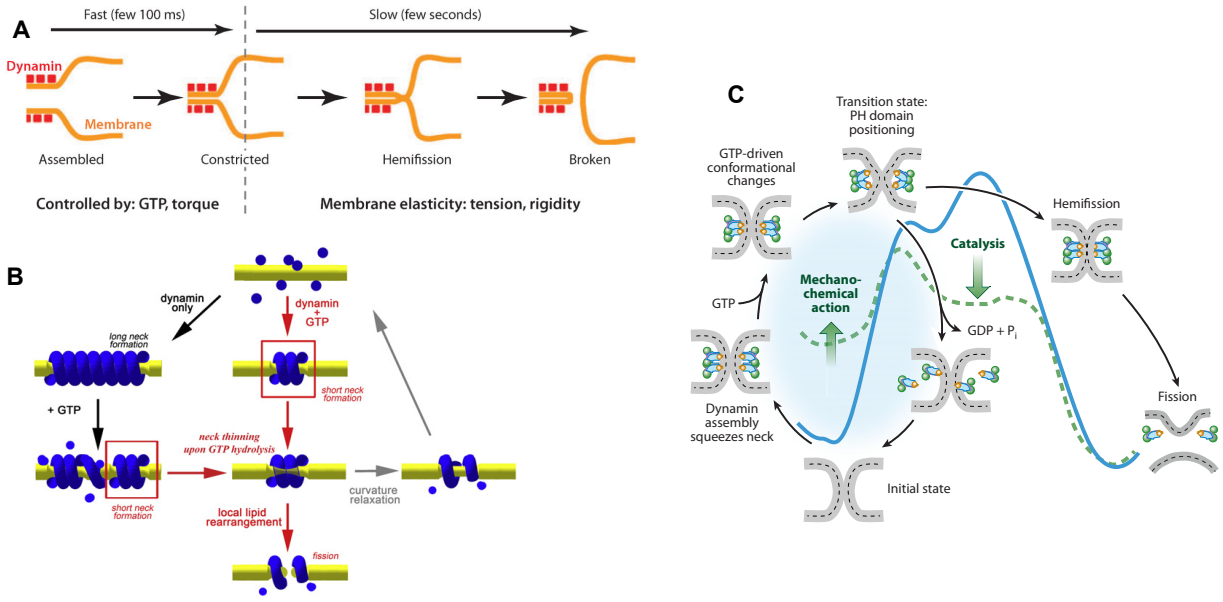

Figure 1-3. Current Models for dynamin-catalyzed membrane fission. (A) Constriction Model. (B) Squeeze and Release Model (C) Hemifission Model. Images are reproduced from Morlot and Roux 2013 (A); Bashkirov et al., 2008 (B); Schmid and Frolov 2011 (C).

1.4 Role of the PH domain

Predictions from mathematical modeling of the PH domain on the membrane suggest that membrane insertion combined with tilting of the domain during GTP hydrolysis would reduce that energy required for the formation of a hemi-fission intermediate (Shnyrova et al., 2013). The PH domain does not regulate membrane targeting of dynamin to necks of coated pits (Bethoney et al., 2009). Instead the PH domain has been hypothesized to play a more direct role in membrane fission because mutations that abolish dynamin function, such as those in centronuclear myopathies, do not affect subcellular localization of dynamin (Bethoney et al., 2009; Kenniston and Lemmon 2010). *In vitro* fluorescence quenching studies with labeled phosphoinositides, are indicative of dynamin mediated PIP_2 clustering at site of fission (Bethoney et al., 2009). This could be directly contributing to lipid phase separation that facilitates fission (Liu et al., 2006). I533, a hydrophobic residue in the variable loop1 of the PH domain has been shown to insert into the membrane (Ramachandran and Pucadyil et al., 2009). Supporting data from CryoEM reconstructions of the constricted tube also indicates a slight tilting of the PH domain from the axis perpendicular to the membrane (Mears et al., 2007; Chappie et al., 2011). Alternately, results from fluorescence spectroscopy and microscopy techniques argue against membrane-insertion by PH domain and instead point towards a more anchor-like role that functions to stabilize the polymer on the membrane (Mehrotra et al., 2014), but how it contributes to the fission reaction still remains unanswered. One possibility could be that GTP hydrolysis triggers further membrane constriction facilitated by deeper membrane insertion by the PH domain leading to the formation of a hemi-fission. Once the inner monolayers fuse the bilayers undergo rapid remodeling culminating into a non-leaky fission event. An alternate possibility can be that GTP hydrolysis triggers disassembly of the polymer, which is coupled to simultaneous reduction in the extent of membrane insertion by the PH domain. This destabilizes the hemi-fission intermediate inducing rapid membrane remodeling precipitating in fission of the underlying membrane (Shnyrova et al., 2013; Mattila et al., 2015). However there are no experimental evidences to support either of these models. The lack of facile assays that provide both spatial and temporal resolution at single event level limit our understanding of the functional relevance of the PH domain in dynamin-catalyzed membrane fission.

Dynamin-catalyzed membrane fission has been a topic of intense research for the last 25 years. Structural studies, Cryo-EM reconstructions, biochemical and biophysical assays,

fluorescence spectroscopy and microscopic approaches have contributed significantly to our current understanding of its function. However its mechanism of fission is still obscure and debated. Although multiple models have been proposed to explain the conformational changes leading to a localized membrane remodeling, currently it is still elusive how GTP hydrolysis triggers changes in scaffold assembly to mediate membrane fission. Another theory that needs more validation is the functional relevance of the PH domain in the fission reaction. In my thesis, I have attempted to address the mechanism of fission by designing a novel assay that allows the real-time monitoring of membrane constriction and fission using correlative quantitative fluorescence microscopy.

Chapter- 2

*S*upported *M*emb*r*ane *T*ubes (SMrT) Assay

2.1 Introduction

*In vitro*reconstitution is an important approach to understand mechanisms underlying complex reactions and cellular processes.Cell biology-based approaches have provided us with a wealth of knowledge regarding the identity and functional relevance of most biological components. *In vitro* reconstitution relies on simulating complex reactions involving myriads of proteins using minimal components under biochemically-regulated environment. One of the best examples where these two different approaches have helped contribute significantly is dynamin. Dynamin is a large multi-domain GTPase and a prototypical member of the dynamin superfamily. Numerous vesiculation processes occurring from the plasma membrane in mammalian cells are dependent on dynamin for fission where it has been shown to formhelical collars around the tubular necks of deeply invaginated coated pits to drive membrane fissionand release nascent vesicles.

Liposomes have been the preferred membrane substrate for most reconstitution studies, and the earliest insights into dynamin function came from *in vitro* reconstitution of dynamin in the presence of liposomes. Although the use of liposomeshasadded significantly to our current understanding of dynamin function, they have drawbacks. Ideally, one would like to visualize the protein in action in real-time with the ability to spatially and temporally resolve discreet stages of the reaction. All *in vitro* biochemical reconstitution efforts with liposomes, to date have relied on end-point and bulk read-outs. Being diffraction limited, they cannot be used for fluorescence microscopy; and the lack of reservoir limits their applicability in assays that require sampling differential curvatures on the same surface.

The use of alternate model membrane systems has helped us overcome these challenges, but have also generated controversy. Discrepancies include ambiguity with respect to our understanding of how GTP hydrolysis is coupled to fission. Dynamin-catalyzed vesicle release was visualized in real-time on membrane tubes drawn out of a lipid reservoir (Roux et al., 2006; Bashkirov et al., 2008; Pucadyil and Schmid 2008). The first reports of addition of dynamin and GTP together to preformed tubes showed rapid kinetics of fission. Addition of GTP to preassembled dynamin was shown to cause twisting and super coiling of dynamin coated tubules, suggesting a rotary movement of the helices relative to each other (Roux et al., 2006; Morlot et al., 2012).Conductance-based measurements on membrane tubes suggest that assembly of dynamin is sufficient to trigger constriction and that the role of GTP hydrolysis is to cause

disassembly of the dynamin scaffold (Bashkirov et al., 2008), but not constriction. This probably suggests that in the absence of GTP, dynamin forms long stable cylindrical scaffolds, which undergo disassembly upon GTP addition. In the constant presence of GTP only short assemblies of dynamin are formed which rapidly undergo fission. Multiple cycles of assembly-disassembly generate membrane curvature and drive fission in a stochastic lipid-dependent manner. These observations are consistent with EM data in presence different nucleotides. There are clearly multiple interpretations onhow GTPase-induced changes in the conformation of the polymer ultimately lead to membrane fission. The fundamental reason underlying these discrepancies is the inability to simultaneously monitor and correlate membrane-remodeling events with polymer dynamics. Due to the nature of the read out in the above mentioned assay systems, mechanistic insights as to how the GTP hydrolysis-induced conformational changes taking place in the polymer are propagated to the underlying membrane tube to cause fission have remained unclear.

To overcome theses challenges we have developed a facile assay system of arrayed supported membrane tubes (SMrT), where the membrane tube dimensions can be controlled to mimic the topology of necks of clathrin-coated buds, the physiological substrate for dynamin. In this chapter I have discussed in detail their characterization and robustness as templates for studying membrane remodeling and vesiculation.Our goal is to develop an assay that would avoid ensemble averaging and enable us to capture the multi-step processes of scaffold assembly, membrane constriction and membrane fission with sufficient time resolution

2.2 Materials and Methods

2.2.1 PEGylation of glass coverslips

Glass coverslips were passivated by covalent attachment of polyethyleneglycol (PEG) according to earlier reports (Turner et al., 2013). Briefly, glass coverslips were cleaned with 3 N NaOH for 5 min and rinsed with water. Clean coverslips were treated with piranha solution (conc. H_2SO_4: 30% H_2O_2 = 3:2 v/v) for 1 hr at room temperature, rinsed with water and dried on a heat block set at 90°C. Dried coverslips were silanized with neat 3-glycidyloxypropyltrimethoxysilane (Sigma) for 5 hrs under vacuum. Silanized coverslips were rinsed with acetone, air-dried and placed in a glass beaker containing molten PEG400 (Sigma) or PEG8000 (USB) maintained at 90°C for 48-60 hrs. Coverslips were rinsed extensively with

water and stored dry in a closed container. Coverslips were sequentially cleaned with 1% SDS, water, methanol and water in between experiments and could be used 4-5 times without significant loss of surface passivation.

2.2.2 Supported Membrane Tethers (SMrT Templates)

Appropriate volumes of lipid stocks (Avanti Polar Lipids) were aliquoted into glass vials,diluted to a final concentration of 1 mM in chloroform and stored at -80 °C. Lipid stockscontained a trace amount (0.5 mol%) of the fluorescent Texas Red DHPE (Invitrogen) lipid probe.Stocks were brought to room temperature before use. A small aliquot (~3 nmol total lipid)was spread on a freshly cleaned ultraPEGylated coverslip and kept under high vacuumor 5 min to remove traces of chloroform. A ~35 µl flow cell (Bioptechs) was assembledby placing a 0.1 mm silicone spacer between the ultraPEGylated coverslip and an ITOcoatedslide. The flow cell was filled with filtered and degassed HKS containing 1 % w/vBSA (Sigma) and left undisturbed for 10 min at room temperature. Hydration of the drylipid leads to the formation of large (~10 µm) vesicles inside the chamber. Supportedmembrane tethers (SMrT) are created by extrusion of the large vesicles to narrowmembrane tethers induced by flowing excess HKS buffer containing 1% BSA at high (~3mm/s particle velocity inside the chamber) flow rates. SMrT templates were judgedready for experiments when the entire membrane reservoir was extruded into tethersthat remained lightly adhered to the surface even in the absence of external buffer flow.

2.2.3 Field emission scanning electron microscopy

SMrT templates containing 5 mol% Cap biotin PE (Avanti Polar Lipids) were incubated with streptavidin (Invitrogen) and processed for scanning electron microscopy inside the flow cell. Templates were fixed with 3% w/v glutaraldehyde (Fischer) for 10 min and rinsed with PBS, treated with 1% SDS and rinsed with excess water. Samples were dehydrated by sequentially passing 10, 20, 40, 60, 80 and 100% ethanol. The flow cell was disassembled and the coverslips were kept under vacuum overnight. Samples were gold-coated using a Q150T Turbo-Pumped Sputter Coater (Quorum Technologies) and imaged on an Ultra Plus Field Emission Scanning Electron Microscope (Zeiss) using a 1.9 kV electron beam and secondary electron detector. SEM images of dynamin-assembled on SMrT templates were compared to the

scaffold thickness estimate from previous TEM images of dynamin-coated membrane tethers[27] to estimate the thickness contributed from gold coating.

2.2.4 Fluorescence Microscopy

Fluorescence imaging was carried out on an Olympus IX71 inverted microscope equipped with an 100X, 1.4 NA oil-immersion objective. Fluorescent probes were excited with a LED light source (Thor Labs) and fluorescence emission was collected through single-band filters (Semrock) with excitation/emission wavelength bandpasses of 482 ± 35 nm/536 ± 40 nm for Alexa488, 562 ± 40 nm/624 ± 40 nm for Texas Red and 628 ± 40 nm/692 ± 40 nm for DiD probes on an Evolve 512 EMCCD camera (Photometrics). Image acquisition was controlled by Metamorph software (Molecular Devices).

2.2.5 FRAP analysis

FRAP was carried out on a Zeiss LSM 780 laser scanning confocal microscope by photo bleaching a region of interest (ROI) and monitoring fluorescence recovery or loss over time. Images were acquired at an optical zoom of 4.0 and argon laser power of 2%. 38 iterations at 100% transmission were used for photo bleaching at a single plane. Image acquisition was controlled by Zen software. Files were first analyzed for bleaching during acquisition. For every tube, the fluorescence intensity profile across the bleached ROI in the first postbleach image was acquired and fitted to a gaussian function to get σ. The e^{-2} width (which accounts for 87% of the bleached region) was calculated according to $\sigma*1.699*2.355$. Background-corrected fluorescence intensity in a 5 pixel ROI placed on the tether was acquired and normalized to the first prebleach intensity. Time per frame information was extracted using the LSM toolkit in Fiji and normalized to render the first postbleach image to time t=0. Intensity *vs* time plots were fitted to a 1D diffusion equation (Ellenberg et al., 1997), which assumes recovery into a completely bleached strip, which was the case in our experiments.

2.3 Results

2.3.1 Supported membrane tubes (SMrT)

Dynamin-catalyzed membrane fission has previously been analyzed using low-tension supported bilayers with excess reservoir or GUVs (Meinecke et al., 2013; Neumann and Schmid, 2013; Pucadyil and Schmid, 2008a) but the bulk nature of the read-outs provide limited insights into the pathway for membrane fission. Fluorescence-based techniques offer the advantage of addressing dynamics of single fission events through direct monitoring of intermediates in the helical scaffold and the underlying membrane tube during the scission reaction. While the widely used assay system of membrane tethers pulled from GUVs have informed us of the membrane-active nature of helical scaffolds using force spectroscopy- and conductance-based measurements, (Bashkirov et al., 2008; Morlot et al., 2012; Roux et al., 2010; Shnyrova et al., 2013), application of fluorescence microscopy-based techniques to such systems is significantly hindered by the out-of-focus movements of tethers in solution, not to mention the experimental challenge in recording statistically significant numbers of fission events since such assay systems are only capable of recording a single fission event at a time.

To circumvent these issues, we developed a facile *in vitro* assay system comprised of an array of membrane tubes resting on a passive surface and housed in a flow-cell to allow accurate monitoring of reaction kinetics using fluorescence microscopy, which we recently described to visualize dynamics of epsin-induced clathrin assembly (Holkar et al., 2015). Briefly, ~1 nmol of a suitable lipid mixture is dried on a PEGylated coverslip and mounted in a flow-cell (see Figure 1A for schematic). Gentle hydration in physiological buffer leads to the formation of large vesicles (Figure 2-1A, white arrows) that are subsequently extruded by controlled buffer flow at high rates (particle velocities of ~30 mm/s) to generate narrow membrane tubes in solution (Figure 2-1A, yellow arrows). With time, membrane tubes settle down and get pinned at discrete sites possibly due to defects on the glass surface that resisted PEGylation. The membrane tubes are therefore not under externally applied tension. We refer to this assay system as supported membrane tubes (SMrT). Scanning electron micrographs of streptavidin-bound, fixed and gold-coated SMrT templates composed of 1,2-dioleoyl-*sn*-glycero-3-phosphatidylcholine (DOPC): 1,2-dioleoyl-*sn*-glycero-3-phosphatidylserine (DOPS): 1,2-dioleoyl-*sn*-glycero-3-phosphoethanolamine-N-(cap biotinyl) (80:15:5 mol%) showed an array of intact membrane tubes that spanned the entire coverslip surface (Figure 2-1B, white arrows). Size estimation of membrane tubes corrected for the streptavidin- and gold-layer thicknesses revealed a mean tube radius of 17.4 ± 4.7 nm (mean ± SD, N = 84, Figure 2-1C), very similar to the dimensions of

necks of deeply invaginated clathrin-coated pits (Iversen et al., 2003). As a reporter for tube fluorescence, we incorporated trace amounts (0.5 mol%) of the fluorescent lipid probe *p*-Texas Red DHPE that equally partitions to regions of low and high membrane curvature (Hsieh et al., 2012) and displays fluorescence properties that are insensitive to protein binding (Jung et al., 2009). FRAP analysis of the lipid probe gives a mobile fraction (R) of ~100% and an apparent diffusion coefficient (D) of 2.4 ± 1.6 $\mu m^2.s^{-1}$ (mean ± SD, N = 10, Figure 2-1D), in agreement with previous reports of lateral mobility of lipids in fluid membrane tethers (Domanov et al., 2011). SMrT templates respond to a hypoosmotic shock by first budding out (Figure 2-1E, yellow arrows) the membrane reservoir from the tube and later undergoing scission at the bud-tube junction (Figure 2-1E, red arrows). The intrinsic membrane tension causes the cut ends of the tube to retract. However, retraction is limited to short extents due to surface pinning sites, which fortuitously allows monitoring of multiple cuts on a single membrane tube. Together, these observations indicate that SMrT templates are fluid-filled membrane tubes and allow the possibility of a high throughput analysis of membrane fission events.

2.3 Discussions

Generation of vesicles from a membrane compartment is fundamental to diverse cellular processes such as nutrient uptake, synaptic transmission and organelle biogenesis. Every vesicle formed in the cell is an outcome of a process called membrane fission wherein a localized curvature stress is applied to a tubular membrane intermediate to force it to undergo scission. Biochemical screens for effectors of membrane fission and a mechanistic analysis of this process requires a tubular membrane template as a substrate. Current techniques to create such substrates necessitate the use of micromanipulators or sophisticated optical traps and require a high level of technical expertise. To circumvent these issues, we present a facile method using readily available commercial equipment to generate an array of membrane tubes supported on a passsivated glass coverslip and housed inside a flow cell. SMrT templates are an array of narrow (~40-50 nm wide) membrane tubes that are pinned to a highly passivated glass coverslip and amenable to microscopic analysis. The method of preparing SMrT templates involves surface passivation of a glass coverslip by covalent attachment of polyethylene glycol (PEG). The covalent attachment allows repeated use of coverslips in multiple rounds of template creation, which makes the assay highly economical. The assay requires order-of-magnitude lower amounts

of lipids (1-2 nmol) per round of template creation, which again makes the assay economical. The use of a commercially available flow cell makes the protocol amenable to be setup in any laboratory. The set-up is housed inside a flow cell, which makes it convenient to flow-in proteins and allows accurate estimation of reaction kinetics. The major methodological advantage of this setup, as compared to the previously established system of tethers pulled out of giant vesicles, is a suppression of the tubule undulations out of the optical focus due to the non-specific attachment of the tubule on the coverslip. This enables following in time and quantitative characterization of the constriction and fission processes. Since the tubule is pinned to the coverslip at multiple points along its entire length, it would ideally serve to decouple different fission events so that each of them can now be observed independently of the others. In conventional tether pulling experiments, these events could only be measured individually and in some cases sporadically; hence limiting their utility, SMrT templates are an array of membrane tubes so the experimental challenge in recording statistically significant numbers of fission events is dramatically reduced. After hydration with buffer and formation of SMrT templates, the area where the lipid is spotted presents itself as a supported lipid bilayer, which in turn can act as an in situ calibration standard (discussed in detail in chapter 4). This allows precise estimation of dimensions of the diffraction-limited membrane tubes using fluorescence microscopy. SMrT templates are novel and can be used as a method to visualize and analyze the process by which proteins sever membrane. The template can also be used to assay for membrane curvature sensitivity of protein binding to membrane surfaces, although unlike conventional tubes they are not amenable to EM based studies. We anticipate SMrT templates to provide an opportunity in future studies involving FRET-based assays to directly link dynamin conformational changes and assembly states with the fission reaction.

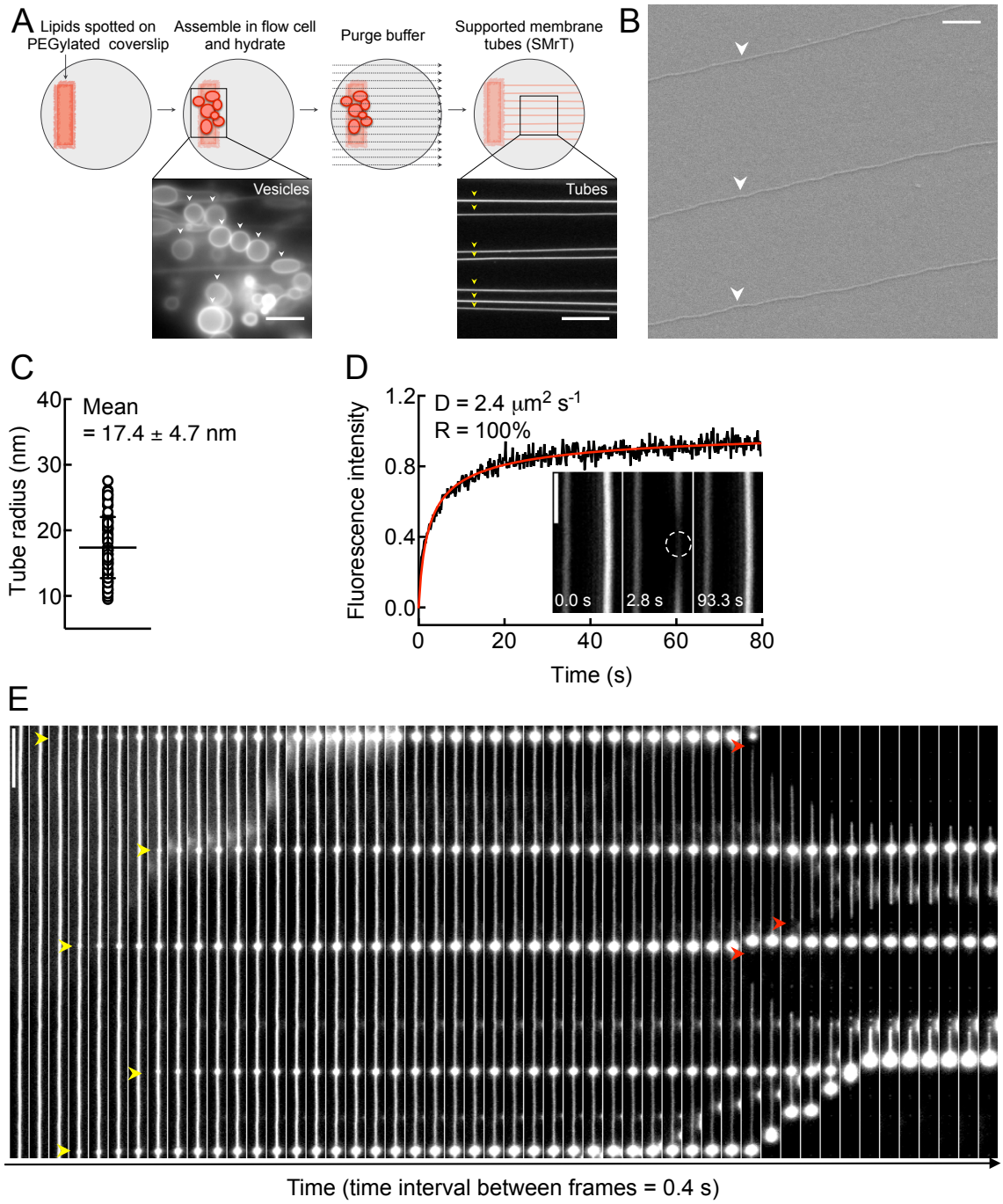

Figure 2-1. Supported membrane tubes (SMrT)(A) Schematic of generation of SMrT templates. A lipid mix spotted on a passivated glass coverslip when hydrated inside the flow cell forms large vesicles (white arrows), which are extruded by flow of buffer to generate membrane tubes (yellow arrows). Scale bars = 10 μm. (B) Scanning electron micrograph (SEM) of SMrT templates (white arrows). Scale bar = 500 nm. (C) Radius of the initial membrane tube from analysis of SEM images. Data represent the mean ± SD (N = 84 tubes). (D) Fluorescence recovery data (black trace) after photobleaching a membrane tube fitted to a one-dimensional recovery equation (red trace). Inset shows micrographs acquired during the FRAP experiment.

Dotted circle marks the bleached region. Scale bar = 2 μm. Data for diffusion coefficient (D) is represented as the mean ± SD (N = 10 tubes). R is the mobile fraction. (E) Panels from a time-lapse movie showing SMrT templates responding to a hypoosmotic shock by first budding out (yellow arrows) the membrane reservoir from the tube and later undergoing scission at the bud-tube junction (red arrows). Scale bar = 10 μm.

Chapter- 3

Mechanistic insights into dynamin-catalyzed membrane fission

3.1 Introduction

Dynamin is a multidomain GTPase that contains an N-terminal G-domain which binds and hydrolyzes GTP, a middle domain, a pleckstrin-homology (PH) domain that binds the plasma membrane-localized phosphatidylinositol-4,5-bisphosphate (PIP_2) lipid and a stalk which makes intramolecular contacts with the middle domain to maintain dynamin as tetramers in solution and intermolecular contacts with adjacent stalks to promote dynamin self-assembly as helical scaffolds on membrane tubes (Faelber et al., 2011; Schmid and Frolov 2011; Ferguson and De Camilli 2012; Chappie and Dyda 2013). A nonleaky membrane tube-severing reaction involving a neck-like intermediate is theorized to involve a tube-constriction step in order that the enclosing lipid bilayer is brought to close proximity, equivalent in distance to the thickness of the lipid bilayer, at which point spontaneous formation of a hemifission intermediate leads to tube scission (Kozlovsky and Kozlov 2003; Frolov et al., 2015). Dynamin can bind negatively charged lipids and spontaneously self-assemble into helical scaffolds which constrict the underlying tube, although the estimated dimensions of the membrane tube under the scaffold range widely from ~7-11 nm in radius (Zhang and Hinshaw 2001; Roux et al., 2010; Bashkirov et al., 2008; Shnyrova et al., 2013). Scaffold assembly reorients catalytic residues in apposing G-domains of dynamin and leads to a ~100-fold stimulation in basal rates of GTP hydrolysis (Chappie et al., 2010). GTP hydrolysis is necessary but its causal relationship to tube severing remains debated (Roux 2014). Conductance measurements on membrane tethers pulled from giant unilamellar vesicles (GUVs) suggest that scaffold assembly *per se* is sufficient for the lipid bilayer to be brought to distances which favor the spontaneous formation of the hemifission intermediate (Bashkirov et al., 2008; Shnyrova et al., 2013). GTP hydrolysis has therefore been proposed to render scaffolds flexible in order to facilitate local sculpting of membrane lipids into non-bilayer configurations to assist tube scission(Shnyrova et al., 2013), or generate a torque to facilitate scission at the junction between the scaffold and the bare membrane (Morlot et al., 2012). Docking of crystal structures of the isolated G-domains locked in the transition state to the cryoEM reconstructions of helical scaffolds as well as recent cryoEM reconstruction of a slow-hydrolyzing dynamin mutant (Sundborger et al., 2014) suggests a concerted state-transition in helical scaffolds facilitates tube scission. The causal relationship between GTP hydrolysis and generation of the hemifission intermediate prior to tube scission thus remains unclear.

3.2 Methods and Material

3.2.1 Expression, purification and fluorescent labeling of proteins

Human dynamin1 was cloned into a pET15B vector with N-terminal 6xHis- and C-terminal StepII tags and confirmed by sequencing. Proteins were expressed in BL21(DE3) in autoinduction medium (Formedium, UK) at 18 °C for 30 hours. Frozen bacterial pellets were resuspended in 20 mM HEPES, 500 mM NaCl and 10 mM Imidazole pH 7.4, supplemented with a protease inhibitor cocktail (Roche) and lysed by sonication. Proteins were first purified on a HiTrap Chelating HP column (GE Lifesciences) against a linear imidazole gradient followed by purification on a StrepTrap HP column (GE Lifesciences) according to standard procedures. Purified proteins were dialyzed against HBS (20 mM HEPES, 150 mM NaCl) supplemented with 1 mM DTT, 1 mM EDTA and 50% v/v glycerol pH 7.4 overnight, flash frozen in liquid N_2 and stored at -80 °C. Purified dynamin1 was labeled with a 5-fold molar excess of thiol-reactive Alexa488 C5 maleimide dye (Invitrogen) for 1 hr at room temperature and quenched with DTT. Free dye was removed by extensive dialysis against HBS containing 1 mM DTT. All labeled proteins were resolved with 10% SDS-PAGE and judged to be free of unreacted dye, which typically migrates with the dye front.

3.2.2 PEGylation of glass coverslips

Glass coverslips were passivated by covalent attachment of polyethyleneglycol (PEG) according to earlier reports (Turner et al., 2013). Briefly, glass coverslips were cleaned with 3 N NaOH for 5 min and rinsed with water. Clean coverslips were treated with piranha solution (conc. H_2SO_4: 30% H_2O_2 = 3:2 v/v) for 1 hr at room temperature, rinsed with water and dried on a heat block set at 90°C. Dried coverslips were silanized with neat 3-glycidyloxypropyltrimethoxysilane (Sigma) for 5 hrs under vacuum. Silanized coverslips were rinsed with acetone, air-dried and placed in a glass beaker containing molten PEG400 (Sigma) or PEG8000 (USB) maintained at 90°C for 48-60 hrs. Coverslips were rinsed extensively with water and stored dry in a closed container. Coverslips were sequentially cleaned with 1% SDS, water, methanol and water in between experiments and could be used 4-5 times without significant loss of surface passivation.

3.2.3 Supported membrane tubes (SMrT)

Lipid stocks (Avanti Polar Lipids) were aliquoted into glass vials in required proportions, diluted to a final concentration of 1 mM total lipid in chloroform and stored at -80 °C. *p*-Texas Red-DHPE isomer was separated from a mixed isomer stock of Texas Red DHPE (Invitrogen) using thin layer chromatography on silica gel plates (Sigma) against 100% methanol as described earlier (Jung et al., 2009). Lipid stocks were brought to room temperature before use. A small aliquot (~1 nmol total lipid) was spread on a freshly cleaned PEGylated coverslip and kept under high vacuum for 5 min to remove traces of chloroform. A ~35 µl flow cell (Bioptechs) was assembled by placing a 0.1 mm silicone spacer between the PEGylated coverslip and an ITO-coated glass slide. The flow cell was filled with filtered and degassed PBS and left undisturbed for 10 min at room temperature. For experiments involving fluorescently labeled dynamin, PEG8000-coated glass coverslips were used and the hydration buffer contained 1% (w/v) BSA (Sigma). Supported membrane tubes (SMrT) were created by extrusion of the large vesicles, formed during hydration, to narrow membrane tubes by flowing excess PBS at high (~30 mm/s particle velocity inside the chamber) flow rates. SMrT templates were judged ready for experiments when the entire membrane reservoir was extruded into tubes that remained pinned at discrete sites to the surface. Freestanding tethers were prepared as described earlier (Neumann et al., 2013).

3.2.4 Scaffold assembly and tube scission assays

SMrT templates were first equilibrated in filtered and degassed HKS (20 mM HEPES, 150 mM KCl, pH 7.4) containing an oxygen scavenger cocktail of 0.2 mg/ml glucose oxidase (Sigma, G-2133), 0.035 mg/ml catalase (Sigma, C-40), 4.5 mg/ml glucose (Sigma) and 1 mM DTT. Dynamin, previously dialyzed overnight against HKS and spun at 100,000g for 20 min to remove aggregates, was reconstituted in HKS to a final concentration of 0.5 µM and flowed into the chamber at a low flow rate of ~1 mm/s in order to minimize focus drifts. Bulk fission kinetics was analyzed by first estimating the time-of-cut for all events occurring on a single membrane tube. Data were ordered in an ascending fashion and subtracted by the time interval for the first, which normalized for difference in the time of arrival of dynamin across different experiments into the field of view. The first 100 cuts were plotted against time and fitted to a linear equation to estimate the rate of fission. Fission for single events was estimated as described in the text. To

avoid fluorescence self-quenching, fluorescently labeled dynamin was mixed with unlabeled dynamin in a 1:1 molar ration during scaffold assembly. GTP (Jena Bioscience) and $MgCl_2$ were added to the assay buffer at final concentrations of 1 mM. All reactions were carried out at 25 °C and imaged as described below.

3.2.5 Fluorescence microscopy

Fluorescence imaging was carried out on an Olympus IX71 inverted microscope equipped with a 100X, 1.4 NA oil-immersion objective. Fluorescent probes were excited with a stable LED light source (Thor Labs) and fluorescence emission was collected through filters (Semrock) with excitation/emission wavelength bandpasses of 482 ± 35 nm/536 ± 40 nm for Alexa488 and 562 ± 40 nm/624 ± 40 nm for Texas Red probes simultaneously on two Evolve 512 EMCCD cameras (Photometrics). Image acquisition was controlled by Metamorph software (Molecular Devices).

3.2.6 Image analysis and intensity calibration

Image analysis of fluorescence micrographs and time-lapse movies were carried out using Fiji (version 1.47) (Schindelinet al., 2012) and a nonlinear regression analysis was carried out using Graphpad Prism (version 5.0a). Scaffolds assembled on membrane tubes were imaged for tube fluorescence. Pixel intensities along the tube length were bimodally distributed and were fitted to a sum of 2 gaussian function. The population with lower mean fluorescence intensity, which represents tube fluorescence under the scaffold, was equated to the earlier reported dynamin-coated tube radius (Roux et al., 2010) to arrive at a calibration constant (Figure3-1-1). The calibration constant was estimated before every experiment that involved equating tube fluorescence to radius to account for intensity fluctuations during image acquisition.

3.3. Results

3.3.1 Dynamin purification and characterization

We engineered the human dynamin1 cDNA with N-terminal $His_6$and C-terminal StrepII tags to facilitate bacterial expression and purification using a 2-step tandem affinity purification protocol (Fig. 3-1A, B). Since bacteria lacks post-translational machinery, and many such

modifications have been proposed to regulate dynamin function, it was pertinent to run the protein through conventional assays that check for fundamental biochemical properties attributed to dynamin. When assaying for GTPase activity, which is a reporter for self-assembly, the protein showed 40-fold stimulation in presence of 100% PS liposomes (Song et al., 1999). Many residues in the stalk domain of dynamin when mutated have been demonstrated to completely impair the ability of the molecule to assemble into higher order oligomers (Song et al., 2004; Ramachandran et al., 2007). Thus, mutants such as R399A and I690K, which are defective in self-assembly, failed to show stimulation in their basal rates of GTPase activity in presence of negatively charged liposomes (Fig. 3-1C). Membrane association of dynamin1 on PIP_2 containing membranes was confirmed under equilibrium conditions by incubating a wide range of concentrations of fluorescently labeled WT protein with SUPER templates composed of DOPC:DOPS:$DOPIP_2$ (85:15:5 mol %) (Fig. 3-1D). We find that full-length dynamin1 displays high affinity for PIP_2 (Fig. 3-1E, K_D= 207.5 ± 19.2 nM), similar to what has been reported earlier using surface plasmon resonance experiments (Kenniston et al., 2010). SUPER templates are supported bilayers with excess membrane reservoir and have been used to demonstrate membrane-remodeling properties of dynamin (Fig. 3-1F, red arrowheads). Upon incubation, dynamin forms long scaffolds that pull membrane tubes that are several microns in length (Fig. 3-1F, blue arrowheads). However, constant presence of GTP inhibits formation of long scaffolds of dynaminand promotes membrane vesiculation (Fig. 3-1F, yellow arrowheads).

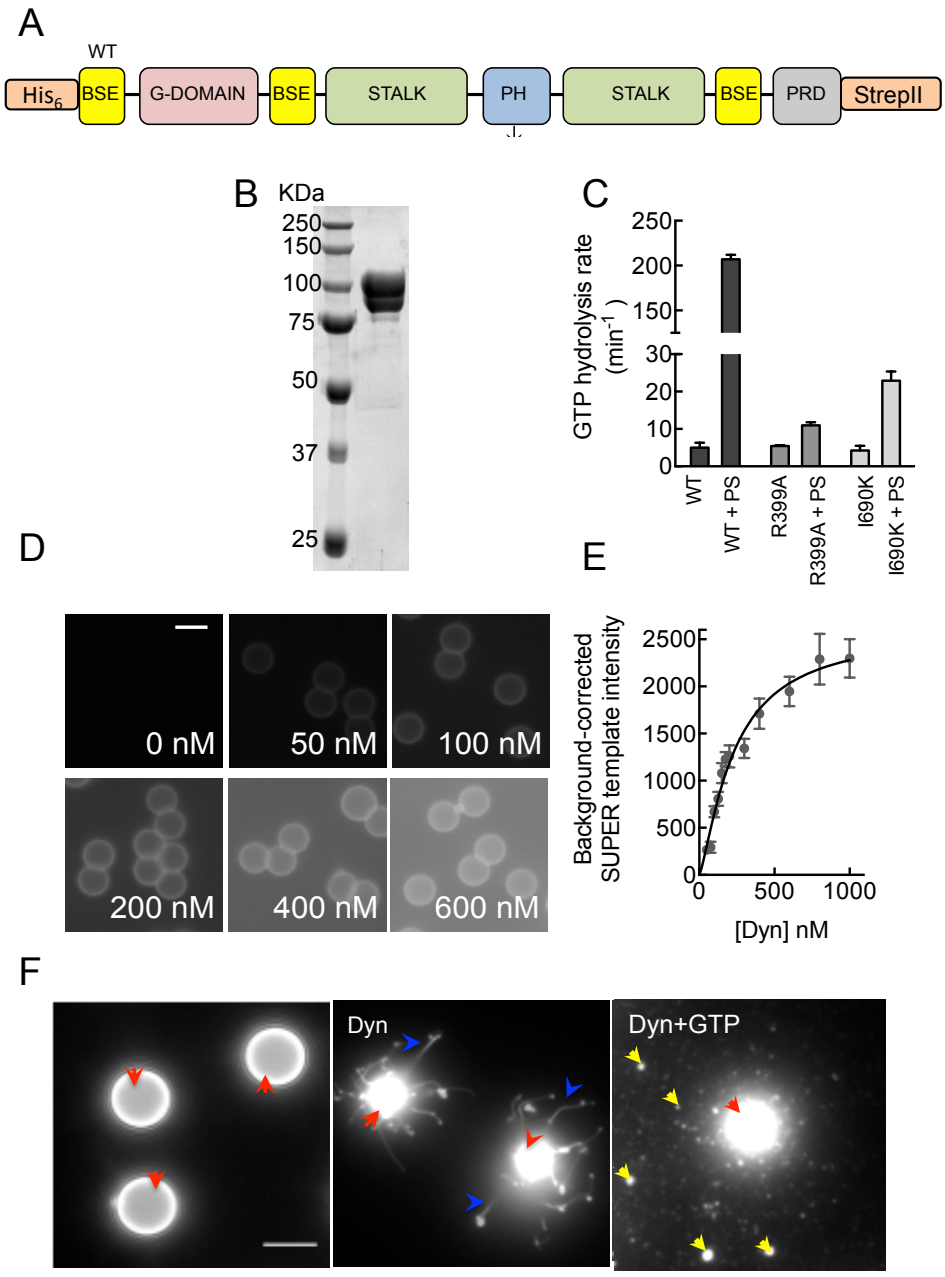

Figure 3-1. Membrane binding and tubulation by dynamin(A) Structure-based domain organization of dynamin1. (B) SDS-PAGE-resolved and Coomassie Blue-stained dynamin after 2-step tandem affinity purification protocol used in the study. (C) Summary of basal and assembly stimulated GTPase activity of WT, R399A and I690K in absence and presence of 100% PS liposomes (Data represents mean±SD from N=3 experiments) (D) Fluorescence micrographs of SUPER templates incubated with increasing concentrations of Alexa Fluor 488 maleimide-labeled dynamin. Scale bar 10 µm. (E)Background-corrected fluorescence associated with SUPER templates of Alexa Fluor 488 maleimide-labeled dynamin fitted to a one-site binding equation. Error bars indicate mean S.D. (F)Panel showing SUPER templates (red arrowheads),tubules (blue arrowheads) generated upon incubation with dynamin and vesicles (yellow arrowheads) released in presence of dynamin and GTP. Scale bar 5 µm.

3.3.2 Dynamin Scaffold Assembly

SMrT templates containing 1,2-dioleoyl-*sn*-glycero-3-phospho-(1'-myo-inositol-4',5'-bisphosphate) (PIP_2) at physiologically-relevant (1 mol%) concentrations were prepared to analyze the determinants and dynamics of dynamin scaffold assembly. Hydration of dried lipids has earlier been suggested to introduce non-uniformity in lipid distribution in the resulting vesicles (Larsen et al., 2011). As a control, we monitored the fluorescence distribution of the PIP_2-specific, PLC δ PH domain on SMrT templates. Fluorescence of Alexa488-labeled PLC δ PH domain was found to be uniform and strongly co-localized with tube fluorescence (Pearson's r = 0.92, $P< 0.0001$, N=10, Fig. 3-2A) indicating a uniform starting distribution of PIP_2 in the membrane. Addition of 0.5 μM Alexa488-labeled dynamin (50% of which contained unlabeled dynamin to prevent fluorescence self-quenching) to SMrT templates and imaged after 10 min revealed scaffolds discretely organized along the length of the tube (Fig. 3-2B, white arrows), each of which constricted the underlying tube and reduced tube fluorescence (Fig. 3-2C, yellow arrows). Scaffold distribution strongly coincided with regions of low tube fluorescence (Fig. 3-2C, Pearson's r = -0.8705, $P< 0.0001$). Since fluorescence of diffraction-limited, membrane-bound objects is proportional to the net membrane surface area (Kunding et al., 2008), we equated the tube fluorescence under scaffolds after their assembly to the previously reported dimensions of constricted dynamin-coated tubes (Roux et al., 2010) and discussed recently (Schlomovitz et al., 2011) to arrive at a calibration constant (Fig. 3-1-1). Based on such calibration, the initial tube fluorescence was back calculated to be 16.4 ± 3.4 nm (mean ± SD, N = 180, Fig. 3-2D), very similar to the value of 17.4 ± 4.7 nm (mean ± SD, N = 84, Fig. 2-1C) estimated from SEM analysis ($P = 0.1578$, Mann-Whitney's test), thus validating a fluorescence intensity-based calculation of tube dimensions (see below).

Scaffold assembly was highly dependent on the starting tube dimensions. For example, while discrete scaffolds and the associated membrane constrictions were apparent on a tube of 12.3 nm radius (Fig. 3-2E), dynamin appeared uniformly bound without any discernable membrane constrictions on a tube of 22 nm radius (Fig. 3-2F). Indeed, scaffold assembly-induced membrane constrictions were only apparent on membrane tubes thinner than a critical ~16 nm radius limit (Fig. 3-2F), consistent with previous estimates of the membrane curvature threshold for dynamin polymerization arrived at from assays using conventional tethers pulled from GUVs (Roux et al., 2010). Thus, membrane curvature is a critical determinant for the

spontaneous switching from a peripherally-bound state to a self-organized, membrane-active helical scaffold. Together, these results set the basis for using SMrT templates as a facile alternative assay system to probe dynamics of scaffold assembly.

Flowing in 0.5 μM dynamin to SMrT templates led to the assembly of multiple scaffolds (Fig. 3-2G, yellow arrows) along the length of the tube. Time-lapse imaging of this process indicated a nucleation and lateral expansion pathway (Movie 1). Qualitatively similar results were obtained with freestanding tethers (Movie 2), but without the inherent out-of-focus movement, which allowed accurate analysis of fluorescence changes at sites of scaffold assembly. Thus, scaffold assembly led to a monotonous decay in tube fluorescence with a slow time constant (τ) of 29.2 ± 18.6 s (mean ± SD, N = 80) that reached a plateau of 43.6 ± 7.4% (mean ± SD, N = 80) of initial fluorescence. The plateau tube fluorescence reached upon scaffold assembly equates to a tube radius of 11.9 ± 1.8 nm (mean ± SD, N = 80). Assuming a 5 nm thick lipid bilayer, the enclosed lumen of the tube at this point should be ~7 nm in radius, which is much wider than the critical distance necessary to form the hemi-fission intermediate (Kozlovsky and Kozlov 2003; Frolov et al., 2015). These estimates are in contrast to the ~2 nm lumenal radius reported from previous conductance-based measurements (Bashkirov et al., 2008; Shnyrova et al., 2013). Thus, while scaffolds are membrane active, their assembly imposes a moderate degree of membrane constriction and with kinetics slower than the typical time scales of dynamin-catalyzed membrane fission events seen *in vivo* (Taylor et al., 2011; Cocucci et al., 2014).

Equating tube fluorescence to tube radius

Step 1: Image acquisition.
Acquire a fluorescence micrograph of SMrT templates with preassembled scaffolds in the tube fluorescence channel

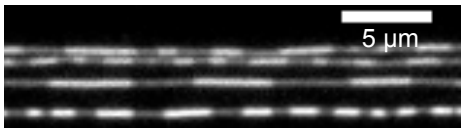

Step 2: Histogram analysis.
Plot histogram (gray) of single pixel tube fluorescence along the length of the tube and fit to a sum of 2 gaussian function (red).
The first peak corresponds to the mean tube fluorescence under the scaffold.

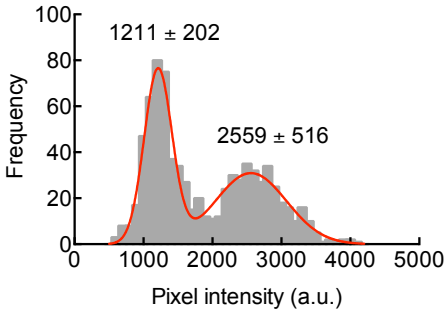

Step 3: Calculate calibration constant.
Since the net tube fluorescence is proportional to the surface area of the tube [Kunding et al. (2008) Biophys. J. 95:1176–1188];
$I = K*R^2$ where, I = tube fluorescence under scaffold; R = tube radius, 11.2 nm [from Roux et al. (2010) Proc. Natl. Acad. Sci. U.S.A. 107:4141–4146]; K = calibration constant

Figure 3-1-1. Calculation of the calibration constant in order to convert tube fluorescence into tube radii.

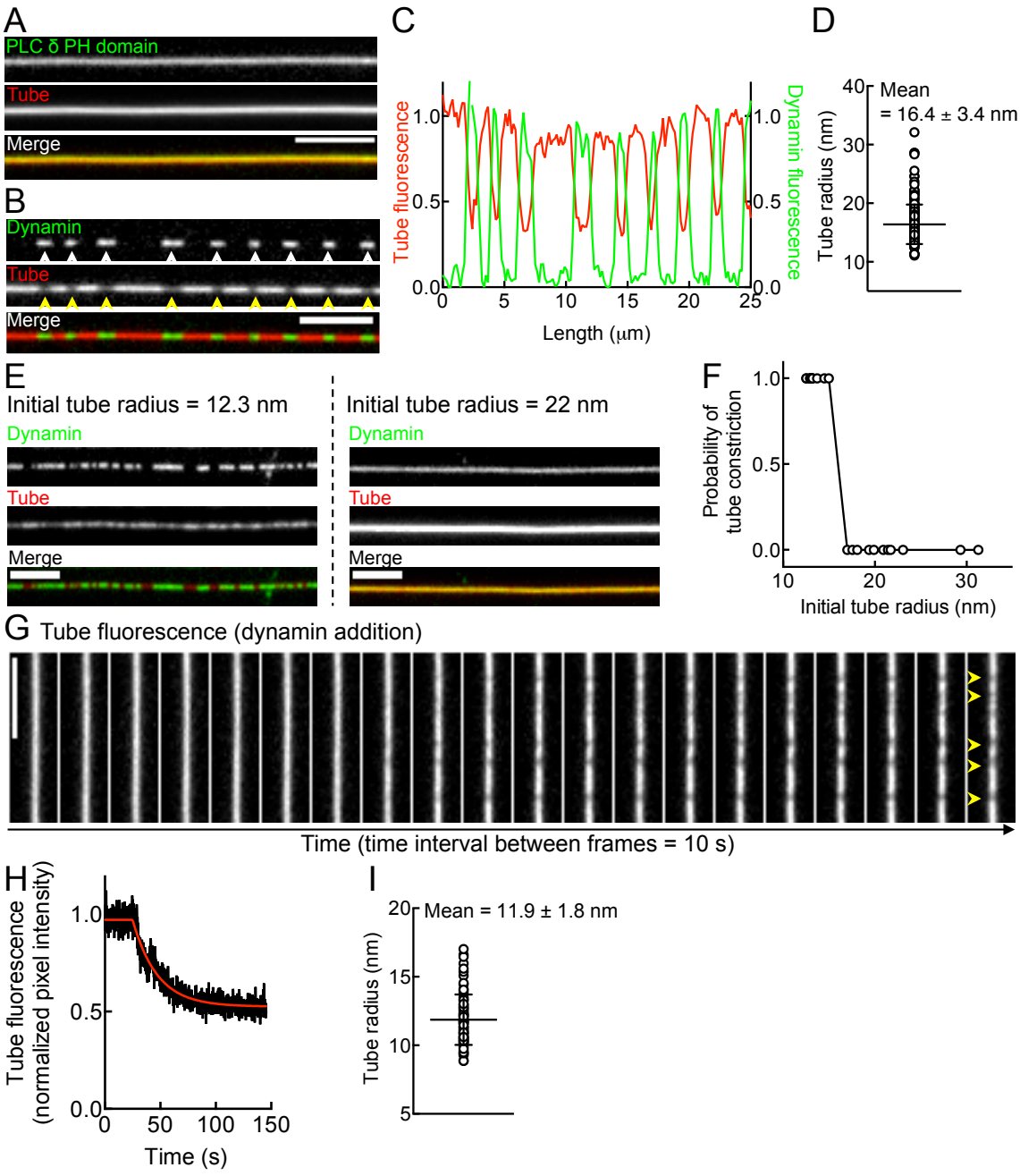

Figure 3-2. Dynamin scaffold assembly (A) Fluorescence micrographs of Alexa488-labeled PLC δ PH domain (green) on a *p*-Texas Red DHPE-labeled tube (red). Scale bar = 5 μm. (B) Fluorescence micrographs of Alexa488-labeled dynamin (white arrows, green) on a *p*-Texas Red DHPE-labeled tube (red) showing sites of tube constriction (yellow arrows). Scale bar = 5 μm. (C) Normalized dynamin and tube fluorescence line profiles of micrographs shown in (B). (D) Radius of the initial membrane tube from calibrated analysis of tube fluorescence (Fig. 3-1-1). Bars represent the mean ± SD (N = 180 tubes). (E) Fluorescence micrographs of dynamin (green) on a tube (red) of 12.3 nm and 22 nm starting radii. Scale bar = 5 μm. (F) Probability of occurrence of scaffold-induced tube constriction as a function of starting tube radius. (G) Panels from a time-lapse movie showing multiple scaffold assembly events (yellow arrows) in response

to dynamin addition (Movie 1). Scale bar = 5 μm. (H) Single pixel fluorescence trace (black) showing kinetics of scaffold assembly-induced tube constriction fitted to an exponential decay function (red). (I) Radius of the membrane tube underlying scaffolds from calibrated analysis of tube fluorescence (Fig. 3-1-1). Bars represent the mean ± SD (N = 80 events).

3.3.3 GTP hydrolysis-induced tube constriction precedes tube scission

Next, we added GTP to preassembled scaffolds on SMrT templates (Fig. 3-3A, yellow arrows). Previous reports with membrane tubes grown from a lipid reservoir and stabilized solely by interactions between dynamin subunits showed scaffold disassembly and tube retraction in response to GTP addition (Roux et al., 2006; Pucadyil and Schmid 2008). In contrast, surface pinning sites render SMrT templates stable to such collateral effects and scaffolds respond to GTP addition in a markedly different manner. Flowing in excess 1 mM GTP caused some of the scaffolds to buckle and then straighten out (Fig. 3-3A, white arrows, Movie 3), suggesting a conformational change. Later, membrane tubes got severed at a site apparently contained within the scaffold (Fig. 3-3A, red arrows, Movie 3). Thus, SMrT templates allow stage-specific monitoring of tube and scaffold dynamics without scaffold disassembly-induced tube retraction seen in previous assays (Roux et al., 2006; Pucadyil and Schmid 2008; Bashkirov et al., 2008).

Simultaneous monitoring of scaffold and tube fluorescence at 100 ms temporal resolution revealed that GTP arrival caused a further decay in tube fluorescence (over that already caused by scaffold assembly) (Fig. 3-3B, *Tube kymograph*). This was followed by scission and tube retraction, marked by the abrupt loss of tube fluorescence (Fig. 3-3B, *Tube kymograph* and Fig. 3-3C). Remarkably, the scaffold (Fig. 3-3B, *Scaffold kymograph*) essentially remained intact while the underlying membrane tube was further constricted in response to GTP hydrolysis. Thus, GTP hydrolysis induces a conformational change in a largely intact scaffold, converting it to a state that displays higher membrane constricting activity. Scission resulted in part of the scaffold being left behind and the other being lost from the field due to tube retraction (Fig. 3-3B, *Scaffold kymograph*). Scaffold splitting in this manner was a common occurrence with wide scaffolds showing multiple splitting events (Fig. 3-3-1) and could represent a passive outcome of separation of the severed ends of the underlying tube. These results indicate that the site where tubes get severed is located within the scaffold and not at its edge, as suggested previously (Morlot et al., 2012). Scaling pixel intensities in Fig.3-3B (*Tube kymograph*) to tube radius (Fig. 3-3D) revealed that GTP hydrolysis induces further constriction of the underlying membrane

tube to approach dimensions of ~7 nm radius prior to scission. Tube constriction preceding severing depends on multiple rounds of GTP hydrolysis since addition of the non-hydrolyzable GTP analogue, GMPPCP, GDP or a transition-state mimic GDP.AlF_4^- to preassembled scaffolds caused no further constriction or scission of the tube (Fig. 3-3-2).

The fission time, defined as the time interval between the onset of tube constriction and scission (Fig. 3-3C); a measure of the catalytic efficiency of the fission apparatus, displayed a high degree of variability (Fig. 3-3C), which could explain the diversity in intermediates seen in the earlier reported electron micrographs of preassembled scaffolds exposed to GTP as they may represent intermediates trapped along the same pathway (Sweitzer and Hinshaw 1998; Danino et al., 2004). Despite this variability, the fission times were strongly correlated to the time constants of tube constriction (Fig. 3-3E, Spearman's r = 0.87, N = 84 scaffolds, $P< 0.0001$) implying that tubes that were constricted faster also got severed faster. GTP hydrolysis could therefore be mechanistically involved in actively remodeling the underlying tube in order for it to reach a critical dimension before scission. If this were the case then despite the observed variability in time constants of tube constriction, tube dimensions reached at the time of scission should be narrowly distributed about a critical prefission tube radius. Since the tube fluorescence decay could be fitted well to an exponential function, we extrapolated the starting tube fluorescence under the helical scaffolds ($F_{assembly}$) to that reached at the time of scission ($F_{prefission}$) from the estimated time constant of GTP hydrolysis-induced tube constriction (τ) and the fission time using the equation $F_{prefission} = F_{assembly}\, e^{-(\text{fission time}/\tau)}$. Conversion of the estimated $F_{prefission}$ to tube dimensions gave us a mean prefission tube radius of 7.3 ± 2.0 nm (mean ± SD, N = 76, Fig. 3-3F). Again, assuming a 5 nm thick lipid bilayer, the enclosed lumen of the prefission intermediate should be 2.3 nm in radius, which is in excellent agreement with the theoretically proposed requirements for the formation of the hemifission intermediate (Kozlovsky and Kozlov 2003; Frolov et al., 2015).

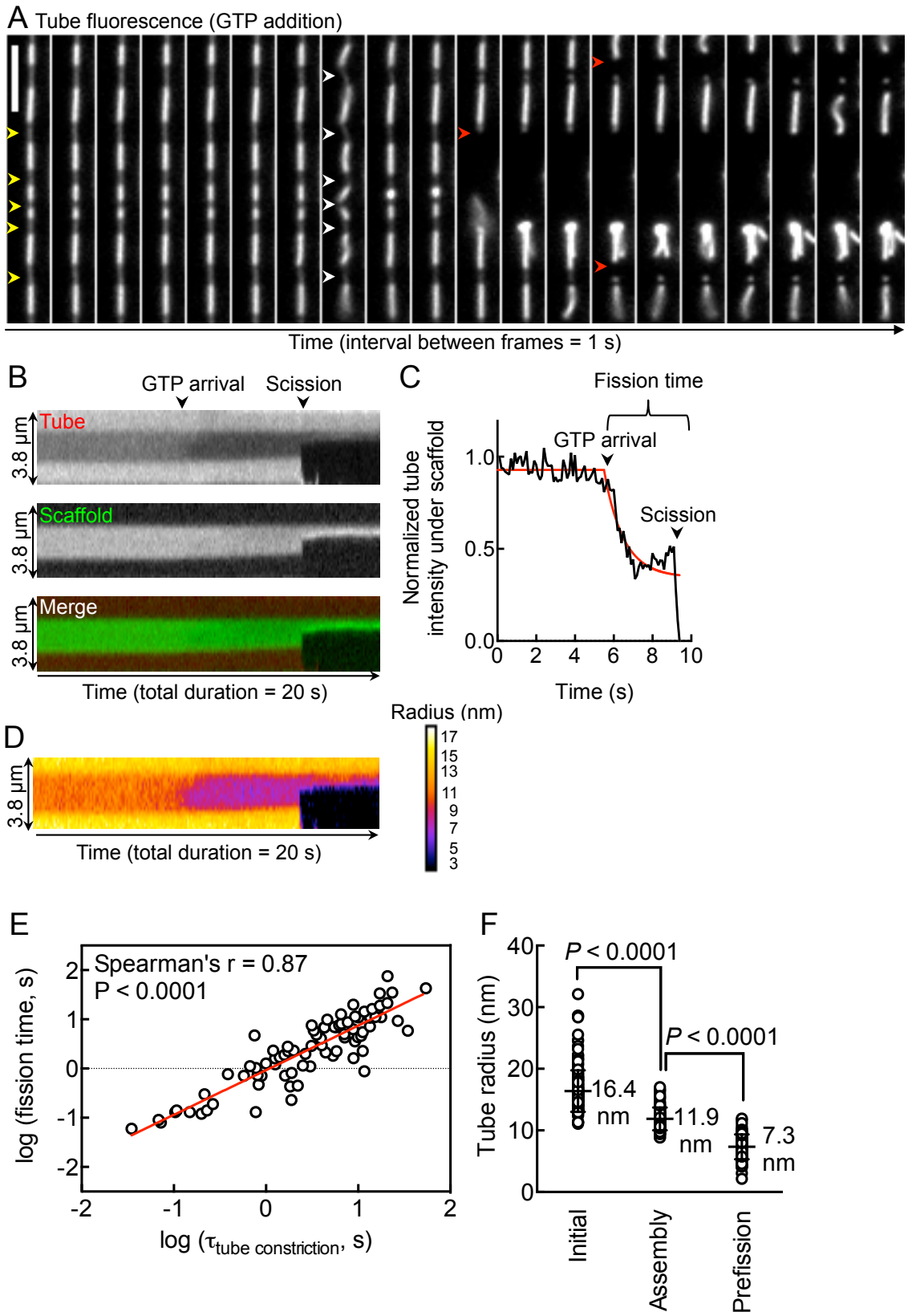
A Tube fluorescence (GTP addition)
Time (interval between frames = 1 s)
B
GTP arrival
Scission
Tube
Scaffold
Merge
3.8 µm
Time (total duration = 20 s)
C
Fission time
GTP arrival
Scission
Normalized tube intensity under scaffold
1.0
0.5
0.0
0 2 4 6 8 10
Time (s)
D
Radius (nm)
17 15 13 11 9 7 5 3
3.8 µm
Time (total duration = 20 s)
E
Spearman's r = 0.87
P < 0.0001
log (fission time, s)
log (τtube constriction, s)
F
P < 0.0001
P < 0.0001
Tube radius (nm)
16.4 nm
11.9 nm
7.3 nm
Initial
Assembly
Prefission

Figure 3-3. GTP hydrolysis-induced tube constriction precedes tube scission (A) Panels from a time-lapse movie monitoring GTP addition to preassembled scaffolds (yellow arrows). Arrival of GTP leads to buckling of some scaffolds (white arrows) that is followed by tube scission (red arrows) (Movie 3). Scale bar = 5 μm. (B) Kymographs from simultaneous dual channel recordings showing tube (red) and scaffold (green) fluorescence. (C) Kinetics of GTP hydrolysis-induced tube constriction, fitted to an exponential decay function (red), prior to scission. (D) Tube fluorescence kymograph in (B) scaled to tube radius. (E) Correlation between fission time and the time constants of GTP hydrolysis-induced tube constriction for 84 tube scission events. (F) Radius of the membrane tube before scaffold assembly (Initial, N = 180), after scaffold assembly (Assembly, N = 80) and before fission (Prefission, N = 76) calculated from calibrated tube fluorescence. Bars represent the mean ± SD. Significance (P) values are calculated using the Mann-Whitney's test.

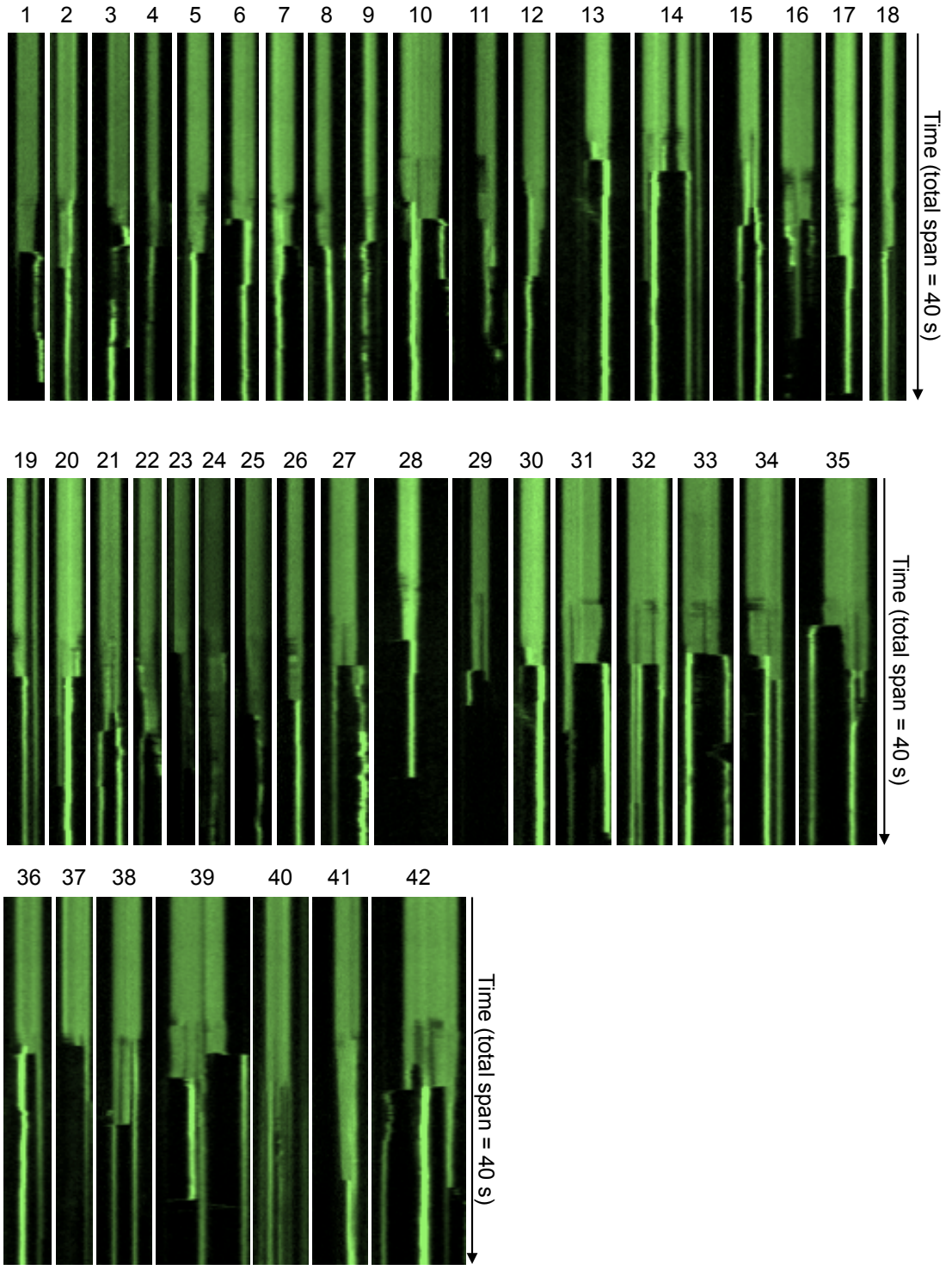

Figure 3-3-1. Examples of splitting of dynamin scaffolds in response to tube scission.

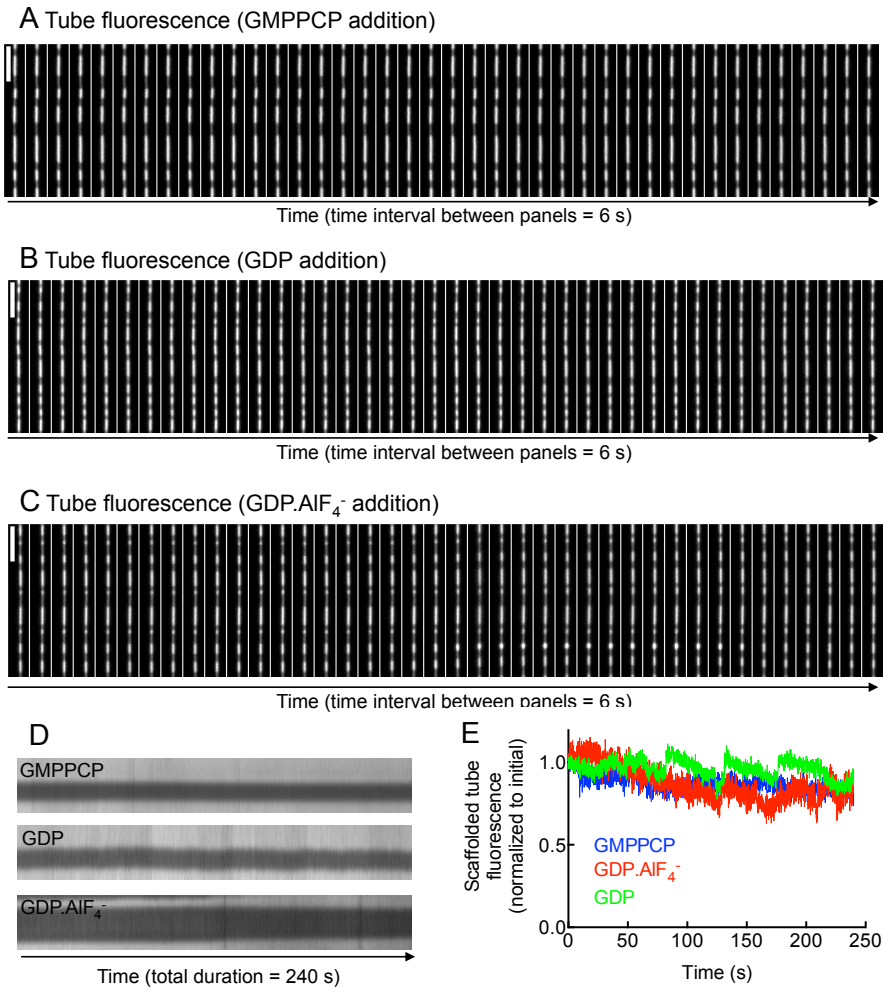

Figure 3-3-2. Panels from a time-lapse movie monitoring scaffolds in response to addition of (A) GMPPCP, (B) GDP, and (C) GDP.AlF_4^- addition to preassembled scaffolds. (D) Kymographs of tube fluorescence in response to addition of GMPPCP, GDP, and GDP.AlF_4^-. (E) Kinetics of changes in tube fluorescence in response to addition of GMPPCP, GDP, and GDP.AlF_4^-.

3.3.4 Coordination between scaffold assembly and tube scission

Stage-specific reconstitution experiments indicate that the scaffold assembly-induced tube constriction is a slow process and generates moderate degree of membrane constriction (Fig. 3-2) whereas GTP hydrolysis-induced tube constriction guarantees tube scission but with highly variable rates (Fig. 3-3). Together, these attributes reflect workings of a stochastic and inefficient membrane fission apparatus. In cells, dynamin catalyzes membrane fission in the constant presence of GTP as short self-limited scaffolds presumably because scission of the underlying

tube occurs early enough before any significant scaffold expansion (Doyon et al., 2011; Shnyrova et al., 2013). Importantly, the time scales reported for the scission reaction are narrowly distributed about ~10-12 s (Taylor et al., 2011; Cocucci et al., 2014). To address this discrepancy, we recreated a physiologically relevant scission reaction by flowing in 0.5 μM dynamin to SMrT templates bathed in excess GTP (1 mM). The arrival of dynamin led to the appearance of multiple tube constriction events, each of which progressed toward tube scission (Fig. 3-4A, red arrows). Surface pinning sites restricted the extent of retraction of the severed ends thus allowing multiple scission events to take place on a single tube (Movie 4). Importantly, the pinning sites also contained collateral disassembly of scaffolds in response to cut-induced loss in membrane tension (Fig. 3-4-1). Kinetic analysis of the tube severing process showed a linear increase in number of fission events with time indicating that each fission event is temporally independent. The bulk fission rate for 1 mM GTP was 6.1 s^{-1} (Fig. 3-4B, red symbols), which dropped to 3.7 s^{-1} with 100 μM GTP (Fig. 3-4B, green symbols) and to 1.9 s^{-1} with 10 μM GTP (Fig. 5B, blue symbols).

The start of each tube-severing event was characterized by a monotonous decay in tube fluorescence before scission-induced tube retraction (Fig. 3-4C), seen as a precipitous drop in the tube fluorescence trace (Fig. 3-4D) and also apparent in recent results monitoring conductance changes in free standing lipid nanotubes (Mattila et al., 2015). Surprisingly, the rate of tube constriction was faster in presence of GTP than was seen with scaffold assembly in the absence of GTP (Fig. 3-4E, $\tau_{scission}$ = 6.5 ± 4.7 s, mean ± SD, N = 21; $\tau_{assembly}$ = 29.2 ± 18.6 s, mean ± SD, N = 73; $P< 0.0001$, Student's t-test). Faster rates of tube constriction and the monotonous nature of the fluorescence decay strongly imply that the above-mentioned GTP hydrolysis-dependent conformational changes in helical scaffolds (Fig. 3-4B) now occur coordinately with scaffold assembly. Thus, scaffold assembly and GTP hydrolysis-induced tube constriction become kinetically inseparable in the constant presence of GTP. The mean fission time for reactions carried out with 1 mM GTP was 12.8 ± 5.8 s (mean ± SD, N = 75 events, Fig. 3-4F), which increases to 19.4 ± 11.7 s (mean ± SD, N = 73 events, $P< 0.0001$, Student's t-test) with 100 μM GTP and to 47.8 ± 19.2 s (mean ± SD, N = 50 events, $P< 0.0001$, Student's t-test) with 10 μM GTP indicating that substrate limitation delays the tube severing reaction possible due to a slowing down of GTPase activity and hence the rate of tube constriction. Importantly, the fission time seen with excess GTP is very similar to the characteristic fission time seen *in vivo*(Taylor et

al., 2011; Cocucci et al., 2014). Based on the estimated *k*cat of 1.4 s^{-1} at room temperature, the mean fission time of 12.8 s indicates a requirement for ~18 cycles of GTP hydrolysis before tube scission.

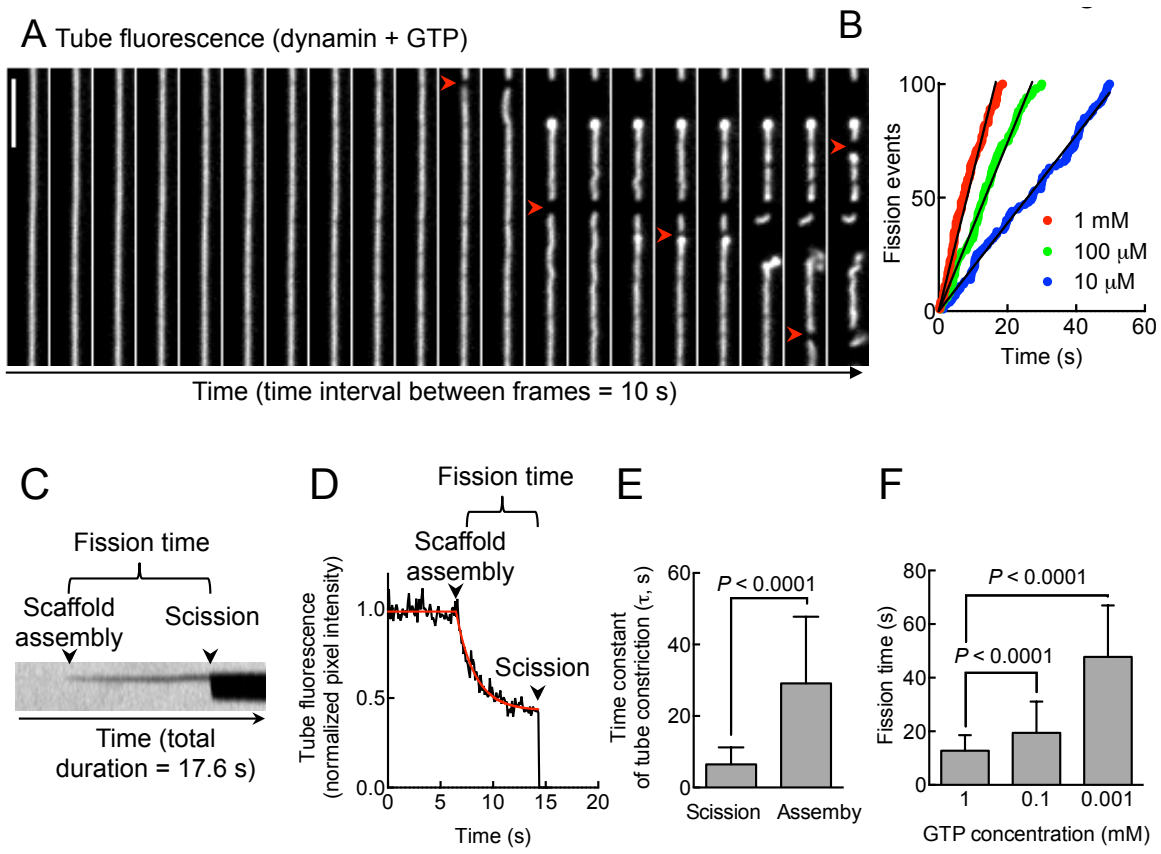

Figure 3-4. Coordination between scaffold assembly and tube scission(A) Panels from a time-lapse movie showing multiple scission events (red arrows) in response to dynamin and GTP addition (Movie 4). Scale bar = 5 μm. (B) Rates of membrane fission in presence of 1 mM, 100 μM and 10 μm GTP fitted to a line (black). Data represents pooled analysis from multiple movies. (C) Kymograph showing tube fluorescence for a single tube scission event. (D) Single pixel fluorescence trace (black) showing kinetics of tube constriction prior to scission fitted to an exponential decay function (red). (E) Time constants of scaffold assembly-induced tube constriction in the absence (assembly, N = 80) and presence (scission, N = 21) of GTP. Data represent the mean ± SD. Significance (P) values are calculated using the Student's t-test. (F) Mean ± SD of fission times for 1 mM (N = 75), 100 μM (N = 73) and 10 μm (N = 50) GTP. Significance (P) values are calculated using the Student's t-test.

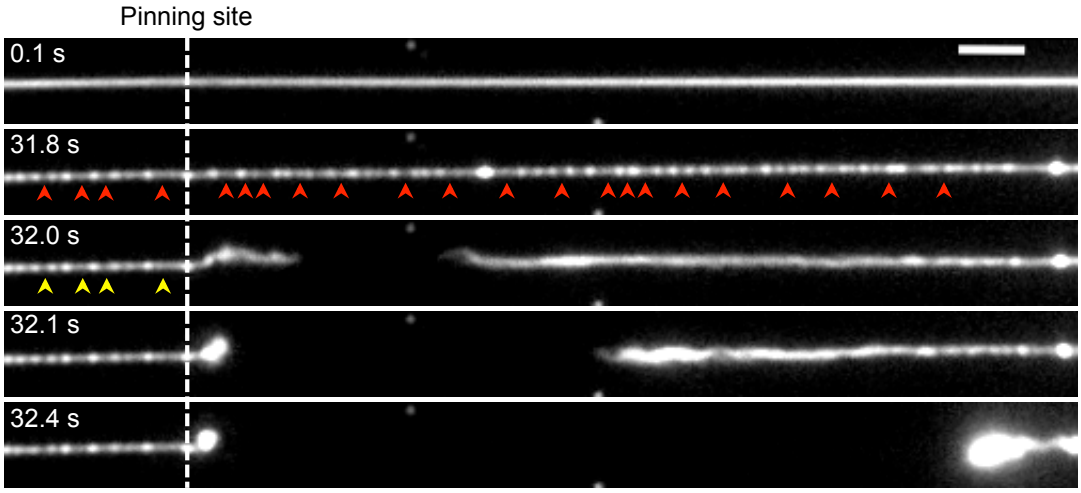

Figure 3-4-1. Effects of surface pinning sites on stability of scaffolds to collateral effects. Shown here is a membrane tube on a highly passivated surface with 1 pinning site in the field of view (marked by the dotted line). Addition of dynamin and GTP leads to formation of scaffolds (red arrows) and a single scission event. Note that scaffolds on the right of the pinning site shown collateral disassembly whereas those on the left of the pinning site remains unaffected (yellow arrows).

3.3.5 Role of I533A in membrane fission

The dynamin PH domain engages the membrane through electrostatic and hydrophobic interactions via residues located in its variable loops (Vallis et al., 1999; Lemmon 2000; Ramachandran et al., 2009). A critical role for the hydrophobic character of the variable loop 1 for dynamin function is seen when an Ile^{533} to Ala mutation renders dynamin incapable of catalyzing membrane fission during clathrin-mediated endocytosis (Ramachandran et al., 2009). With the suite of assays described above for the stage-specific monitoring of dynamin function, we reanalyzed the molecular basis of the defect associated with I533A (Ramachandran et al., 2009; Shnyrova et al., 2013). Addition of 0.5 μM I533A to SMrT templates containing 1 mol% PIP_2 led to the formation of scaffolds that constricted the underlying membrane tube (Fig. 3-5A), consistent with earlier results (Shnyrova et al., 2013). I533A scaffolds were however severely restricted in length (Fig. 3-5A) compared to those formed by WT dynamin (Fig. 3-5B,C), yet their assembly was similarly sensitive to the starting membrane curvature as WT dynamin with no constrictions apparent on membrane tubes wider than ~17 nm radius (Fig. 3-5C). Increasing the concentration of PIP_2 to 5 mol% rescued the apparent self-assembly defect associated with I533A with scaffold lengths similar to that seen with WT dynamin (Fig. 3-5B). Furthermore, increasing the PIP_2 concentration extended the curvature selectivity for scaffold assembly-

induced constriction to ~32 nm (Fig. 3-5C). Interestingly, even on 5 mol% PIP_2-containing SMrT templates, kymographs of tube fluorescence changes in response to growth of I533A scaffolds were characterized by jagged boundaries between the scaffold and the membrane (Fig. 3-5D, red arrows) which is unlike that seen for WT dynamin, indicating a laterally mobile and less stably entrenched scaffold in the membrane. In addition, the limiting tube radius seen after self-assembly of I533A scaffolds was 13.8 ± 1.2 nm (mean ± SD, N = 29, Fig. 3-5E), which is significantly higher than 11.9 ± 1.8 nm (mean ± SD, N = 80, $P< 0.0001$, Student's t-test) seen with WT dynamin indicating that I533A scaffolds are less effective in tube constriction. In conjunctions with recent studies indicating a dramatically lowered degree of assembly-induced self-quenching of fluorescently labeled I533A (Ramachandran et al., 2009), these results reflect characteristics of a less 'compact' scaffold. Addition of I533A to SMrT templates containing 1 mol% PIP_2 in the constant presence of GTP showed no tube scission (Fig. 3-5F), consistent with earlier results (Shnyrova et al., 2013). Remarkably however, we observed no signs of tube constriction during the entire course of the experiment. Preassembling I533A to allow formation of scaffolds (Fig. 3-5G, yellow arrows) and then adding GTP caused scission of the tube (Fig. 3-5G, red arrows). Thus, the molecular basis for the earlier observed membrane fission defect lies in the inability of I533A to form stable scaffolds under conditions of constant GTP turnover and not *per se* in membrane fission. We probed if the rescue in scaffold assembly by increasing the PIP_2 concentration from 1 to 5 mol%seen earlier (Fig. 3-5A, B) was sufficient to allow formation of stable scaffolds in the constant presence of GTP. Addition of 0.5 μM I533A to SMrT templates containing 5 mol% PIP_2 in the constant presence of GTP indeed led to scaffold assembly and tube scission (Fig. 3-5H). The bulk fission rate for I533A under these conditions was 4.2 s^{-1} (Fig. 3-5I, red symbols) while that for WT dynamin with 1 mol% PIP_2 was 6.8 s^{-1} (Fig.3-5I, gray symbols) and for 5 mol% PIP_2 was 9.6 s^{-1} (Fig. 3-5I, blue symbols) indicating only a partial rescue of its membrane recruitment defect. Importantly, I533A on 5 mol% PIP_2-containing SMrT templates showed a fission time of 8.7 ± 4.0 s (mean ± SD, N = 35, Fig. 3-5J), which was significantly lower than 12.8 ± 5.8 (mean ± SD, N = 75, $P = 0.0003$, Student's t-test, Fig. 3-5J) for WT dynamin acting on 1 mol% PIP_2 and than 11.0 ± 5.0 (mean ± SD, N = 243, $P = 0.01$, Student's t test, Fig. 3-5J) on 5 mol% PIP_2. The fission time defines the actual duration for which dynamin works to affect membrane fission and therefore serves as a direct parameter for

its catalytic efficiency. Our results therefore imply that I533A is in fact better at catalyzing membrane fission than WT dynamin.

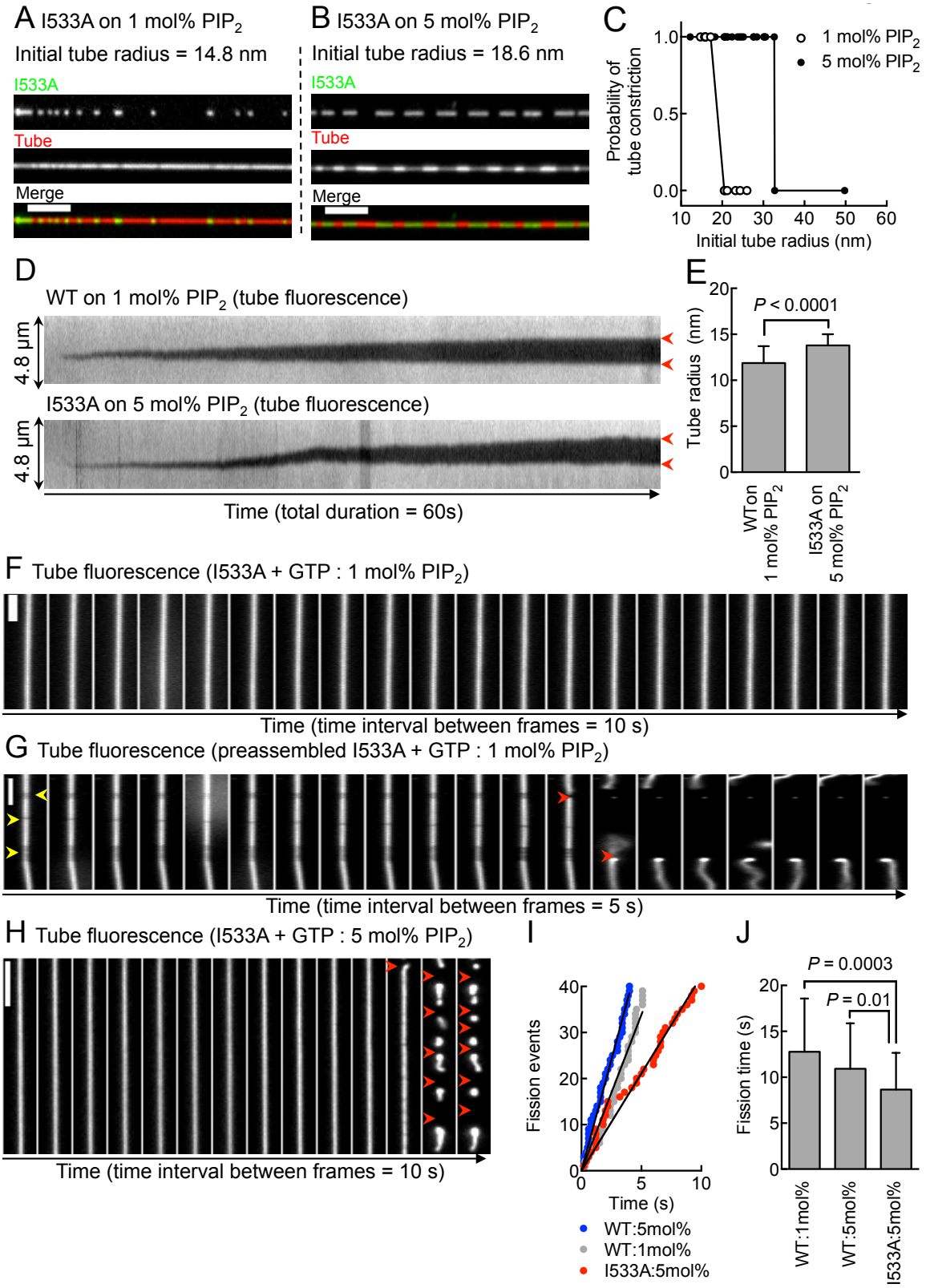

Figure 3-5.Role of I533A in membrane fission. Fluorescence micrographs of Alexa488-labeled dynamin I533A (green) on a *p*-Texas Red DHPE-labeled tube (red) containing 1 (A) and 5 (B) mol% PIP_2. Scale bars = 5 μm. (C) Probability of occurrence of I533A scaffold-induced tube constriction as a function of starting tube radius for 1 (open symbols) and 5 (closed symbols) mol% PIP_2. (D) Kymographs of scaffold assembly-induced tube constriction for WT on 1 mol% PIP_2 and I533A on 5 mol% PIP_2 tubes. The boundary between the scaffold and the bare membrane is marked by red arrows. (E) Radius of the membrane tube after assembly of WT (N = N = 80) on 1 mol% PIP_2 and I533A scaffolds (N = 29) on 5 mol% PIP_2 calculated from calibrated tube fluorescence. Significance (P) values are calculated using the Student's t-test. (F) Panels from a time-lapse movie showing addition of I533A to SMrT templates containing 1 mol% PIP_2 in presence of GTP. (G) Panels from a time-lapse movie showing addition of GTP to preassembled I533A scaffolds (yellow arrows) on 1 mol% PIP2 containing SMrT templates. Red arrows mark sites of tube scission. (H) Panels from a time-lapse movie showing addition of I533A to SMrT templates containing 5 mol% PIP2 in presence of GTP. Red arrows mark sites of tube scission. (I) Rates of membrane fission for I533A on SMrT templates containing 5 mol% PIP_2 (red symbols) and for WT on SMrT templates containing 1 mol% (gray symbols) and 5 mol% (red symbols) PIP_2. Data represents pooled analysis from multiple movies. (J) Mean ± SD of fission times for WT on 1 mol% (N = 75) and 5 mol% (N = 243) PIP_2-containing SMrT templates. The same calculated for I533A on 1 mol% (N = 35) PIP_2-containing SMrT templates. Significance (P) values are calculated using the Student's t-test.

Discussion

Our results reveal elegant design principlesof an autonomous fission apparatus thatutilizes scaffold assembly and assembly-stimulated GTP hydrolysis to constrict and sever membrane tubes. Tube scission appears to be localized within the region confined by the scaffold and is in contrast to the earlier proposed mechanistic framework that invokes curvature stress generated at the edge of the dynamin scaffold and the bare membrane to affect fission(Morlot et al., 2012). Our results are in agreement with recent molecular dynamics simulations where the point of rupture of the head-group region of lipids was found to be localized to the central zone of the constriction and not directly at its edges (Fuhrmans et al., 2014). We find that an intrinsic coordination between scaffold assembly and assembly-stimulated GTP hydrolysis, achieved when carried out under physiologically relevant conditions of constant presence of GTP, is sufficient to render dynamin capable of orchestrating a highly deterministic fission reaction with characteristic fission times similar to that seen *in vivo*. The nature of conformational changes we observe wherein the outer scaffold retains its general architecture while the underlying membrane tube is constricted in response to GTP hydrolysis is quite unlike those described

earlier. Previous CryoEM results on dynamin lacking the C-terminal unstructured PRD assembled on membranes suggest constriction of both the outer scaffold as well as the underlying membrane tube in response to GTP binding (Zhang and Hinshaw 2001; Mears et al., 2007; Chappie et al., 2011). Our results with full-length dynamin however suggest that tube constriction is only apparent when helical scaffolds engage in multiple rounds of GTP hydrolysis. Under the present conditions, fluorescence labeling of dynamin1 occurs preferentially at Cys^{708} present in the stalk (Liu et al., 2011). Thus, if the helical scaffold was merely peripherally associated and constantly adapting to the underlying tube dimensions, its fluorescence should have declined upon tube constriction, which is not the case. We speculate that GTP hydrolysis effectively leads to the conversion of the scaffold to a state that displays higher membrane constricting activity, possibly one that imposes a deeper footprint on the underlying membrane (see Fig. 3-6) and is consistent with the recently proposed transmission of conformational changes from the bundle signaling element (BSE) to the PH domain (Mattlila et al., 2015). Nevertheless, a mere state transition appears to be insufficient as multiple rounds of GTP-hydrolysis are necessary to constantly remodel the underlying tube to reach critical dimensions before scission. While analysis of the precise conformational changes is beyond the scope of this report, we anticipate the use of SMrT templates to allow dynamic fluorescence-based detection of conformational changes occurring in dynamin and other self-assembling proteins that remodel membranes.

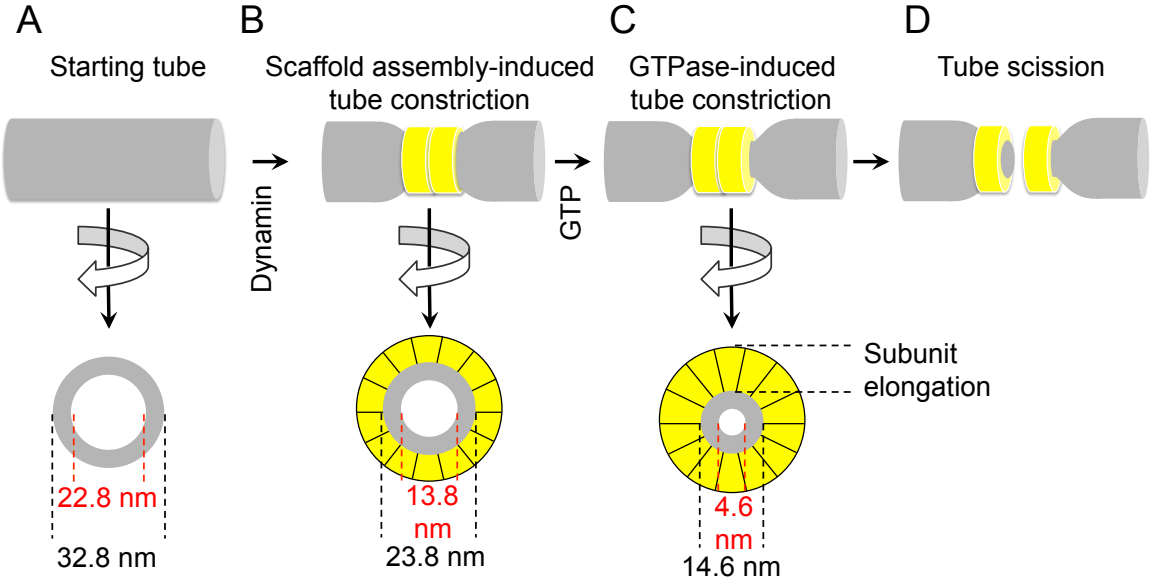

Figure 3-6. Proposed mechanism of dynamin-catalyzed tube scission. Dynamin addition to SMrT templates (A) leads to self-assembly of a scaffold (yellow) (B), which constricts the underlying tube (gray) to an outer diameter of 23.8 nm. GTP hydrolysis by an intact scaffold induces further tube constriction that reduces the outer tube diameter to 14.6 nm (C), possibly by elongation of each subunit of the scaffold so as to impress a deeper footprint on the underlying membrane. Upon reaching this stage, the tube undergoes scission (D) with a concomitant splitting of the scaffold.

Conductance measurements using membrane nanotubes containing low PIP_2 concentrations have indicated that I533A can bind and constrict the membrane tube in the absence of GTP (Shnyrova et al., 2013) and recent spectroscopic analysis suggests that it adopts an alternate, less-stable orientation on the membrane (Mehrotra et al., 2014). Indeed, with the stage-specific reconstitution methods available with SMrT templates, our results indicate that I533A forms scaffolds that are shorter in length; less stably bound on the membrane and constrict the underlying tube to a lesser degree than WT. I533A fails to catalyze membrane fission under conditions of constant GTP turnover, a result that was interpreted to reflect the requirement for stable membrane insertion of hydrophobic residues to facilitate local sculpting of lipids into non-bilayer configurations to promote membrane fission (Shnyrova et al., 2013). Direct visualization of the membrane fission reaction however identifies the defect in I533A to be not with membrane fission but in stable scaffolding of the membrane in the constant presence of GTP. In fact, overwhelming the membrane recruitment defect by favoring an electrosctatic mode of association renders I533A perfectly capable of catalyzing membrane fission, with a catalytic efficiency that is significantly better than that seen with WT. It is tempting to speculate that the mechanism by which dynamin orchestrates membrane fission represents a trade-off between robust anchoring to the membrane and a sluggish catalysis of the fission pathway.

Chapter- 4

PH domain catalyzes dynamin-induced membrane fission

4.1 Introduction

Membrane fission is governed by the general principle that a protein scaffold drives constriction of the underlying membrane, bringing them in close proximity, until they spontaneously fuse (Chernomordik et al., 2003). Since this process involves the formation of a narrow neck-like intermediate, membrane fission is an energetically unfavorable process (Kozlovsky and Kozlov, 2003). Dynamin was the first protein shown to be directly involved in membrane fission (Koenig and Ikeda 1983; van der Bliek 1993). The dynamin superfamily of proteins is characterized by the presence of three conserved core domains; the G-domain, bundle-signaling element (BSE) and the stalk (Chappie et al., 2013). The G-domain binds and hydrolyzes GTP, the stalk maintains dynamin as a tetramer in solution and promotes dynamin self-assembly as helical scaffolds on the membrane, while the BSE acts as a toggle switch to stimulate its basal GTPase activity upon self-assembly (Faelber et al., 2012). Dynamin1, the neuronal isoform of classical dynamins, functions to catalyze membrane fission during fast synaptic vesicle recycling events (Schmid et al., 2011). Unlike other members of the dynamin superfamily that contain the characteristic core domains, classical dynamins are unique as they contain a well-defined membrane binding, pleckstrin-homology domain (PHD) in the middle and a proline-arginine rich domain (PRD) at the C-terminus. The PHD binds phosphatidylinositol-4,5-bisphosphate (PIP_2) while the PRD binds SH3-domain containing endocytic accessory proteins (Okamotoet al., 1997). Coincidence detection of the plasma membrane-localized PIP_2 and endocytic accessory proteins causes dynamin to be specifically recruited to emergent sites of membrane fission(Ferguson and De Camilli2012).

The importance of the PHD is underscored by the observation that mutations in centronuclear myopathy (CNM) and Charcot-Marie-Tooth (CMT) disease patients are predominantly located in the PHD (Durieux et al., 2010). These mutations map to a region on the PHD distant from those required for lipid binding (Kenniston et al., 2010). Considering that dynamin functions are critical for survival (Ferguson and De Camilli2012), their presence in surviving patients suggest that the PHD plays a subtle role in dynamin function. The functional relevance of the PHD in dynamin function remains debated. Early data from cells indicate that the partial or complete deletion of the PHD does not alter the subcellular localization of dynamin (Achiriloaie et al., 1999,Vallis et al., 1999), suggesting that the 109-residue globular domain plays more than a membrane-targeting role. The isolated PHD has very low affinity for

negatively charged lipids, including PIP_2 (Klein et al., 1998), but increases in avidity upon dynamin self-assembly. The crystal structure of the PHD identifies a β-sandwich core with 3 variable loops (VL1, VL2 and VL3) that together constitute the PIP_2-binding pocket (MA Lemmon 2000). VL1 contains both hydrophobic and polar residues and partially inserts into the lipid bilayer (Ramachandran et al.,2009). VL2 and VL3 are relatively polar in nature but are important for dynamin function, as evidenced by mutation studies (Liu et al., 2011).

An active role for the PHD in dynamin function stems from observations that mutations disrupting the hydrophobicity of the VL1 loop tend to show reduced membrane remodeling and fission activity (Ramachandran et al., 2009). Furthermore, theoretical considerations suggest a role for residues in this loop in splaying of lipids in the membrane in order to facilitate fission (Shnyrova et al., 2013). Despite these observations, the specific role of the PHD in membrane fission has been difficult to interpret from mutagenesis approaches since the above-described mutations alter dynamics and orientation of the PHD on the membrane (Mehrotra et al., 2014). Consequently, defects such as the inability to form stable scaffolds in the constant presence of GTP weigh-in significantly and complicate understanding the role of the PHD in membrane fission (Chapter 3)

4.2Materials and Methods

4.2.1 Expression, purification and fluorescent labeling of proteins

Full-length human dynamin1 (WT) was cloned with a C-terminal StrepII tag in pET15B vector. Residues 520-629 corresponding to the PHDwere deleted and replaced with 6xHis to generate the ΔPH construct. All clones were confirmed by sequencing. Proteins were expressed in BL21(DE3) in autoinduction medium (Formedium, UK) at 18 °C for 30 hours and purified as described earlier (Chapter 3). Purified proteins were labeled with extrinsic, cysteine-reactive Alexa-488 C5 or Alexa-647C5 maleimide fluorescent probes (Invitrogen) as described earlier (Chapter 3).

4.2.2 Preparation of liposomes, SUPER and SMrT templates

Lipids stocks (Avanti Polar) were aliquoted in the following proportions to generate PIP_2- or CL-containing mixtures; DOPC:DOPS:$DOPIP_2$ (84:15:1 mol%) and DOPC:DOPS:CL

(80:15:5 mol%). When necessary, trace amounts of the fluorescent lipid probe *p*-Texas Red DHPE was incorporated to a final concentration of 1 mol%. For liposomes, dried lipid mixtures were hydrated in assay buffer (20 mM Hepes, pH 7.5, 150 mM KCl) to a final concentration of 1 mM and extruded through 100 nm polycarbonate membranes (Whatman). SUPER templates were prepared with PIP_2- or CL-containing liposomes as previously reported (Pucadyil et al., 2010). SMrT templates were prepared as described previously (Chapter 3).

4.2.3 Liposome binding assays

WT or ΔPH, both at a final concentration of 1 μM, were incubated with 100 μM of PIP_2- and CL-containing liposomes, respectively, for 30 min at room temperature. The liposome-bound (pellet, P) and free (supernatant, S) protein fractions were separated by high-speed (100,000 g) centrifugation. Samples were resolved on a 10% SDS PAGE and stained with CBB.

4.2.4 GTPase assay

WT or ΔPH, both at a final concentration of 0.1 μM, were incubated with 10 μM of PIP_2- or CL-containing liposomes, respectively, in assay buffer containing 1 mM GTP (Jena Bioscience, Germany) and 1 mM $MgCl_2$ for 30 min at 37° C. GTP hydrolysis was monitored over time using a malachite green-based colorimetric assay (Baykov et al., 1988).

4.2.5 SUPER template tubulation assays

Glass-bottomed Lab-Tek (Nunc) chambers were passivated with 2 mg/ml BSA (Sigma) and filled with 200 μl of assay buffer containing 2 μM of WT or ΔPH. A small aliquot (20 μl) of the stock of SUPER templates was added to the chamber, incubated for 10 min at room temperature and imaged as described below.

4.2.6 Electron microscopy

WT or ΔPH, at a final concentration of 4 μM, were incubated with 1 mM GMPPCP (Jena Bioscience, Germany) and 1 mM $MgCl_2$ in low-salt assay buffer (20 mM HEPES, pH 7.5, 35 mM NaCl) for 2 hr at room temperature. The mixture was then adsorbed onto carbon-coated grids, stained with 1% uranyl acetate and imaged with a 200 keV electron microscope.

4.2.7 SMrT templates assays

SMrT templates assays to monitor scaffold assembly and membrane fission were carried out as 25 °C as described earlier (Chapter 3).

4.2.8 Fluorescence microscopy

Fluorescence imaging was carried out on an Olympus IX71 inverted microscope through a 100x, 1.4 NA oil-immersion objective equipped with an Evolve 512 EMCCD camera (Photometrics).

4.2.9 Statistical analysis

All nonlinear regression analyses were carried out using Graphpad Prism (version 5.0a).

4.2.10 Image analysis for conversion of tube fluorescence to radius

Image analysis of fluorescence micrographs and time-lapse movies were carried out using Fiji (version 1.47) (Schindelin et al., 2012) The membrane tubes were labeled with the fluorescent lipid probe *p*-Texas red DHPE, which partitions equally to regions of low and high membrane curvature (Hsieh et al., 2012), exhibits fluorescence properties that are insensitive to protein binding (Jung et al., 2009), and displays unrestricted diffusion in membrane tubes (Chapter 3). Tube fluorescence to radius conversion was carried out using the supported lipid bilayer (SLB) formed at the source of SMrT template preparations as an *in situ* calibration standard (Fig. 4-2-2A). This conversion is based on the premise that the fluorescence intensity of diffraction-limited, membrane-bound objects is proportional to the net membrane area (Kunding et al., 2008) . Before each experiment, fluorescence micrographs of the SLB and tubes were acquired and corrected for background. The integrated fluorescence intensity of ROIs of different sizes placed on the SLB (Fig. 4-2-2B) was plotted against their respective area to get calibration constant K_1 (Fig. 4-2-2C). The integrated fluorescence of ROIs of length (l) placed on tubes (Fig. 4-2-2D) was then converted to net membrane area using K_1, following which radius (r) of the tube was calculated from $r = \text{area}/(2\pi l)$. The estimated tube radius (r) was then plotted against the maximum pixel intensity in ROIs placed on tubes to get calibration constant K_2 (Fig. 4-2-2E). Tube fluorescence can then directly be converted to tube radius by dividing pixel intensities in a micrograph with K_2. Errors arising from fluctuations in tube fluorescence in still

micrographs or time-lapse movies of tubes account for <10% coefficient-of-variation (COV) of mean fluorescence (Fig. 4-2-2F). We validated this approach by estimating the tube radius under a dynamin scaffold. A kymograph of a 10 s movie of a preassembled dynamin scaffold was first acquired (Fig. 4-2-2G). All pixels in the kymograph were converted to tube radius by dividing their intensity by K_2. A histogram of tube radii was then fitted to a sum of 2 gaussian (Fig. 4-2-2H). The low value peak, corresponding to the tube radius under the scaffold, gave us an estimate of 7.9 ± 0.6 nm (mean ± SD, n = 15) (Fig. 4-2-2I). These estimates reflect the tube radius from the center of the lumen to the center of the bilayer. Addition of 2.5 nm to this estimate to account for the 5 nm thick lipid bilayer brings the tube radius under a dynamin scaffold to 10.4 nm, in good agreement with the value of 11.2 nm reported earlier from force spectroscopy (Roux et al., 2010).

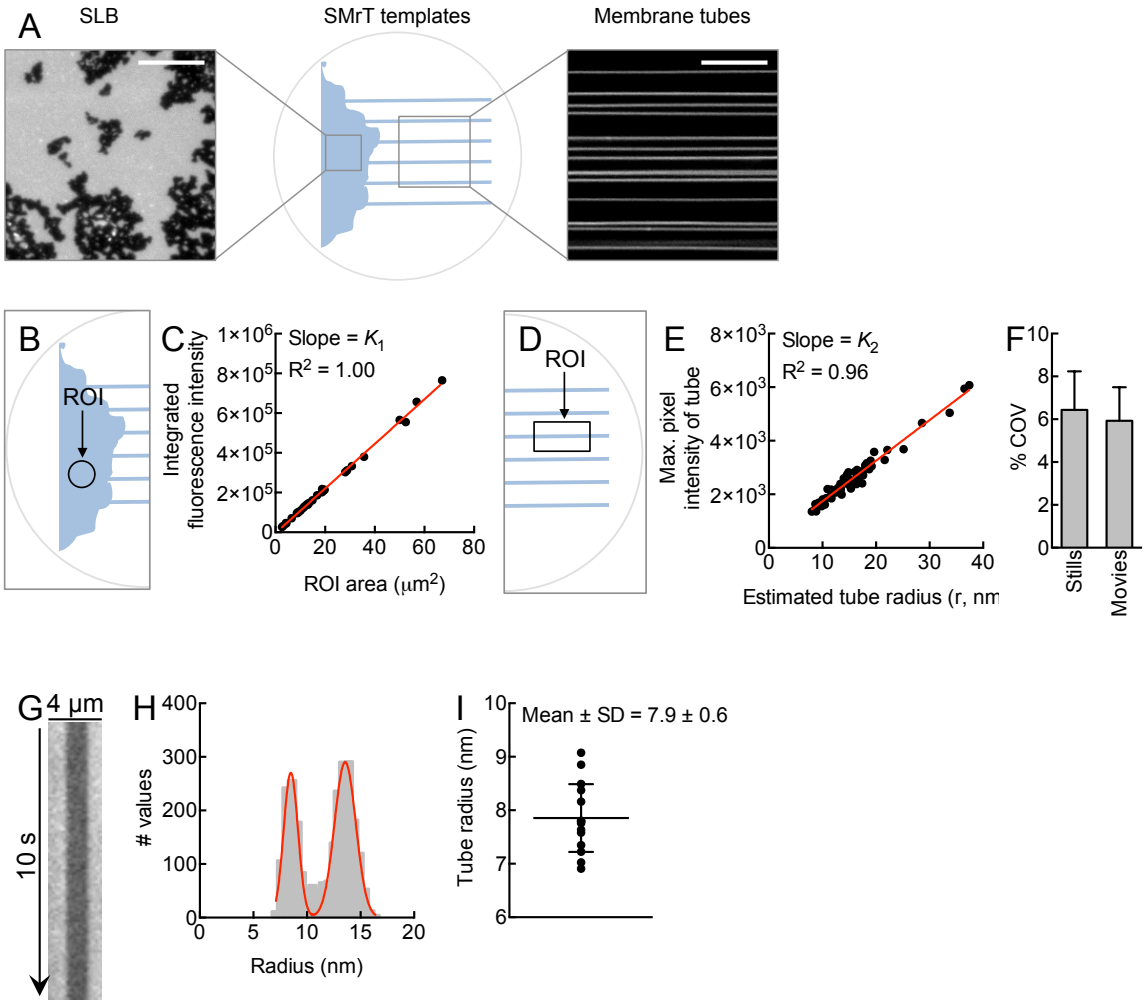

Figure 4-2-2. Procedure for converting tube fluorescence to radius(A) Schematic of SMrT templates showing the supported lipid bilayer (SLB) at source and membrane tubes. Scale bar = 10 μm. (B) Schematic of the SLB and the ROI position. (C) Plot of integrated fluorescence intensity in ROI against the area of ROI. (D) Schematic of membrane tubes and the ROI position. (E) Plot of maximum pixel intensity in ROI to tube radius. (F) Plot showing the coefficient-of-variation (COV) about the mean fluorescence intensity for still and time-lapse images of membrane tubes. Data represents the mean ± SD (n≥ 20, N=1). (G) Kymograph of tube fluorescence about a dynamin scaffold. Dark and light portions reflect regions under and adjacent to the scaffold on the tube, respectively. (H) Histogram of tube radii calculated from pixels of the kymograph shown in (G) and fitted to a sum of 2 gaussian. (I) Estimated tube radius under the dynamin scaffold.

4.3 Results

4.3.1 A functionally active dynamin construct lacking the PHD

To specifically delineate the contribution of the PHD in dynamin function, we used an alternate approach of engineering a dynamin construct where the 109-residue long PHD is replaced by 6 His residues. This construct, which we refer to as ΔPH (see Fig. 4-1A), can be recruited to membranes containing the chelator lipid (CL), DGS NTA(Ni^{2+}) (Kubalek et al., 1994). Thus, the ΔPH allows us to monitor consequences of a lack of PHD while on the membrane. PolyHis-CL interactions have been widely used to artificially recruit proteins to analyze a range of membrane-localized processes such as Rab-effector interactions(Christis et al., 2012), clathrin recruitment by adaptors (Kelly et al., 2014) and mechanisms of membrane curvature generation (Stachowiak et al., 2012).

We first tested ΔPH in assays previously used to monitor dynamin function *in vitro*. ΔPH binds to and sediments with CL-containing liposomes to levels comparable to that seen with WT on PIP_2-containing liposomes (Fig. 4-1B,C). Dynamin self-assembles to form helical scaffolds on membranes, which in turn stimulates its basal GTP hydrolysis rates (Chappie et al., 2010). Thus, assembly-stimulated GTPase activity reflects proper orientation of the G-domains within the scaffold. We find that the ΔPH displays identical rates of lipid-stimulated GTPase activity on CL-containing liposomes as seen with WT on PIP_2-containing liposomes (Fig. 4-1D). Next, we analyzed ΔPH for its ability to catalyze membrane fission in presence of GTP on our previously described assay system of supported membrane tubes (SMrT) (Chapter 2). Remarkably, we find that the ΔPH severs membrane tubes (Fig. 4-1E). These results indicate that the PHD is entirely dispensable for membrane fission. However, ΔPH was 10-fold slower in cutting tubes than WT

(Fig. 4-1F, $WT_{fission\ rate}$ = 6.7 cuts.s^{-1}, $\Delta PH_{fission\ rate}$ = 0.6 cuts.s^{-1}, Movie 5). We analyzed the molecular basis of a delayed fission reaction with ΔPH using stage-specific assays that monitor dynamin function at the single-event resolution.

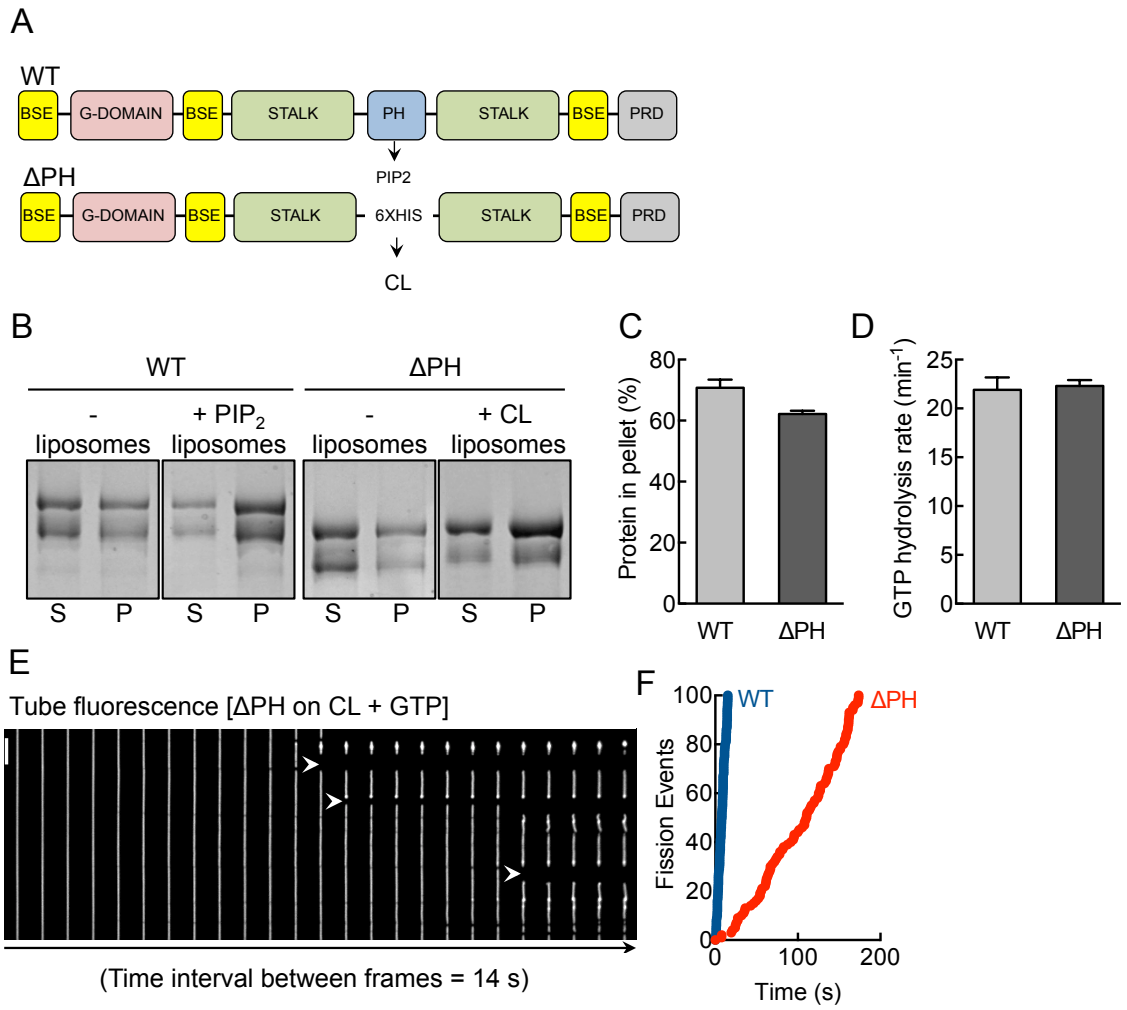

Figure 4-1. A functionally active dynamin construct lacking the PHD (A) Schematic representation of WT dynamin showing the bundle-signaling element (BSE), GTPase domain (G-domain), stalk, pleckstrin-homology domain (PHD) and the proline-arginine rich domain (PRD). The ΔPH construct has the entire PH domain deleted and replaced with a 6His linker. (B) CBB-stained SDS-PAGE of WT and ΔPH in the absence and presence of PIP_2- and CL-containing liposomes after sedimentation showing protein amounts in the supernatant (S) and pellet (P) fractions. (C) Densitometric analysis of gels shown in (B) indicating the fraction of protein in the pellet. Data represent mean ± SD (N = 2). (D) Assembly-stimulated GTP hydrolysis rates of WT and ΔPH in presence of PIP_2- or CL-containing liposomes, respectively. Data represent mean ± SD (N = 3). (E) Panels from a time-lapse sequence showing addition of ΔPH to SMrT templates in presence of GTP. White arrowheads mark sites of scission. (F)

Cumulative fission rates of WT and ΔPH. Data represent pooled analysis from n ≥ 19tubes in N = 3 independent experiments.

4.3.2 PHD is a kinetic regulator of dynamin self-assembly

We first monitored ΔPH functions in a membrane-independent, dynamin self-assembly assay using negative stain EM (Carr and Hinshaw,1997). Incubation of WT with a non-hydrolyzable GTP analog, GMPPCP, under low-salt conditions promotes dynamin self-assembly into rings/spirals (Fig. 4-2A). Under similar conditions, ΔPH formed fewer assemblies, and those that formed appeared to be incomplete, crescent-shaped structures (Fig. 4-2A). These results are in contrast to previous reports where the removal of PHD was seen to promote dynamin self-assembly (Vallis et al., 1999; Kenniston et al., 2010; Reubold et al., 2015). We believe these differences arise from the use of a full-length construct and deletion of the entire PHD in our case as opposed to a full-length construct with partial deletion of the PHD (Achiriloaie et al., 1999) or a construct lacking both the PHD and the PRD (Reubold et al., 2015). Consistent with a defect in self-assembly in solution, ΔPH failed to remodel planar CL-containing SUPER templates into long membrane tubes (Fig. 4-2B), suggesting together that the PHD positively contributes to cooperative self-association between dynamin molecules. Surprisingly, when added to SMrT templates and visualized after 10 min, we find fluorescently labeled ΔPH organized as discrete scaffolds (Fig. 4-2C, white arrowheads). Moreover, like is seen with WT, ΔPH scaffolds constrict the underlying tube and reduce tube fluorescence (Fig. 4-2C, red arrowheads). Together, these results suggest that a curved membrane rescues the self-assembly defect in ΔPH. Importantly, despite the membranes having different concentrations of the lipid that recruits WT and ΔPH to the membrane, the mean scaffold density seen with ΔPH was similar to that seen for WT (Fig. 4-2D) suggesting that ΔPH is not compromised with respect to membrane binding.

A closer look at dynamics of scaffold formation revealed subtle defects associated with ΔPH. We assayed scaffold expansion and tube constriction abilities of ΔPH from the drop in tube fluorescence under scaffolds (Fig. 4-2C). Kymographs generated from time-lapse movies following dynamin addition to SMrT templates indicate that ΔPH scaffolds nucleate and laterally expand on the tube (Fig. 4-2E), similar to that seen for WT. However, analysis of multiple single events of scaffold formation revealed significantly slower kinetics of scaffold expansion for ΔPH compared to that seen for WT (Fig. 4-2F, τ_{WT} = 61 ± 28 s, mean ± SD, n = 17; $\tau_{\Delta PH}$ = 187 ± 156

s, mean ± SD, n = 18). As a control, a 6xHis-mEGFP is recruited to membrane tubes containing 5 mol% CL with a τof ~25 s indicating that the slow kinetics of scaffold expansion seen with ΔPH is not due to reduced accessibility for CL. Scaffold assembly led to a monotonous decay in tube fluorescence indicating tube constriction at the site of the growing scaffold for both WT and ΔPH. However, the kinetics of assembly-induced tube constriction was 4-fold slower for ΔPH compared to that seen for WT (Fig. 4-2G, τ_{WT} = 20 ± 14 s, mean ± SD, n = 173; $\tau_{\Delta PH}$ = 86 ± 63 s, mean ± SD, n = 73). Strikingly, scaling pixel intensities to tube dimensions (Fig. 4-2-2) revealed that at equilibrium, ΔPH scaffolds appeared to constrict the underlying membrane tube to ~7 nm radius, similar to that seen with WT (Fig. 4-2H). These results indicate that ΔPH is membrane active and highlight a role for the PHD in facilitating the rate but not the extent of dynamin assembly-induced membrane constriction.

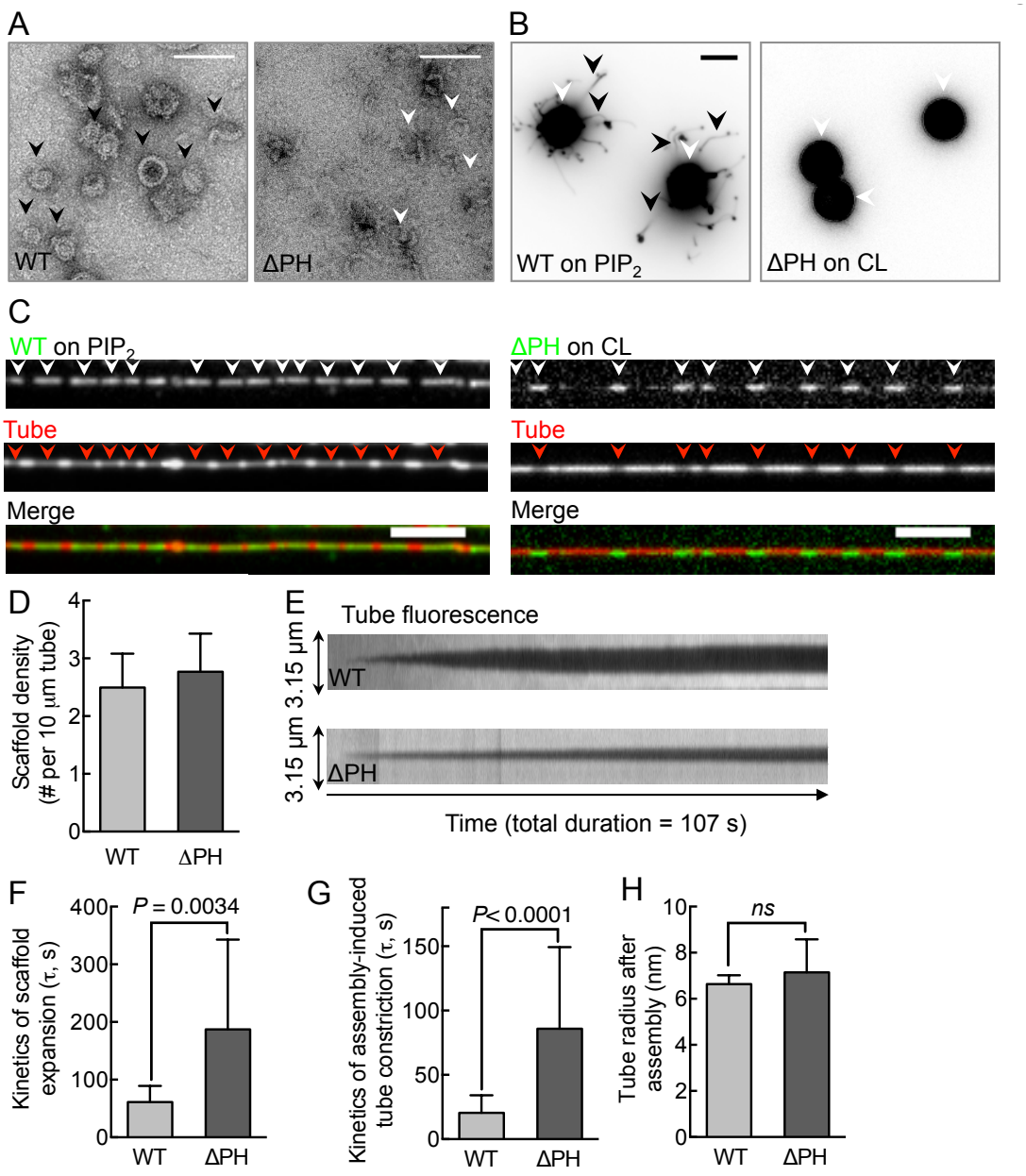

Figure 4-2. The PHD kinetically regulates dynamin self-assembly. (A) Representative negative-stained EM of WT and ΔPH in presence of GMPPCP under low-salt conditions. Black arrowheads mark WT dynamin rings and white arrowheads mark crescent-shaped structures and incomplete rings seen with ΔPH. Scale bar = 100 nm. (B) SUPER templates (white arrowheads) showing membrane tubules (black arrowheads) with WT but not ΔPH. Images are inverted in contrast for clarity. Scale bar = 5 μm. (C) Fluorescence micrographs showing the distribution of Alexa488-labeled (green) WT and ΔPH on a *p*-Texas Red DHPE-labeled (red) membrane tube. White arrowheads mark dynamin scaffolds and red arrowheads mark sites of tube constriction. Scale bars = 5 μm. (D) Scaffold density for WT and ΔPH. Data represent mean ± SD (n = 3, N = 3). (E) Kymographs of scaffold assembly-induced tube constriction for WT and ΔPH. (F) Time constants (τ) of scaffold expansion for WT and ΔPH. Data represent mean ± SD (n ≥ 20, N = 3,

Student's t-test). (G) Time constant (τ) of scaffold assembly-induced tube constriction. Data represent mean ± SD (n ≥ 20, N = 3, Student's t-test). (F) Radius of membrane tube underlying scaffolds from calibrated analysis of tube dimensions (see Fig. 4-2-1). Data represent mean ± SD (n ≥ 20, N = 3, Student's t-test).

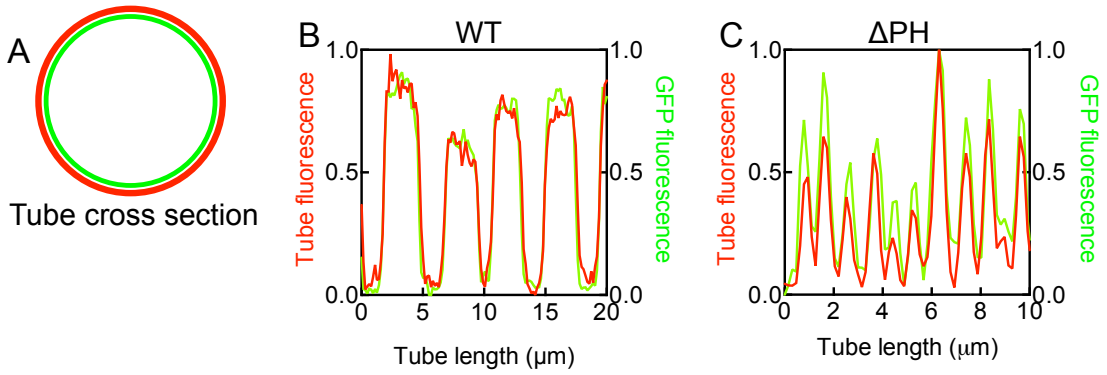

Figure 4-2-1. Validation of tube constriction (A) Schematic cross-sectional view of a membrane tube labeled with *p*-Texas Red DHPE (red) and containing mEGFP (green) recruited to the inner monolayer. Line profiles of tube (red) and mEGFP (green) fluorescence after scaffold assembly with WT (B) and ΔPH (C). The coincidence in fluorescence indicates that the drop seen in tube fluorescence is due to tube constriction.

4.3.3 A catalytic role for the PHD in dynamin-induced membrane fission

Swapping the native PHD-PIP_2 interaction for a generic polyHis-CL association preserves dynamin's ability to self-assemble on and constrict membrane tubes. This prompted us to monitor the effects of GTP addition to preassembled ΔPH scaffolds. Our experiments with WT have earlier shown that the addition of GTP to preassembled scaffolds leads to further tube constriction, which is followed by tube scission (Chapter 3). Kinetics of GTPase-induced tube constriction provides specific insights into mechanochemical functions of dynamin. Importantly, fission time, defined as the time interval between the onset of tube constriction and the cut under a preassembled scaffold, indicates the actual catalytic efficiency of dynamin since such analysis overcomes complications arising from upstream defects associated with membrane binding and self-assembly. GTP-addition to preassembled ΔPH scaffolds led to tube constriction followed by a cut (Fig. 4-3A, Movie 6). Single pixel tube fluorescence traces acquired from under a ΔPH (Fig. 4-3B, red trace) and WT (Fig. 10B, blue trace) scaffold showed similar trends of GTPase-induced tube constriction prior to scission, with the important distinction that ΔPH fission events were characterized by a prolonged fission time. Analysis of multiple single tube scission events revealed that the kinetics of GTPase-induced tube constriction with ΔPH was only marginally

slower than that seen with WT (Fig. 4-3C, τ_{WT} = 2.3 ± 3.0 s, mean ± SD, n = 44; $\tau_{\Delta PH}$ = 4.7 ± 4.8 s, mean ± SD, n = 39). Furthermore, scaling pixel intensities to tube dimensions (Fig. 4-2-2) revealed that ΔPH scaffolds constrict tube dimensions down to ~3 nm radius prior to the cut, similar to that seen for WT (Fig. 4-3D). Thus, the mechanochemical coupling between GTPase-induced conformational changes in the scaffold and tube constriction is managed quite well even in the absence of a PHD. Remarkably, upon reaching these critical dimensions (~3 nm tube radius), ΔPH appeared to stall for variable time periods while reactions with WT appeared to undergo near spontaneous membrane scission. Consequently, the fission time for ΔPH reactions shows a wide distribution centered about a mean value that is ~12-fold longer than that seen with WT (Fig. 4-3E, Fission time$_{WT}$= 9.8 ± 5.5 s, mean ± SD, n = 88; Fission time$_{\Delta PH}$= 117.5 ± 46.6 s, mean ± SD, n = 44). Taken together, the 10-fold slower cutting rates with ΔPH (Fig. 4-1F) can be explained by slower rates of scaffold assembly and prolonged fission times. In addition to the kinetic delay in tube constriction, our results point to a role of the PHD that is downstream of coupling GTP hydrolysis to membrane constriction. We find instead, that the presence of a PHD in dynamin potently facilitates transformation of a highly constricted prefission tube intermediate to a cut.

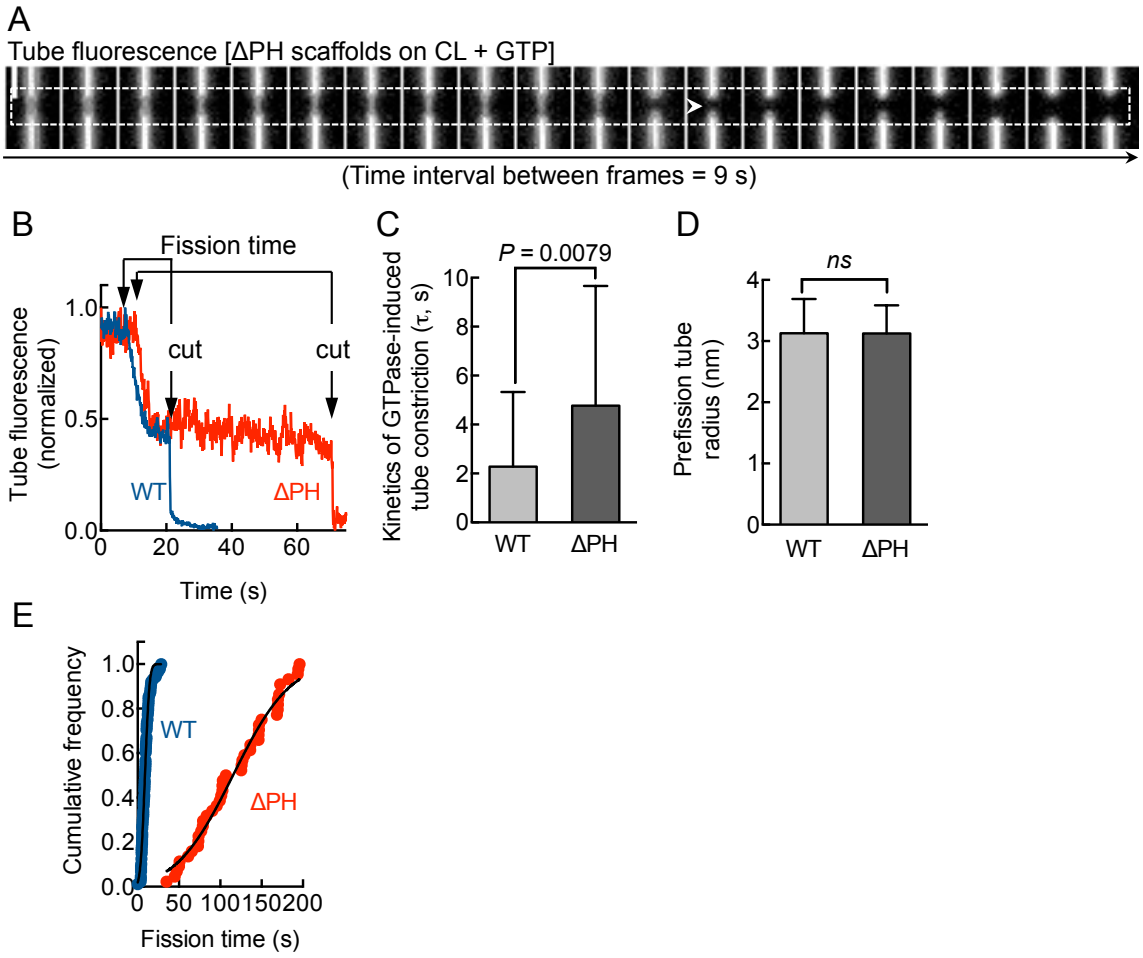

Figure 4-3. Catalytic role of the PHD in dynamin-induced membrane fission (A) Panels from a time-lapse movie monitoring tube fluorescence changes under a ΔPH scaffold (marked by the dotted line) in response to GTP addition. White arrowhead marks site of scission. Scale bar = 5 μm. (B) Single pixel tube fluorescence changes in response to GTP addition to a WT (blue) and ΔPH (red) scaffold. Fission time represents the time period between onset of constriction and the cut in the tube. (C) Time constants of GTPase-induced tube constriction. Data represent the mean ± SD ($n \geq 40$, N=3, Student's t-test). (D) Tube radius of the prefission intermediate. Data represent the mean ± SD ($n \geq 40$, N=3, Student's t-test).(E) Cumulative frequency distribution of fission time for WT and ΔPH. ($n \geq 40$, N=3).

4.3.4 Global determinants for efficient catalysis of membrane fission

Previous work indicates an important role for membrane insertion by VL1 in dynamin-induced membrane fission (Ramachandran et al., 2009) (Fig. 4-4A). Using the suite of stage-specific fluorescence-based assays described here, we recently showed that the primary defect associated with altering the hydrophobicity of VL1 by introducing the I533A mutation is an

inability to form stable scaffolds in the constant presence of GTP(Chapter 3), events that are upstream of membrane fission *per se*. In fact, the fission defect with I533A can be overcome when preassembled on membrane tubes. To comprehensively address if residues in VL1 indeed affect membrane fission, we substituted I533 with residues of varying hydrophobicity and tested them for fission times on preassembled scaffolds. To our surprise, none of the mutants displayed a phenotype as severe as that seen with ΔPH (Fig. 4-2B). Moreover, we find little correlation between residue hydrophobicity at the 533 position to fission time (Fig. 4-4C). These results suggest contribution of additional residues in the PHD in catalyzing fission or a global effect ascribable to the entire PHD.

To test the latter possibility, we asked if defects associated with ΔPHscaffolds could be overcome by providing a PHD in *trans*. For this, we added equimolar concentrations of ΔPHand WT to CL-containing membrane tubes. Using orthogonally labeled ΔPHand WT constructs, we find WT to coassemble with ΔPH to form mixed scaffolds (Fig. 4-4D). Thus, WT fluorescence (green) strongly coincided with ΔPH fluorescence (red) (Fig. 4-4E). Conversely, addition of equimolar concentrations of WT and ΔPH to PIP_2-containing membrane tubes also led to the formation of mixed scaffolds (Fig. 4-4F,G). The ratio of WT:ΔPH fluorescence was lower on CL containing-tubes and higher on PIP_2 containing-tubes (Fig. 4-4H), and is consistent with the differences in scaffold assembly rates seen for each of these constructs (Fig. 4-2F). Since scaffold assembly is attributed to proper alignment of the stalk regions (Faelber et al., 2011; Ford et al., 2011), the ability for ΔPH to co-assemble with WT suggests that the ΔPH and WT are architecturally similar at the G-domain:stalk:BSE interface.

Mixed scaffolds on CL containing-tubes displayed a significant enhancement in kinetics of assembly-induced tube constriction seen earlier with ΔPH alone (Fig. 4-4I; $\tau_{\Delta PH} = 85.9 \pm 63.5$ s, mean ± SD, n = 73; $\tau_{\Delta PH:WT} = 51.6 \pm 28.3$ s, mean ± SD, n = 11). Surprisingly, mixed scaffolds on PIP_2 containing-tubes also showed enhancement in kinetics of assembly-induced tube constriction seen with WT (Fig. 4-4I; $\tau_{WT} = 20.4 \pm 13.7$ s, mean ± SD, n = 173; $\tau_{\Delta PH:WT} = 15.9 \pm 6.4$ s, mean ± SD, n = 13). Next, we added GTP to preassembled mixed scaffolds (Figure 4-4E) and monitored their response over time. While kinetics of GTPase-induced tube constriction with mixed scaffolds showed marginal changes (Fig.4-4-1), we find the fission time to be significantly affected. Thus, mixed scaffolds on CL containing-tubes showed fission times that were ~4-fold faster than that seen ΔPH scaffolds, approaching estimates seen for WT on PIP_2-

containing tubes (Fig. 4-4J, Fission time$_{\Delta PH}$ = 117.5 ± 46.6, mean ± SD, n = 44;Fission time$_{\Delta PH:WT}$ = 27.9 ± 12.7, mean ± SD, n = 43). Thus, organizing a PHD on a membrane lacking PIP_2 is sufficient to markedly improve the fission defect seen with ΔPH. Again surprisingly, mixed scaffolds on PIP_2-containing tubes displayed fission times that were 2-fold smaller than that seen with WT (Fig. 4-4J, Fission time $_{WT}$ = 9.8 ± 5.5, mean ± SD, n = 88; Fission time$_{WT:\Delta PH}$ = 4.2 ± 1.5, mean ± SD, n = 22). Together, these results lead us to conclude that dynamin scaffolds display a gain-of-function when interspersed with ΔPH constructs. How can this be explained mechanistically? Combining our analysis with WT, ΔPH and mixed scaffolds along with the I533 mutants, we find that fission time correlates quite well with kinetics of assembly-induced tube constriction (Fig. 4-4K), rather than kinetics of GTPase-induced tube constriction (Fig.4-4-1). Together, the specific structural features of the PHD as well as the global organization of multiple PHDs within the scaffold influence the efficiency of the fission process. Importantly, such contributions appear to be intrinsic to how the PHD interacts with or packs on the membrane rather than from a GTP hydrolysis-dependent process.

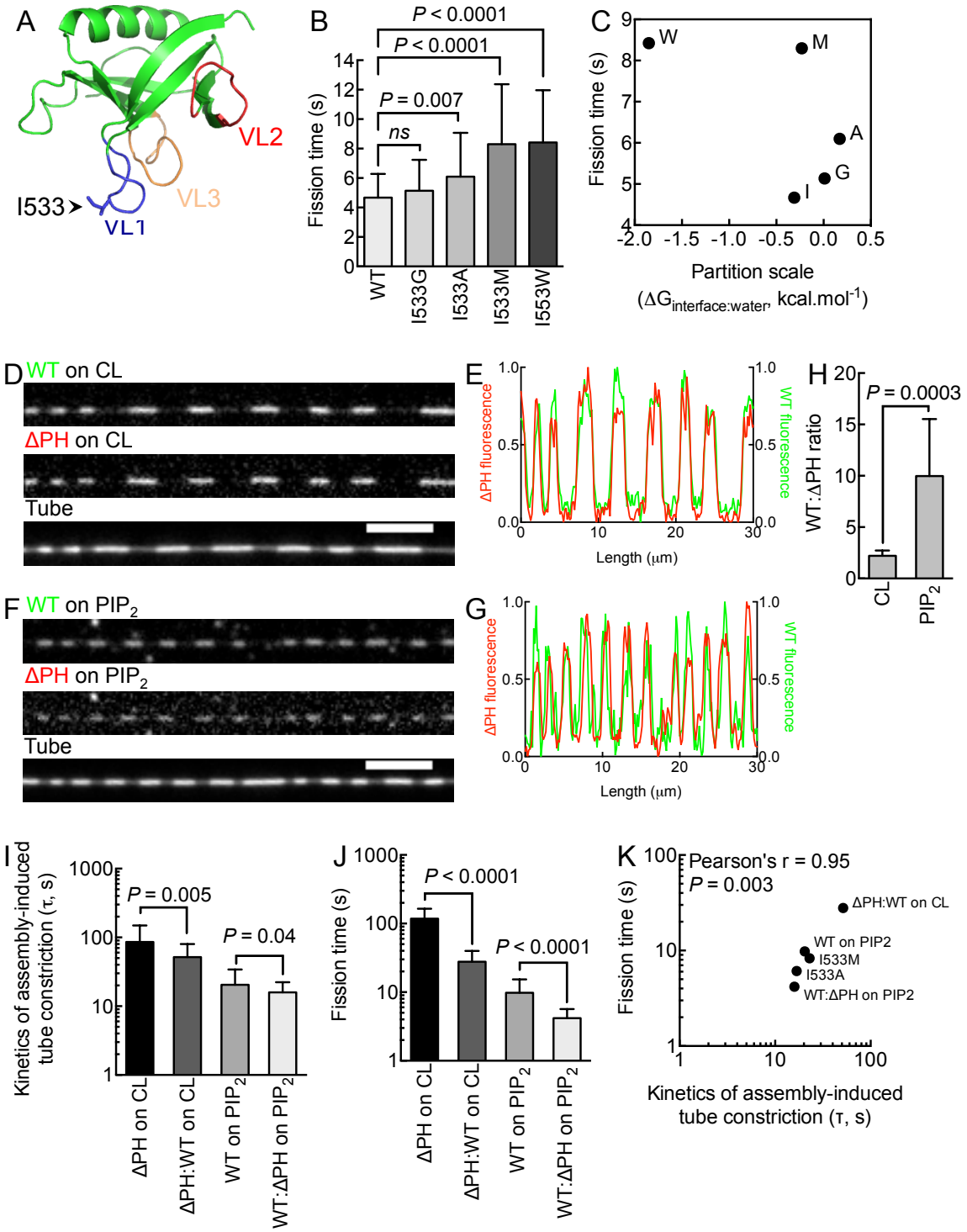

Figure 4-4. Determinants for efficient catalysis of membrane fission(A) Structure of the dynamin1 PHD (PDB code: 1DYN) indicating the position of VL1, 2 and 3 and the I533 residue at the tip of VL1. (B) Fission time for I533 substituted with different residues. Data represent the mean ± SD (n > 40, N=3, Student's t-test). (C) Lack of correlation between residue partition preference (Wimley and White scale) and fission time for the I533 mutants. Fluorescence micrographs (D,F) and line profiles (E,G) of Alexa 647-labeled WT (green) and Alexa 488-

labeled ΔPH (red) scaffolds (white arrowheads) co-assembled on a CL-containing (D) and PIP_2-containing (E) tube. (H) Fluorescence ratio of WT and ΔPH on CL- and PIP_2-containing tubes. Data represent the mean ± SD (n > 10 scaffolds, Student's t-test). (I) Time constants of scaffold assembly-induced tube constriction (I) and fission time (J) for pure (ΔPH or WT) and mixed scaffolds (ΔPH:WT). Data represent the mean ± SD (n≥ 20, N=3, Student's t-test). (K) Correlation between time constant (τ) of assembly-induced tube constriction and fission time. Data represent compiled analysis with pure, mixed and I533 mutants.

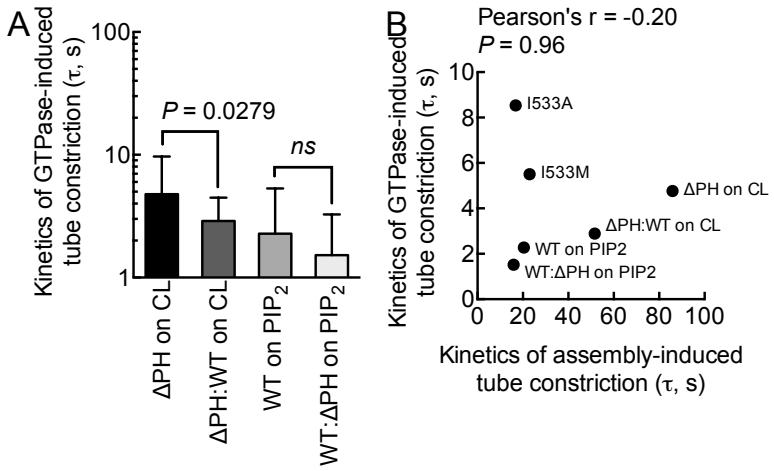

Figure 4-4-1**. Role of the PHD in GTPase-induced membrane constriction**(A) Time constants of GTPase-induced tube constriction for pure (ΔPH or WT) and mixed (ΔPH:WT) scaffolds. Data represent the mean ± SD (n≥ 20, N=3, Student's t-test). (B) Lack of correlation between time constant (τ) of GTPase-induced tube constriction and fission time.

4.3 Discussion

Results from previous studies showing nucleotide-dependent changes to the average distance between the G-domain and PHD in solution (Solomaha et al., 2005) and dissociation of scaffolds in response to GTP hydrolysis (Ramachandran et al., 2007) were interpreted to reflect a functional coupling between the PHD and the G-domain. In addition, the origins of assembly-stimulated GTPase activity were interpreted to reflect a scenario where the PHD transmits assembly-dependent conformational changes in the scaffold to the G domain (Chappie et al., 2010; Chappie et al., 2011). If the PHD were specifically involved in such coupling, the ΔPH construct should have demonstrated effects in bulk rates of GTP hydrolysis and GTPase-induced tube constriction, which is not the case. Furthermore, scaffolds formed in the absence of the PHD constrict tubes to similar extents as WT indicating that the G-domain:stalk:BSE region is solely capable of transmitting conformational changes resulting from GTP hydrolysis to membrane

constriction. The most striking defect in the absence of the PHD is the lingering presence of a prefission intermediate even after the tube has reached the critical dimension, which from theory, is speculated to spontaneously lead to scission (Kozlovsky and Kozlov, 2003). Recent reports have indicated that locking the G-domains in the transition state also results in a highly constricted tube intermediate (Mattila et al., 2015). We think it unlikely that the two intermediates are the same since; (a) the intermediate reported earlier emerges only when the GTPase cycle is stalled while the one we find appears as the scaffold continues to hydrolyze GTP, (b) the intermediate we find stalls with variable efficiency leading to a deregulated fission process, and (c) this intermediate manifests with mutants or constructs that also demonstrate an inability to efficiently manage a GTPase-independent membrane constriction thereby rendering it a function not of dynamin's GTPase cycle but to how it assembles on the membrane.

The long-lived prefission intermediate reveals the necessity for an additional energetic input to be overcome for tube scission. Given that the defect in the absence of the PHD manifests in highly variable fission times, we think the PHD catalyzes tube constriction and scission by exerting small, *k*T-level energy inputs to the underlying lipid bilayer. Surprisingly, mixed scaffolds that contain ΔPH and WT fare better than pure scaffolds in both tube constriction and fission. The 109-residue long PHD occupies a significant volume within the dynamin scaffold (Chappie et al., 2011). Thus, WT when present alongside ΔPH in a mixed scaffold should provide an uneven membrane interacting surface. Such organization should therefore result in the lipid bilayer adopting a fluctuating 'corrugated' configuration (Fig. 4-5). Perhaps, the energetic inputs from the PHD originate from maintaining such a fluctuating bilayer configuration, an effect suggested in recent coarse-grained simulations (Fuhrmans et al., 2015). We speculate that greater the amplitude of such fluctuations, faster would be the progress of tube constriction and fission reactions. Thus, scaffolds comprised of ΔPH would produce the least degree of such undulations followed by WT and mixed scaffolds in that order.

Our results from monitoring partial reactions leading to membrane fission indicate the PHD to be dispensable for membrane fission. The consequence however is a sluggish scaffold assembly and membrane fission reaction. Our results help understand the influence of the PHD in the spatiotemporal regulation of discreet stages of dynamin function. Thus, the PHD acts by enhancing cooperativity between dynamin subunits thereby allowing the rapid formation of scaffolds that constrict the necks of emergent vesicles. Following this, the PHD aids in the rapid

formation of a possible hemi-fused intermediate causing the neck to undergo scission. From an evolutionary standpoint, the PHD appears a recent addition in classical dynamins. In fact, functions of membrane association appear to be managed by disordered loops among the bacterial and mitochondrial dynamins. Thus, the physiologic requirement for a fast-acting membrane fission apparatus appears to have been fulfilled by the adoption of the PHD by the classical dynamins.

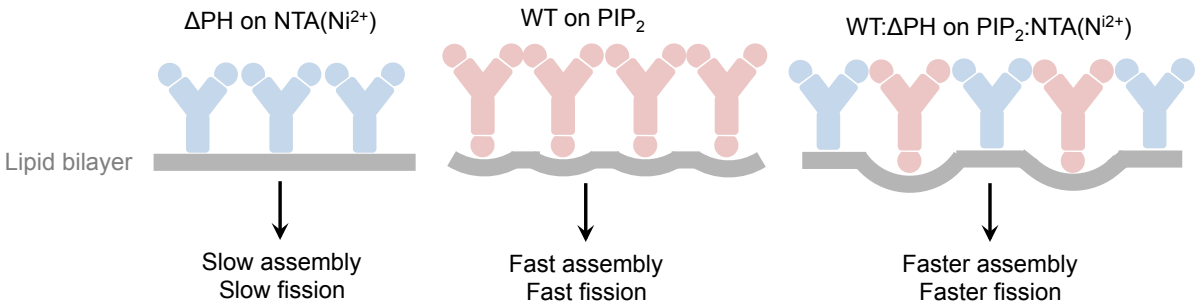

Figure 4-5. Proposed model depicting different bilayer topology adopted in presence and absence of PHD

Chapter- 5

Summary and Future Perspective

5.1 Summary

Biological membranes undergo dynamic remodeling during vesicular transport, wherein proteins are sorted into a membrane bud that is severed to form a vesicle. This process allows cells to take up nutrients, ensures inheritance of organelles after cell division and manages synaptic transmission thus making it fundamental to life. Formation of a membrane bound carrier necessitates dynamic interplay between protein and membrane. Protein complexes extensively remodel membranes generating highly curved intermediates during membrane budding and fission. While the identity and function of key proteins in vesicular transport has been established through hypomorphic mutants or conditional knockouts; we are still unclear about the molecular determinants and spatio-temporal signatures of participant proteins. The complex environment of the cell presents a hurdle in appreciating the broad design principles by which proteins involved in membrane trafficking manage membrane remodeling leading to vesicle release. *In vitro* reconstitution is an important approach to understand mechanisms underlying complex reactions and cellular processes. It relies on simulating cellular processes using minimal components under biochemically-regulated environment.

Liposomes have been the preferred membrane substrate for most reconstitution studies, and the earliest insights into protein induced shape changes in bilayer topology came from incubation of brain cytosol with liposomes. Their small size precludes spatially resolved dynamic analysis using fluorescence microscopy. Due to the bulk nature of these assay systems, mechanistic insights as to how different conformational states of the protein are propagated to the underlying membrane tube have also remained unclear. The use of alternate model membrane systems has helped us overcome these challenges, but have also generated controversy. Quantitative analysis of fluorescence changes on the widely used assay system of membrane tethers pulled from giant unilamellar vesicles and supported bilayers with excess reservoir (SUPER) is difficult because of their out-of-focus movements in solution, not to mention the experimental challenge in recording statistically significant numbers of events because these systems allow recording of only a single fission event.

This thesis describes a novel assay system of arrayed supported membrane tubes (SMrT), which resemble the highly curved membrane intermediates generated during vesicle formation. Using real-time fluorescence microscopy with high temporal resolution, I independently tested

dynamin, core component of clathrin-mediated endocytosis. Internalization of receptors from the plasma membrane via CME proceeds with the deformation of the donor membrane into a bud, encapsulation of proteins, separation of bud from the parent membrane and subsequent fusion with the donor compartment. Although critical to vesicular transport, the molecular mechanisms underlying membrane budding and fission remain poorly understood. In particular, the actual dynamics of lipid bilayer division and the corresponding role of protein machinery driving this process are poorly characterized. Dynamin is recruited to the constricted neck of mature CCPs, where GTP hydrolysis by dynamin collar severs the neck catalyzing release of a clathrin-coated vesicle. Using a correlative fluorescence microscopy-based analysis of scaffold dynamics and membrane topological intermediates generated during clathrin assembly and fission reaction we have not only identified the potential role of membrane curvature in defining the neck for recruitment of dynamin but also a GTP hydrolysis-dependent membrane constriction process catalyzed by an intact dynamin scaffold that culminates in a highly constricted tubular intermediate of 7.2 nm radius prior to scission.

5.2 Future Perspective

While dynamin is capable of binding negatively-charged membranes in vitro, it relies on interactions with several SH3 domain-containing Endocytic Accesory Proteins (EAPs) that act as adaptors to link dynamin function to specific cellular processes. Proteins like Amphiphysin 1 (amph1), Endophilin (endo) have been shown to localize to the necks of clathrin-coated pits (Okamoto et al. 1997; Grabs et al., 1997; Shupliakov et al., 1997; Ringstad et al., 1997; Takei et al., 1999; Yoshida et al 2004; Meinecke et al., 2013).Another BAR family member Syndapin (Sdp) act as an adaptor to recruit dynamin to specialized forms clathrin-independent synaptic vesicle biogenesis (Clayton et al., 2009) and to caveolae-dependent forms of vesicular transport processes (Senju et al., 2011). In addition, complexes of dynamin and Grb2 and the F-actin binding proteins (Abp1) appear to be required for the specific uptake of epidermal growth factor receptors (Huang et al., 2004) and link endocytosis to the actin cytoskeleton (Kessels et al., 2001), respectively. Together, these results suggest that it is a complex of dynamin with these proteins that act as physiological effectors of membrane fission. Dynamin's interaction with these proteins appears to be important in generating clathrin-coated vesicles as attempts to block these interactions have been shown to significantly impair CME. In cells, BAR domain-containing

proteins like amphiphysin, endophilin and syndapin, have been shown to interact with the PRD of dynamin and recruit dynamin specifically to the necks of coated pits. Interactions of dynamin with BAR-domain containing proteins have been relatively well studied and have formed the basis for understanding the regulatory aspects EAPs on dynamin function. The BAR domain is a crescent-shaped module with positively charged residues at its concave surface that promotes electrostatic interactions with negatively charged membranes (Tarricone et al., 2001; Peter et al., 2004; Blood and Voth, 2006). Amph1 and endo are BAR family members that posses an amphipathic helix at the N-terminus of their BAR domains, which partially inserts into the lipid bilayer potentially allowing them to sense/generate membrane curvature. While BAR domain containing proteins manage recruiting dynamin to necks of coated pits, their effects on dynamin's membrane fission activity remains relatively less well studied.

A recent report shows involvement of endophilin in an endocytic pathway that is independent of AP2 and clathrin, however requires dynamin to mediate vesicle release (Boucrot et al., 2015). Independently another study using Endophilin A-2, highlights its ability to form scaffolds and act as a force-generator thereby assisting dynamin to mediate scission on membrane tubes pulled from GUVs (Renard et al., 2015). However the results are qualitative and there is no mechanistic insight into how it compares to the fission characteristics of dynamin alone and other accessory proteins.I speculate that, a complex of dynamin with these membrane-active proteins (endo, amph1, sdp) would display altered GTPase-dependent dynamics on the membrane and as a consequence show altered membrane fission activity. Also since dynamin function critically depends on its tendency to self-assemble into helical polymers, presence of EAPs such as Abp1 and Grb2 that engages the C-terminal PRD domain could very likely interfere with self-assembly and therefore membrane fission.

On a broad perspective, given its simplicity, high-throughput nature and potential applicability, we anticipate our assay system of SMrT templates to be of substantial utility in understanding the mechanisms by which protein scaffolds function during vesicular transport. With the suite of assays now available, it becomes possible to independently test the ability of each of the BAR-protein to sense and generate curvature on our system of SMrT templates. Using this assay it we can also address question related to the regulatory role of EAPs in CME. In the context of dynamin, some of these questions can be addressed quantitatively relating to analysis of characteristics of membrane fission events catalyzed by dynamin:EAP complexes,

and (ii) To correlate possible differences observed in fission characteristics to differences in membrane binding, self-assembly and GTPase-induced disassembly of dynamin:EAP complexes.

References

1. Bashkirov, P. V. *et al.* GTPase Cycle of Dynamin Is Coupled to Membrane Squeeze and Release, Leading to Spontaneous Fission. *Cell***135,** 1276–1286 (2008).
2. Bethoney KA1, King MC, Hinshaw JE, Ostap EM, Lemmon MA. A possible effector role for the pleckstrin homology (PH) domain of dynamin. *Proc Natl Acad Sci U S A.* **106**, 13359-64 (2009).
3. Cao H, Garcia F, McNiven MA. Differential distribution of dynamin isoforms in mammalian cells. *Mol. Biol. Cell***9**,2595–609 (1998).
4. Carr JF, Hinshaw JE. J Biol Chem. Dynamin assembles into spirals under physiological salt conditions upon the addition of GDP and gamma-phosphate analogues. *J Biol Chem*. **272**, 28030-5 (1997).
5. Chang-Ileto B. et al. Synaptojanin 1-mediated PI(4,5)P_2 hydrolysis is modulated by membrane curvature and facilitates membrane fission. Dev. *Cell***20**, 206– 218 (2011).
6. Chantal Christis and Sean Munrocorresponding. The small G protein Arl1 directs the trans-Golgi–specific targeting of the Arf1 exchange factors BIG1 and BIG2. *J Cell Biol.* **196**, 327–335 (2012).
7. Chappie JS, Acharya S, Leonard M, Schmid SL, Dyda F. G domain dimerization controls dynamin's assembly-stimulated GTPase activity. *Nature***27**,465(7297):435-40 (2010)
8. Chappie, J. S. & Dyda, F. Building a fission machine–structural insights into dynamin assembly and activation. *Journal of Cell Science* (2013).
9. Chappie, J. S. *et al.* A Pseudoatomic Model of the Dynamin Polymer Identifies a Hydrolysis-Dependent Powerstroke. *Cell***147,** 209–222 (2011).
10. Chen MS, Obar RA, Schroeder CC, Austin TW, Poodry CA, et al. Multiple forms of dynamin are encoded by shibire, a *Drosophila* gene involved in endocytosis. *Nature***351**, 583–86 (1991).
11. Chernomordik LV, Kozlov MM . Protein-lipid interplay in fusion and fission of biological membranes. *Annu. Rev. Biochem.***72**,175-207 (2003).
12. Christis C1, Munro S. The small G protein Arl1 directs the trans-Golgi-specific targeting of the Arf1 exchange factors BIG1 and BIG2. *J Cell Biol.***196**, 327-35 (2012).
13. Clayton EL, Anggono V, Smillie KJ, Chau N, Robinson PJ, Cousin MA. The phospho-dependent dynamin-syndapin interaction triggers activity-dependent bulk

endocytosis of synaptic vesicles. *J. Neurosci.* **29**, 7706-7717 (2009).

14. Cocucci, E., Gaudin, R. & Kirchhausen, T. Dynamin recruitment and membrane scission at the neck of a clathrin-coated pit. *Mol. Biol. Cell***25,** 3595–3609 (2014).
15. Cook T, Mesa K, Urrutia R. Three dynamin-encoding genes are differentially expressed in developing rat brain. J.Neurochem. 67:927–31.
16. Cook TA, Urrutia R, McNiven MA. (1994). Identification of dynamin 2, an isoform ubiquitously expressed in rat tissues. *Proc. Natl. Acad. Sci. USA***91**, 644–48 (1996).
17. Cremona O, Di Paolo G, Wenk MR, Lu¨ thi A, Kim WT, Takei K, Daniell L, Nemoto Y, Shears SB, Flavell RA, et al. Essential role of phosphoinositide metabolism in synaptic vesicle recycling. *Cell***99**,179–188 (1999).
18. Damke H, Baba T, Warnock DE, Schmid SL. Induction of mutant dynamin specifically blocks endocytic coated vesicle formation. *J. Cell Biol.***127**, 915–34 (1994).
19. Damke, H., T. Baba, D.E. Warnock, and S.L. Schmid. Induction of mutant dynamin specifically blocks endocytic coated vesicle formation. *J Cell Bio.l***127**, 915–934 (1994).
20. Danino, D., Moon, K.-H. & Hinshaw, J. E. Rapid constriction of lipid bilayers by the mechanochemical enzyme dynamin. *J Struct Biol* **147,** 259–267 (2004).
21. Diatloff-Zito C, Gordon AJ, Duchaud E, Merlin G. Isolation of an ubiquitously expressed cDNA encoding human dynamin II, a member of the large GTP-binding protein family. *Gene***163,** 301–6 (1995).
22. Domanov, Y. A. *et al.* Mobility in geometrically confined membranes. *Proc. Natl. Acad. Sci. U.S.A.***108,** 12605–12610 (2011).
23. Doyon, J. B. *et al.* Rapid and efficient clathrin-mediated endocytosis revealed in genome-edited mammalian cells. *Nat. Cell Biol* 1–20 (2011).
24. Durieux AC, Vignaud A, Prudhon B, Viou MT, Beuvin M, Vassilopoulos S, Fraysse B, Ferry A, Lainé J, Romero NB, Guicheney P, Bitoun M. Hum. A centronuclear myopathy-dynamin 2 mutation impairs skeletal muscle structure and function in mice. *Mol Genet*. **19**, 4820-36 (2010).
25. Ellenberg, J. *et al.* Nuclear membrane dynamics and reassembly in living cells: targeting of an inner nuclear membrane protein in interphase and mitosis. *J Cell Biol.***138,** 1193–1206 (1997).
26. Emmanuel Boucrot, Antonio P. A. Ferreira, Leonardo Almeida-Souza, Sylvain Debard,

Yvonne Vallis, Gillian Howard, Laetitia Bertot, Nathalie Sauvonnet & Harvey T. McMahon.. Endophilin marks and controls a clathrin-independent endocytic pathway . *Nature* **517**, 460–465 (2015).

27. Faelber, K., M. Held, S. Gao, Y. Posor, V. Haucke, F. Noé, and O. Daumke. Structural insights into dynamin-mediated membrane fission. *Structure* **20**, 1621– 1628 (2012).
28. Faelber, K., Y. Posor, S. Gao, M. Held, Y. Roske, D. Schulze, V. Haucke, F. Noé, and O. Daumke. Crystal structure of nucleotide-free dynamin. *Nature***477**, 556–560 (2011).
29. Farsad K, Ringstad N, Takei K, Floyd SR, Rose K, De Camilli P. Generation of high curvature membranes mediated by direct endophilin bilayer interactions. *J Cell Biol*. **155**, 193-200 (2001).
30. Ferguson SM, Brasnjo G, Hayashi M, Wölfel M, Collesi C, Giovedi S, Raimondi A, Gong LW, Ariel P, Paradise S, O'toole E, Flavell R, Cremona O, Miesenböck G, Ryan TA, De Camilli P. A selective activity-dependent requirement for dynamin 1 in synaptic vesicle endocytosis. *Science*.**316**, 570-4 (2007).
31. Ferguson SM, Raimondi A, Paradise S, Shen H, Mesaki K, Ferguson A, Destaing O, Ko G, Takasaki J, Cremona O, O' Toole E, De Camilli P. Coordinated actions of actin and BAR proteins upstream of dynamin at endocytic clathrin-coated pits. *Dev Cell.* **17**, 811-22 (2009).
32. Ferguson, S. M. & Pietro De Camilli. Dynamin, a membrane-remodelling GTPase. *Nature Publishing Group* 1–14 (2012).
33. Ferguson, S., A. Raimondi, S. Paradise, H. Shen, K. Mesaki, A. Ferguson, O. Destaing, G. Ko, J. Takasaki, O. Cremona, E.O. Toole, and Pietro De Camilli.. Coordinated Actions of Actin and BAR Proteins Upstream of Dynamin at Endocytic Clathrin-Coated Pits. *Developmental Cell.***17**, 811–822 (2009).
34. Ford, M.G.J., S. Jenni, and J. Nunnari. The crystal structure of dynamin. *Nature* **477**, 561–566 (2011).
35. Fröhlich C, Grabiger S, Schwefel D, Faelber K, Rosenbaum E, Mears J, Rocks O, Daumke O. Structural insights into oligomerization and mitochondrial remodelling of dynamin 1-like protein. *EMBO J.***32**, 1280-92 (2013).
36. Frolov, V. A., Escalada, A., Akimov, S. A. & Shnyrova, A. V. Geometry of membrane fission. *Chemistry and Physics of Lipids***185,** 129–140 (2015).

37. Fuhrmans, M. & Müller, M. Coarse-grained simulation of dynamin-mediated fission. *Soft Matter* – (2014).

38. Gao S, von der Malsburg A, Dick A, Faelber K, Schröder GF, Haller O, Kochs G, Daumke O. Structure of myxovirus resistance protein a reveals intra- and intermolecular domain interactions required for the antiviral function. *Immunity***35**, 514-25 (2011).

39. Grabs D, Slepnev VI, Songyang Z, David C, Lynch M, Cantley LC, DeCamilli P. The SH3 domain of amphiphysin binds the proline-rich domain of dynamin at a single site that defines a new SH3 binding consensus sequence. *J Biol Chem*. **272**, 13419- 13425 (1997).

40. Grigliatti TA, Hall L, Rosenbluth R, Suzuki DT. Temperature-sensitive mutations in *Drosophila melanogaster*. XIV. A selection of immobile adults. *Mol. Gen. Genet.***120**, 107–14 (1973).

41. Herskovits JS, Shpetner HS, Burgess CC, Vallee RB. Microtubules and *Src* homology 3 domains stimulate the dynamin GTPase via its C-terminal domain. *Proc. Natl. Acad. Sci. USA***90**, 11468–72 (1993).

42. Heymann JA, Hinshaw JE.Dynamins at a glance. *J Cell Sci.***122**, 3427-31 (2009).

43. Hsieh, W.T. *et al.* Curvature Sorting of Peripheral Proteins on Solid-Supported Wavy Membranes. *Langmuir***28,** 12838–12843 (2012).

44. Huang F, Khvorova A, Marshall W, Sorkin A. Analysis of clathrin-mediated endocytosis of epidermal growth factor receptor by RNA interference. *J. Biol Chem.***279**,16657-16661 (2004).

45. Itoh T, Erdmann KS, Roux A, Habermann B, Werner H, De Camilli P. Dynamin and the actin cytoskeleton cooperatively regulate plasma membrane invagination by BAR and F-BAR proteins. *Dev Cell.* **9**, 791-804. (2005)

46. Iversen, T. G., Skretting, G., van Deurs, B. & Sandvig, K. Clathrin-coated pits with long, dynamin-wrapped necks upon expression of a clathrin antisense RNA. *Proc. Natl. Acad. Sci. U.S.A.***100,** 5175 (2003).

47. Jon A Kenniston and Mark A Lemmon. Dynamin GTPase regulation is altered by PH domain mutations found in centronuclear myopathy patients. *EMBO J.* **29**, 3054–3067 (2010).

48. Jung, H., Robison, A. D. & Cremer, P. S. Detecting Protein−Ligand Binding on Supported Bilayers by Local pH Modulation. *J. Am. Chem. Soc.***131,** 1006–1014 (2009).

49. Kaksonen M, Toret CP, Drubin DG. A modular design for the clathrin- and actin-mediated endocytosis machinery. *Cell*. **123**, 305-20 (2005).
50. Kessels MM, Engqvist-Goldstein AE, Drubin DG, Qualmann B. Mammalian Abp1, a signal-responsive F-actin-binding protein, links the actin cytoskeleton to endocytosis via the GTPase dynamin. *J. Cell Biol.***153**, 351-366 (2001).
51. Koenig, J., K. Saito, and K. Ikeda. 1983. Reversible control of synaptic transmission in a single gene mutant of Drosophila melanogaster. *J Cell Biol* 96, 1517–1522.
52. Kosaka T & Ikeda K. Reversible blockage of membrane retrieval and endocytosis in the garland cell of the temperature-sensitive mutant of *Drosophila* melanogaster, shibirets1. *J. Cell Biol.***97**, 499–507 (1983).
53. Kozlovsky, Y. & Kozlov, M. M. Membrane fission: model for intermediate structures. *Biophys. J* **85,** 85–96 (2003).
54. Kubalek EW, Le Grice SF, Brown PO. Two-dimensional crystallization of histidine-tagged, HIV-1 reverse transcriptase promoted by a novel nickel-chelating lipid. *J Struct Biol.***113**, 117-23 (1994)
55. Kunding, A. H., Mortensen, M. W., Christensen, S. M. & Stamou, D. A fluorescence-based technique to construct size distributions from single-object measurements: application to the extrusion of lipid vesicles. *Biophysical Journal***95,** 1176–1188 (2008).
56. Larsen, J., Hatzakis, N. S. & Stamou, D. Observation of Inhomogeneity in the Lipid Composition of Individual Nanoscale Liposomes. *J. Am. Chem. Soc.***133,** 10685–10687 (2011).
57. Lippincott-Schwartz J, Snapp E, Kenworthy A. Studying protein dynamics in living cells. *Nat Rev Mol Cell Biol*. **2**, 444-56 (2001).
58. Liu, Y. W. *et al.* Differential curvature sensing and generating activities of dynamin isoforms provide opportunities for tissue-specific regulation. *Proc. Natl. Acad. Sci. U.S.A.***108,** E234 (2011).
59. Liu, Y.W., M.C. Surka, T. Schroeter, V. Lukiyanchuk, and S.L. Schmid. Isoform and splice-variant specific functions of dynamin-2 revealed by analysis of conditional knock-out cells. *Mol. Biol. Cell*. **19**, 5347–5359 (2008).
60. Lundmark R, Carlsson SR. Regulated membrane recruitment of dynamin-2 mediated by sorting nexin 9. *J Biol Chem*. **279**, 42694-702 (2004).

61. M A Lemmon, K. M. F. Signal-dependent membrane targeting by pleckstrin homology (PH) domains. *Biochem. J.***350,** 1 (2000).
62. Marks B & McMahon HT. Calcium triggers calcineurin-dependent synaptic vesicle recycling in mammalian nerve terminals. *Curr.Biol.***8**, 740–49 (1998).
63. Martens S, McMahon HT. Mechanisms of membrane fusion: disparate players and common principles. *Nat Rev Mol Cell Biol*. **9**, 543-56 (2008).
64. Mattila, J.P. *et al.* A hemi-fission intermediate links two mechanistically distinct stages of membrane fission. *Nature*. doi:10.1038/nature14509(2015)
65. McMahon HT, Wigge P, Smith C (1997): Clathrin interacts specifically with amphiphysin and is displaced by dynamin. FEBS Lett. 413:319-322.
66. McPherson PS, Garcia EP, Slepnev VI, David C, Zhang X, et al. A presynaptic inositol-5-phosphatase. *Nature***379,** 353–57 (1996).
67. Mears, J. A., Ray, P. & Hinshaw, J. E. A Corkscrew Model for Dynamin Constriction. *Structure***15,** 1190–1202 (2007).
68. Mehrotra, N., Nichols, J. & Ramachandran, R. Alternate pleckstrin homology domain orientations regulate dynamin-catalyzed membrane fission. *Mol. Biol. Cell***25,** 879–890 (2014).
69. Meinecke M, Boucrot E, Camdere G, Hon WC, Mittal R, McMahon HT. Cooperative recruitment of dynamin and BIN/amph1/Rvs (BAR) domain-containing proteins leads to GTP-dependent membrane scission. *J Biol Chem.* **288**, 6651-61(2013).
70. Mircea Achiriloaie, Barbara Barylko, and Joseph P. Albanesi Essential Role Of The Dynamin Pleckstrin Homology Domain In Receptor-Mediated Endocytosis. *Mol. Cell Biol.***19**,1410–1415 (1999)
71. Morlot, S. *et al.* Membrane Shape at the Edge of the Dynamin Helix Sets Location and Duration of the Fission Reaction. *Cell***151,** 619–629 (2012).
72. Morlot, S., Roux. A. Mechanics of dynamin-mediated membrane fission. *Annu Rev Biophys.* **42**, 629–649 (2013).
73. Muhlberg AB, Warnock DE, Schmid SL. Domain structure and intramolecular regulation of dynamin GTPase. *EMBO J.***16**, 6676-83 (1997).
74. Nakata T, Takemura R, Hirokawa N. A novel member of the dynamin family of GTP binding proteins is expressed specifically in the testis. *J. Cell Sci.***10**, 1–5 (1993).

75. Naslavsky N, Caplan S. EHD proteins: key conductors of endocytic transport. *Trends Cell Biol.***21**,122-31 (2011).

76. Neumann, S., Pucadyil, T. J. & Schmid, S. L. Analyzing membrane remodeling and fission using supported bilayers with excess membrane reservoir. *Nature Protocols***8,** 213–222 (2013).

77. Newman-Smith ED, Shurland DL, van der Bliek AM. Assignment of the dynamin-1 gene (DNM1) to human chromosome 9q34 by fluorescence in situ hybridization and somatic cell hybrid analysis. *Genomics***41**, 286–89 (1997).

78. Niemann A, Berger P, Suter U. Pathomechanisms of mutant proteins in Charcot-Marie-Tooth disease. *Neuromolecular Med*. **8**, 217-42 (2006).

79. Obar RA, Collins CA, Hammarback JA, Shpetner HS, Vallee RB. Molecular cloning of the microtubule-associated mechano-chemical enzyme dynamin reveals homology with a new family of GTP-binding proteins. *Nature* **347**, 256–61(1990).

80. Okamoto PM, Herskovits JS, Vallee RB. Role of the basic, proline-rich region of dynamin in Src homology 3 domain binding and endocytosis. *J Biol Chem.***272**,11629-35 (1997).

81. Peter BJ, Kent HM, Mills IG, Vallis Y, Butler PJ, Evans PR, McMahon HT. BAR domains as sensors of membrane curvature: the amph1 BAR structure. *Science* **30**, 495–499. (2004).

82. Pucadyil, T. J. & Schmid, S. L. Real-time visualization of dynamin-catalyzed membrane fission and vesicle release. *Cell***135,** 1263–1275 (2008).

83. Ramachandran, R. *et al.* Membrane insertion of the pleckstrin homology domain variable loop 1 is critical for dynamin-catalyzed vesicle scission. *Mol. Biol. Cell***20,** 4630–4639 (2009).

84. Ramachandran, R., and S.L. Schmid. Real-time detection reveals that effectors couple dynamin's GTP-dependent conformational changes to the membrane. *EMBO J*. **27**, 27–37 (2007).

85. Renard HF, Simunovic M, Lemière J, Boucrot E, Garcia-Castillo MD, Arumugam S, Chambon V, Lamaze C, Wunder C, Kenworthy AK, Schmidt AA, McMahon HT, Sykes C, Bassereau P, Johannes L. Endophilin-A2 functions in membrane scission in clathrin-independent endocytosis. *Nature***517**, 493-6 (2015).

86. Reubold TF, Faelber K, Plattner N, Posor Y, Ketel K, Curth U, Schlegel J, Anand R,

Manstein DJ, Noé F, Haucke V, Daumke O, Eschenburg S. Crystal structure of the dynamin tetramer. *Nature*. **525**, 404-8 (2015).

87. Ringstad N, Nemoto Y, De Camilli P. The SH3p4/Sh3p8/SH3p13 protein family: binding partners for synaptojanin and dynamin via a Grb2-like Src homology 3 domain. *Proc Natl Acad Sci* **94**, 8569-74 (1997).
88. Rothman JE. Mechanisms of intracellular protein transport. *Nature.* **372**, 55-63 (1994).
89. Roux, A. *et al.* Membrane curvature controls dynamin polymerization. *Proc. Natl. Acad. Sci. U.S.A.***107,** 4141–4146 (2010).
90. Roux, A. Reaching a consensus on the mechanism of dynamin? *F1000Prime Rep***6,** 86 (2014).
91. Roux, A., Uyhazi, K., Frost, A. & De Camilli, P. GTP-dependent twisting of dynamin implicates constriction and tension in membrane fission. *Nature***441,** 528–531 (2006).
92. Schekman R, Orci L. Coat proteins and vesicle budding. *Science.***271**, 1526-33 (1996).
93. Schindelin, J. *et al.* Fiji: an open-source platform for biological-image analysis. *Nature Methods***9,** 676–682 (2012).
94. Schmid SL, Frolov VA. Dynamin: functional design of a membrane fission catalyst. *Annu Rev Cell Dev Biol*. **27**, 79-105 (2011)
95. Schmid SL. Clathrin-coated vesicle formation and protein sorting: an integrated process. *Annu Rev Biochem.***66**, 511-48 (1997).
96. Schmid, S. L. & Frolov, V. A. Dynamin: Functional Design of a Membrane Fission Catalyst. *Annu. Rev. Cell Dev. Biol.***27,** 79–105 (2011).
97. Senju Y, Itoh Y, Takano K, Hamada S, Suetsugu S.. Essential role of PACSIN2/syndapin-II in caveolae membrane sculpting. *J. Cell Sci.***124**, 2032-2040 (2011).
98. Shlomovitz, R., Gov, N. S. & Roux, A. Membrane-mediated interactions and the dynamics of dynamin oligomers on membrane tubes. *New J. Phys.***13,** 065008 (2011).
99. Shnyrova, A.V., P.V. Bashkirov, S.A. Akimov, T.J. Pucadyil, J. Zimmerberg, S.L. Schmid, and V.A. Frolov. Geometric catalysis of membrane fission driven by flexible dynamin rings. *Science***339,** 1433–1436 (2013).
100. Shpetner HS, Vallee RB. Identification of dynamin, a novel mechanochemical enzyme that mediates interactions between microtubules. *Cell.***59**, 421-32 (1989).
101. Shupliakov O, Löw P, Grabs D, Gad H, Chen H, David C, Takei K, De Camilli P, Brodin

L. Synaptic vesicle endocytosis impaired by disruption of dynamin-SH3 domain interactions. *Science.* **276**, 259-63 (1997).

102. Shupliakov O. et al. Synaptic vesicle endocytosis impaired by disruption of dynamin-SH3 domain interactions. *Science***276**, 259–263 (1997).
103. Solomaha E, Palfrey HC. Conformational changes in dynamin on GTP binding and oligomerization reported by intrinsic and extrinsic fluorescence. *Biochem J.* **391**, 601-11(2005).
104. Stachowiak Jeanne C et al. Membrane bending by protein–protein crowding. *Nature Cell Biology***14**, 944–949 (2012).
105. Stowell, M., Marks, B., Wigge, P. & McMahon, H. T. Nucleotide-dependent conformational changes in dynamin: evidence for a mechanochemical molecular spring. *Nat. Cell Biol.***1,** 27–32 (1999).
106. Sundborger, A. C. *et al.* A dynamin mutant defines a superconstricted prefission state. *Cell Reports***8,** 734–742 (2014).
107. Sweitzer, S. M. & Hinshaw, J. E. Dynamin undergoes a GTP-dependent conformational change causing vesiculation. *Cell***93,** 1021–1029 (1998).
108. Takei K, Slepnev VI, Haucke V, De Camilli P. Functional partnership between amphiphysin and dynamin in clathrin-mediated endocytosis. *Nat. Cell Biol.***1**, 33–39 (1999).
109. Takei K, Slepnev VI, Haucke V, De Camilli P. Functional partnership between amph1 and dynamin in clathrin-mediated endocytosis. *Nat. Cell Biol.* **1**, 33–39 (1999).
110. Tamm LK, Crane J, Kiessling V. Membrane fusion: a structural perspective on the interplay of lipids and proteins. *Curr Opin Struct Biol.***13**, 453-66 (2003). Review.
111. Tanford C.Protein-lipid interactions. *Neurosci Res Program Bull.***11**, 193-5 (1973).
112. Tarricone C, Xiao B, Justin N, Walker PA, Rittinger K, Gamblin SJ, Smerdon SJ. The structural basis of Arfaptin-mediated cross-talk between Rac and Arf signalling pathways. *Nature***411**, 215–219 (2001).
113. Taylor, M. J., Perrais, D. & Merrifield, C. J. A High Precision Survey of the Molecular Dynamics of Mammalian Clathrin-Mediated Endocytosis. *Plos Biol***9,** e1000604 (2011).
114. Tuma PL, Stachniak MC, Collins CA. Activation of dynamin GTPase by acidic phospholipids and endogenous rat brain vesicles. *J Biol Chem.***268**,1 7240-6 (1993).

115. Turner, D. K. *et al.* Reduction of Artifacts in Fluorescence Correlation Spectroscopy Due to Sample Adsorption on Optical Glass Surfaces. *appl spectrosc***67,** 692–698 (2013).

116. Urrutia R, Henley JR, Cook T, McNiven MA. The dynamins: redundant or distinct functions for an expanding family of related GTPases?*Proc. Natl. Acad. Sci. USA* **94**, 377–84 (1997).

117. Vaid KS, Guttman JA, Babyak N, Deng W, McNiven MA, Mochizuki N, Finlay BB, Vogl AW. The role of dynamin 3 in the testis. *J Cell Physiol***210**, 644-54 (2007).

118. Vallis, Y., Wigge, P., Marks, B., Evans, P. R. & McMahon, H. T. Importance of the pleckstrin homology domain of dynamin in clathrin-mediated endocytosis. *Curr. Biol.***9,** 257–260 (1999).

119. van der Bliek AM & Meyerowitz EM. Dynamin-like protein encoded by the *Drosophila shibire*gene associated with vesicular traffic.*Nature***351**, 411–414 (1991).

120. van der Bliek AM, Redelmeier TE, Damke H, Tisdale EJ, Meyerowitz EM, Schmid SL. Mutations in human dynamin block an intermediate stage in coated vesicle formation. *J Cell Biol*. **122**, 553-63 (1993).

121. Warnock DE, Schmid SL. Dynamin GTPase, a force-generating molecular switch. *BioEssays***18**, 885–93 (1996).

122. Wickner W. Membrane fusion: five lipids, four SNAREs, three chaperones, two nucleotides, and a Rab, all dancing in a ring on yeast vacuoles. *Annu Rev Cell Dev Biol.* **26**,115-36 (2010).

123. Wigge P & McMahon HT. The amphiphysin family of proteins and their role in endocytosis at the synapse. *Trends Neurosci*. **21**, 339–344 (1998).

124. Yoshida Y et al. The stimulatory action of amph1 on dynamin function is dependent on lipid bilayer curvature. *EMBO J.* **1**, 3483-91 (2004).

125. Zhang, P. & Hinshaw, J. E. Three-dimensional reconstruction of dynamin in the constricted state. *Nat. Cell Biol.***3,** 922–926 (2001).